UNIVERSITI TEKNOLOGI MARA

AI-ENHANCED FAULT-TOLERANT CONTROL OF BIDIRECTIONAL DUAL ACTIVE BRIDGE CONVERTERS USING WAVELET-BASED NEURAL CLASSIFICATION

MOHAMAD SYAZWAN BIN MOHAMED

MSc

March 2026

UNIVERSITI TEKNOLOGI MARA

AI-ENHANCED FAULT-TOLERANT CONTROL OF BIDIRECTIONAL DUAL ACTIVE BRIDGE CONVERTERS USING WAVELET-BASED NEURAL CLASSIFICATION

MOHAMAD SYAZWAN BIN MOHAMED

Thesis submitted in fulfilment
of the requirements for the degree of
Master of Science
(ELECTRICAL ENGINEERING)

FACULTY OF ELECTRICAL ENGINEERING

March 2026

CONFIRMATION BY PANEL OF EXAMINERS

I certify that a Panel of Examiners has met on 27 November 2025 to conduct the final examination of Mohd Zuli Bin Jaafar on his Masters of Science thesis entitled "AI-Enhanced Fault-Tolerant Control Of Bidirectional Dual Active Bridge Converters Using Wavelet-Based Neural Classification" in accordance with Universiti Teknologi MARA Act 1976 (Akta 173). The Panel of Examiner recommends that the student be awarded the relevant degree. The Panel of Examiners was as follows:

Nor Diyana Md Sin
Associate Professor
Faculty of Electrical Engineering
Universiti Teknologi MARA
(Chairman)

Khairul Safuan Muhammad
Senior Lecturer
Faculty of Electrical Engineering
Universiti Teknologi MARA
(Internal Examiner)

Mohd Azlan Abu
Senior Lecturer
Faculty of Applied Sciences
Universiti Teknologi Malaysia
(External Examiner)

PROFESSOR DR HJH ZURAEDA IBRAHIM
Dean
Institute of Postgraduates Studies
Universiti Teknologi MARA

Date: 6 March 2026

AUTHOR'S DECLARATION

I declare that the work in this thesis was carried out in accordance with the regulations of Universiti Teknologi MARA. It is original and is the results of my own work, unless otherwise indicated or acknowledged as referenced work. This thesis has not been submitted to any other academic institution or non-academic institution for any degree or qualification.

I, hereby, acknowledge that I have been supplied with the Academic Rules and Regulations for Postgraduate, Universiti Teknologi MARA, regulating the conduct of my study and research.

Name of Student	:	MOHAMAD SYAZWAN BIN MOHAMED
Student ID. No.	:	2023241928
Programme	:	Master of Science (Electrical Engineering) – CEEE750
Faculty	:	Electrical Engineering
Thesis Title	:	AI-Enhanced Fault-Tolerant Control of Bidirectional Dual Active Bridge Converters Using Wavelet-Based Neural Classification
Signature of Student	:	
Date	:	6 March 2026

ABSTRACT

This thesis presents a simulation-based fault-tolerant control strategy for a bidirectional Dual Active Bridge (DAB) converter, motivated by the growing demand for reliable and efficient power conversion in applications such as electric vehicles, battery energy storage systems, and renewable energy integration. Although DAB converters are widely adopted due to their high efficiency and bidirectional capability, their performance can be significantly degraded by open-circuit switch faults, which may compromise system stability and power continuity. To address this issue, a fault detection and diagnosis framework combining wavelet-based feature extraction and Artificial Neural Network (ANN) classification is proposed. Inductor current signals obtained from a MATLAB/Simulink model of the DAB converter are decomposed using discrete wavelet transform to extract time–frequency features that characterise both normal and faulty operating conditions. These features are used to train an ANN classifier to distinguish between normal operation and open-circuit faults at individual switches. The ANN training converged within six epochs and achieved a Mean Squared Error (MSE) of 1.43×10^{-15}, indicating fast convergence and stable learning behaviour under the simulated conditions. Simulation results demonstrate that the proposed method is capable of detecting open-circuit faults at switches T1, T2, T5, and T6 within approximately 0.21–0.23 s. Following fault identification, a redundancy-based passive fault-tolerant control strategy is activated, allowing the converter to recover stable operation within approximately 0.28–0.29s. The post-fault current waveforms return to within predefined tolerance bands with reduced oscillations, confirming the effectiveness of the proposed approach in maintaining bidirectional power flow during fault conditions. Overall, the results indicate that the integration of wavelet-based signal processing and ANN-based fault diagnosis can enhance the reliability of DAB converters under open-circuit fault scenarios in a simulated environment.

ACKNOWLEDGEMENT

I am deeply grateful for the continuous support, insightful guidance, and patience shown by Assoc Prof Muhamad Nabil Hidayat throughout the course of this research. His expertise and encouragement have been invaluable in navigating the complexities of this project. I also wish to extend my sincere appreciation to my co-supervisor, Ts. Dr. Kanendra Naidu, for providing me with invaluable insights into controller designs and for sharing his wealth of knowledge and practical experience, which greatly enhanced my understanding and approach to this work.

I would also like to extend my appreciation to the technical staff and colleagues at College of Engineering for their support and assistance during the experimental and simulation phases of this project. Their willingness to share their expertise and offer advice when challenges arose enriched my learning experience.

Finally, this thesis is dedicated to the loving memory of my very dear father and mother for the vision and determination to educate me. This piece of victory is dedicated to both of you.

TABLE OF CONTENTS

LIST OF TABLES

LIST OF FIGURES

LIST OF SYMBOLS

Symbols

cD_1, cD_2, cD_3	Wavelet detail coefficients
$e(t)$	Error signal at time t
f_s	Switching frequency
K_i	Integral gain
K_d	Derivative gain
K_p	Proportional gain (used in PID/PI controller)
L	Inductance of Transformer or DAB System
$m(t)$	Control signal output
P	Power Transferred Across the Converter
V_1	Voltage at the Primary Side of DAB
V_2	Voltage at the Secondary Side of DAB Converter
V_actual	Actual voltage (used in hysteresis control)
V_ref	Reference voltage (used in hysteresis control)
θ	Phase Shift Angle Between Bridges

LIST OF ABBREVIATIONS

Abbreviations

ANN	Artificial Neural Network
APM	Airborne Particulate Matter
AI	Artificial Intelligence
AFTC	Active Fault-Tolerant Control
Cuk	Ćuk Converter
DAB	Dual Active Bridge
DC	Direct Current
EV	Electric Vehicle
FDD	Fault Detection and Diagnosis
FLC	Fuzzy Logic Controller
HIL	Hardware-in-the-Loop
IGBT	Insulated-Gate Bipolar Transistor
ML	Machine Learning
MOSFET	Metal–Oxide–Semiconductor Field-Effect Transistor
MPC	Model Predictive Control
MRAC	Model Reference Adaptive Control
NNC	Neural Network Controller
PCA	Principal Component Analysis
PD	Proportional-Derivative

PID	Proportional-Integral-Derivative
PI	Proportional-Integral
PFTC	Passive Fault-Tolerant Control
QSAR	Quantitative Structure-Activity Relationship
SEPIC	Single-Ended Primary-Inductor Converter
SMC	Sliding Mode Controller
UPS	Uninterruptible Power Supply
V2G	Vehicle-to-Grid
ZCS	Zero-Current Switching
ZVS	Zero-Voltage Switching

LIST OF NOMENCLATURE

Nomenclatures

Ah	Measured in ampere-hours (Ah), represents electric charge, typically for battery capacity.
C	Measured in farads (F), capacitance is a component's ability to store electric charge.
D	Duty cycle (unitless), expresses the ON-time ratio of a switching period.
e(t)	Error signal (unit varies), difference between reference and actual output.
f	Measured in hertz (Hz), frequency represents the number of AC cycles per second.
I	Measured in amperes (A), current refers to the flow of electric charge in a circuit.
Ki	Integral gain (1/s), corrects cumulative error over time.
Kd	Derivative gain (s), reacts to rate of error change.
Kp	Proportional gain (unit varies), determines control output relative to error.
L	Measured in henries (H), inductance describes a coil's opposition to current change.
m(t)	Control signal (unit varies), manipulated output from the controller.
P	Measured in watts (W), power indicates the rate of energy transfer.
R	Measured in ohms (Ω), resistance quantifies opposition to current flow.
t	Measured in seconds (s), time describes the duration of circuit events.

V	Measured in volts (V), voltage is the electric potential difference between two points.
V_actual	Measured in volts (V), actual voltage is the real-time output being controlled.
V_ref	Measured in volts (V), reference voltage is the target level in control systems.
θ	Measured in radians (rad), represents phase shift in switching control.

CHAPTER 1
INTRODUCTION

1.1 Research Background

The Bidirectional DAB Converter has become a cornerstone in modern power electronics due to its adaptability, efficiency, and ability to manage bidirectional power flow [1]. Its architecture, which consists of DAB on both the input and output sides, allows seamless power transfer in either direction [2]. This feature makes DAB converters ideal for a wide range of applications, including electric vehicle (EV) charging, renewable energy systems, energy storage, and grid support. With the growing emphasis on sustainable energy and the need to stabilize power supply systems, DAB converters are instrumental in managing energy flow between sources, storage, and loads [3]. However, as these systems grow in complexity, ensuring their reliability and resilience under various fault conditions has become critical. Fault tolerance is an essential aspect of power electronics, particularly in applications where continuous operation is vital [4]. Traditional converters are susceptible to faults, such as open circuit and short circuit failures in semiconductor switches, which can lead to catastrophic system failures, interrupt operations, and increase maintenance costs [5].

In the case of a DAB converter, the challenge is even greater, as bidirectional power flow requires the system to quickly detect, isolate, and adapt to faults to maintain stability. Without effective fault tolerance, faults in DAB converters could disrupt power systems, leading to downtime and increased costs [6]. This has led to a growing body of research focused on developing fault tolerant topologies and intelligent control strategies for DAB converters to ensure they remain operational under fault conditions.

One of the most promising approaches in recent research involves integrating artificial intelligence (AI) with signal processing techniques to enhance fault detection and tolerance [7]. Specifically, the combination of artificial neural networks (ANNs) with wavelet-based feature extraction has emerged as a powerful method for fault management in DAB converters [8]. Wavelet analysis is particularly effective for capturing transient behaviours and oscillations in electrical waveforms, which are often indicative of faults [9]. Unlike Fourier analysis, which provides frequency information without localization in time, wavelet analysis decomposes signals into both time and

frequency domains, making it ideal for detecting sudden changes associated with faults [10]. By extracting these unique features, wavelet analysis can help identify distinct patterns that correspond to different types of faults, thus enabling precise and rapid fault detection. After extracting features with wavelet decomposition, these features can be used to train an ANN, which is adept at recognizing complex patterns in data [11]. The ANN learns to classify various operational states of the DAB converter, distinguishing between normal and faulty conditions and identifying specific fault types [12]. Once trained, the ANN can quickly analyse incoming waveform data to detect and classify faults in real time, triggering appropriate responses to maintain system stability [13]. This intelligent fault management approach allows the DAB converter to not only detect faults but also adapt its operation, accordingly, leveraging redundancy or adjusting control strategies to ensure uninterrupted power flow [14].

The fault tolerant DAB converter topology proposed in this research integrates redundancy with intelligent control mechanisms [15]. Redundant switches are included in the design, which can be activated when faults are detected, thereby maintaining continuous operation [16]. The ANN's ability to identify faults based on the waveform data alone augmented by wavelet extracted features enables the system to respond swiftly to faults, reducing the risk of cascading failures. This design not only enhances the reliability of the DAB converter but also contributes to the resilience of the larger power system [17]. Such resilience is critical in applications like EV charging stations, which require uninterrupted service, and in renewable energy systems, where fluctuations in supply and demand make fault tolerance essential for grid stability [18]. The significance of this research extends beyond the technical advancement of DAB converters. It demonstrates a paradigm shift in power electronics toward more adaptive, intelligent systems that can handle the complexities of modern energy systems [19]. As the grid evolves to accommodate decentralized and variable renewable energy sources, the demand for converters that can adapt to fluctuating conditions and withstand faults will only increase. This research provides a blueprint for designing next generation power converters that incorporate AI driven fault tolerance, thus paving the way for more resilient and sustainable energy systems.

Furthermore, the integration of wavelet-based feature extraction and ANN classification represents a valuable contribution to the broader field of intelligent power electronics [20]. This approach exemplifies how advanced data processing techniques can be applied to power systems, enhancing their performance and robustness. By

leveraging wavelet transforms to capture subtle fault characteristics and using ANNs for rapid classification, the proposed fault tolerant DAB converter showcases how AI and signal processing can work in tandem to improve system reliability [21]. This methodology has potential applications beyond DAB converters, extending to other critical components in power systems that require fault tolerant capabilities. Ultimately, this research addresses a critical need in the energy industry: the ability to maintain reliable power flow in the face of faults. By developing an intelligent, fault tolerant DAB converter, this work contributes to the advancement of resilient power systems that are essential for modern applications such as renewable energy integration, smart grids, and EV infrastructure. The proposed converter is not only a technical innovation but also a step toward sustainable and reliable energy solutions, aligning with global efforts to achieve a more robust and flexible energy grid.

1.2 Motivation for This Work

In today's rapidly evolving energy landscape, reliability, efficiency, and adaptability are more important than ever. As the world shifts toward renewable energy systems, electric vehicles, and smart grid technologies, the need for robust and intelligent power converters becomes critical [22]. At the heart of many of these applications is the DAB converter, prized for its ability to transfer energy bidirectionally with high efficiency and compact design.

However, as promising as DAB converters are, they also come with challenges particularly when it comes to fault tolerance and real time fault detection [23]. In high stakes systems like EV charging or grid connected batteries, even a brief power disruption caused by an undetected fault can lead to equipment damage, energy loss, or safety risks. Traditional fault detection methods often fall short in speed or accuracy, especially in dynamic environments [24].

This is what drives the core motivation behind this work: the need to enhance the fault tolerance of DAB converters using intelligent, fast, and accurate control strategies. By integrating wavelet-based feature extraction with artificial neural networks (ANNs), this research aims to create a converter that can not only operate efficiently under normal conditions but also quickly detect and recover from faults, maintaining system stability with minimal downtime.

The ultimate goal is to contribute to the development of smarter, safer, and more resilient power systems ones that can meet the growing demands of modern energy applications while minimizing failure risks. This work combines power electronics, signal processing, and AI to push the boundaries of what current converters can do and to help pave the way for next generation energy solutions.

1.3 Problem Statement

Modern energy systems increasingly depend on advanced power electronic converters to enable efficient and flexible energy exchange between multiple sources and loads. Among these converters, the bidirectional DAB converter has gained significant attention due to its high-power density, galvanic isolation, and capability for bidirectional power transfer. Despite these advantages, maintaining stable, efficient, and reliable operation of DAB converters under varying load and operating conditions remains a significant challenge. Conventional switching and control strategies are often

based on fixed modulation schemes or simplified control assumptions, which may not respond effectively to dynamic current variations. As a result, such methods can lead to increased power losses, reduced efficiency, and degraded system performance, particularly in applications requiring frequent bidirectional power flow. This highlights the need for an improved switching strategy that incorporates current-based control to ensure stable and efficient operation across a wide range of operating conditions.

In addition to control challenges, fault detection in bidirectional DAB converters represents a critical concern for system reliability and safety. Traditional fault detection techniques commonly rely on threshold-based monitoring, rule-based logic, or hardware protection circuits. While these approaches are relatively simple to implement, they often suffer from limited sensitivity, slow response time, and an inability to accurately detect subtle or early-stage faults. In particular, open-circuit switch faults can be difficult to identify using conventional methods because they may not produce immediate or obvious changes in system signals. As a consequence, such faults may remain undetected until they lead to severe performance degradation or component damage. This limitation exposes a clear gap between existing fault detection methods and the increasing reliability demands of modern power electronic systems.

Recent advancements in data-driven and intelligent diagnostic techniques provide an opportunity to address these shortcomings. Artificial neural networks offer the ability to learn complex nonlinear relationships from system data and can distinguish between normal and faulty operating conditions with higher accuracy than traditional methods. When combined with effective feature extraction techniques, such as wavelet-based analysis, ANN-based fault detection can capture both time-domain and frequency-domain characteristics of converter signals. This enables faster and more reliable detection of open-circuit faults compared to conventional approaches, particularly in dynamic operating environments. However, the application of such intelligent fault detection methods to bidirectional DAB converters remains relatively limited and requires further investigation and validation.

Furthermore, the effectiveness of any proposed switching strategy or fault detection mechanism must be demonstrated through systematic evaluation before practical deployment. Experimental validation, while desirable, is often constrained by cost, time, and hardware availability. MATLAB and Simulink simulations provide a flexible and powerful platform for modelling converter behaviour, implementing control algorithms, and evaluating fault detection performance under controlled yet

realistic conditions. Without comprehensive simulation-based validation, it is difficult to assess whether proposed techniques can achieve the desired improvements in efficiency, stability, and fault tolerance. Therefore, there exists a clear need for a structured simulation framework that can validate both an improved current-controlled switching strategy and an intelligent ANN-based fault detection mechanism for bidirectional DAB converters.

1.4 Research Objectives

The objectives of this research focus on addressing key challenges in the design and operation of bidirectional DAB fault tolerant converter topology. These objectives aim to ensure the reliability, efficiency, and seamless operation of the DAB converter under normal and fault conditions.

a) To develop a current controller-based switching strategy to enables efficient and stable bidirectional power transfer in a DAB converter.
b) To develop open circuit fault detection mechanism for BDC using feature extraction method in ANN to enable fast and accurate identification of faulty switches, thereby supporting reliable fault-tolerant operation.
c) To validate both techniques using simulation for evaluating the performance, reliability, and fault-tolerant capability of the proposed switching strategy and fault-detection mechanism.

1.5 Research Question

1) How can a current controller-based switching strategy enhance the efficiency and stability of bidirectional power transfer in DAB converter?
2) What are the major challenges in ensuring reliable operation of a DAB converter under fault conditions, especially open circuit faults?
3) Can artificial neural networks (ANN) effectively detect open circuit faults in Bidirectional DC Converters (BDC) through feature extraction techniques?

1.6 Significance of Study

This study aims to contribute meaningfully to the development of smarter, more reliable power conversion systems, especially in today's world where energy efficiency and system resilience are more important than ever. The DAB converter has gained popularity due to its ability to manage bidirectional power flow, but like any advanced system, it faces real challenges especially when operating under unpredictable conditions or faults [25].

By proposing a current controller-based switching strategy, this research hopes to make DAB converters more efficient and adaptable, which can benefit a wide range of applications, from electric vehicles to renewable energy systems [26]. Furthermore, by introducing artificial neural networks (ANN) for detecting open circuit faults, this study takes a proactive step toward making power systems smarter and more self-aware capable of identifying problems before they lead to serious failures [27].

Validating everything through simulation in MATLAB ensures that the ideas are not just theoretical, but practical and ready for future real-world application. In essence, this research brings together modern control strategies and intelligent fault detection to build a foundation for more robust, efficient, and reliable energy systems. It's a step forward not just in technology, but in creating solutions that matter in everyday energy challenges.

1.7 Assumption

This study is built upon a few key assumptions to ensure the research remains focused, manageable, and meaningful. Firstly, it is assumed that the simulation environment in MATLAB accurately represents the real-world behaviour of the DAB converter under both normal and fault conditions. While simulations cannot capture every possible real-world factor, they are assumed to be reliable enough for validating the proposed control and fault detection strategies.

Secondly, it is assumed that the system components such as switches, transformers, and sensors operate under ideal or near ideal conditions in the simulation. Factors like component aging, noise, and environmental effects such as temperature or humidity are not included in this stage of the research. Third, the artificial neural network (ANN) model used for fault detection is assumed to be properly trained with

clean and relevant input data. It is also assumed that the selected features for training are representative enough to allow the model to recognize patterns and detect open circuit faults accurately.

Lastly, this study assumes that the focus on open circuit faults is sufficient to demonstrate the capability and value of using ANN for fault detection in bidirectional DC converters. While other fault types exist, this research concentrates on a specific type to maintain clarity and depth. These assumptions help keep the research scope clear and enable a deeper exploration of the proposed strategies, laying a strong foundation for future studies that can build upon or expand these ideas.

1.8 Ethical Committee

This research was conducted with careful attention to ethical standards, ensuring that all activities carried out during the study were aligned with principles of honesty, integrity, and respect for academic and professional norms.

Since this project is simulation based and does not involve human participants, animals, or sensitive personal data, the ethical risks are minimal. However, the researcher has remained committed to upholding ethical practices throughout the study. All simulation tools, particularly MATLAB and any machine learning (ML) libraries, were used with proper licensing and within the allowed scope of use. Data used to train the artificial neural network was generated within the simulation environment and does not involve any third party or proprietary datasets. No part of the work was copied or plagiarized from other sources, and full credit has been given to all references, frameworks, and tools used in the development of this project.

Should this study progress toward hardware implementation or real-world testing in the future, ethical approval will be sought from the appropriate institutional review board or ethics committee to ensure the continued responsible conduct of research. This project has been developed in good faith, with the intention of contributing positively to the field of electrical and electronic engineering.

1.9 Thesis Scope and Limitation

This study focuses on the development of a fault-resilient control and fault detection framework for a bidirectional DAB converter, which is widely used in modern

energy systems such as electric vehicles, renewable energy integration, and battery energy storage applications. The scope of the research is defined by the objective of improving both power transfer efficiency and system reliability under normal operating conditions as well as under specific fault scenarios. In this work, a current controller-based switching strategy is investigated to enhance the stability and efficiency of bidirectional power flow within the DAB converter. In parallel, an intelligent fault detection mechanism is developed with particular emphasis on identifying open-circuit faults in converter switches. This fault detection approach employs wavelet-based feature extraction combined with an artificial neural network to enable accurate classification and early detection of fault conditions. The performance of the proposed switching strategy and fault detection mechanism is evaluated and validated entirely through MATLAB and Simulink simulations, allowing systematic analysis under controlled and repeatable operating conditions.

At the same time, several limitations are inherent in the scope of this research and must be acknowledged. All modelling, analysis, and validation are conducted in a simulation environment, and therefore real-world hardware effects such as temperature variation, electromagnetic interference, switching noise, component aging, and unpredictable load behaviour are not fully captured. As a result, hardware implementation, real-time testing, and experimental verification are beyond the scope of the present study. Furthermore, the fault detection framework is limited to open-circuit faults occurring in individual switches of the DAB converter. Other fault types, including short-circuit faults, soft or incipient faults, sensor failures, transformer-related faults, and component-level degradations, are intentionally excluded. The analysis also assumes that only one switch is faulty at any given time, and scenarios involving multiple simultaneous switch failures are not considered.

In addition, the artificial neural network used for fault identification is trained and tested exclusively using data generated from simulations. Its performance therefore depends on the quality and representativeness of the simulated signals, and its effectiveness may vary if applied to different converter topologies or real-world systems without additional retraining or parameter tuning. While the proposed switching strategy is designed to improve efficiency and stability, its application in larger or more complex power systems involving multiple converters, fluctuating grid conditions, or hybrid energy sources may require further optimization. Despite these limitations, the study provides a focused and in-depth investigation into intelligent control and fault

detection for DAB converters and establishes a solid foundation for future work. Potential extensions include hardware implementation, real-time validation, consideration of multiple and mixed fault types, and deployment in large-scale energy conversion systems.

1.10 Thesis Outline

This thesis is thoughtfully organized to guide the reader through the development, implementation, and evaluation of an AI enhanced fault tolerant control strategy for a DAB converter. Each chapter builds upon the last, presenting a clear and logical progression from foundational understanding to technical execution and final insights.

The first chapter, Introduction, lays the groundwork for the study by explaining the importance of fault tolerance in modern power converters especially in critical applications like electric vehicle charging and renewable energy systems. It outlines the research motivation, defines the problem being addressed, and clearly states the objectives and significance of the study. This chapter also introduces the core concept of using artificial intelligence, specifically neural networks, paired with wavelet-based feature extraction to enhance fault detection in power conversion systems.

In the second chapter, Literature Review, the thesis explores existing methods and technologies related to fault tolerant control, fault diagnosis, and AI applications in power electronics. It reviews the use of artificial neural networks and wavelet transform techniques in similar contexts and critically analyses previous work on DAB converters. This helps identify research gaps and provides a solid justification for the proposed approach, positioning it within the broader context of current technological advancements.

Chapter three, Methodology, details how the proposed system was designed and developed. This includes the structure of the DAB converter, the use of wavelet analysis to extract relevant signal features, and the configuration of the neural network model used for fault classification. The simulation setup, data generation, and training procedures are also described in this chapter to ensure the work is transparent, logical, and reproducible.

The fourth chapter, Results and Discussion, presents the outcomes of the simulation-based testing and offers a detailed interpretation of the findings. This chapter

evaluates how the proposed strategy performs under both normal and fault conditions using MATLAB and Simulink environments. Various performance metrics such as detection accuracy, response time, and system robustness are discussed. Graphical results and statistical analyses are used to show how effectively the system can detect and classify open circuit faults. This chapter also reflects on the findings in relation to the research goals and existing literature, while acknowledging limitations and potential improvements.

Finally, chapter five, Conclusion and Future Work, wraps up the research by summarizing the key contributions and outcomes of the study. It reinforces the importance of integrating AI and wavelet-based methods in building smarter, more resilient DAB converters. This chapter also outlines possible directions for future research, including real time hardware implementation, expanding the fault detection system to handle a wider variety of faults, and experimenting with alternative AI models. The goal is to provide a strong foundation for future innovation and encourage the continued advancement of fault tolerant power conversion technologies.

CHAPTER 2
LITERATURE REVIEW

2.1 Introduction

As energy systems become increasingly reliant on power electronics, ensuring the reliability and fault tolerance of converters has emerged as a key area of research [28]. Among the various converter topologies, DAB converter has gained significant attention due to its bidirectional power transfer capability, high power density, and galvanic isolation [29]. DAB converters are especially well suited for applications such as electric vehicle (EV) charging, renewable energy systems, and energy storage, where power needs to flow efficiently in both directions. However, like all power converters, DAB systems are vulnerable to faults that can severely disrupt performance and reduce system lifespan [30].

Traditional methods of fault detection in converters often rely on threshold-based techniques, look up tables, or predefined rule sets [31]. While these approaches are straightforward, they tend to lack adaptability and struggle to detect complex or subtle faults, such as early-stage open circuit failures in switches or components. These limitations have motivated researchers to explore more intelligent and data driven approaches to fault detection particularly those that can learn from patterns in electrical signals.

One area that has shown great promise is the use of Artificial Neural Networks (ANNs) for fault classification [32]. ANNs can recognize non-linear relationships in large datasets, making them well suited for interpreting converter behaviour under various operating conditions. Prior studies have used ANNs for fault diagnosis in different types of converters and power systems, reporting improved detection speed and accuracy compared to conventional methods [33].

Wavelet Transform (WT) has become a widely accepted method for analysing non-stationary signals in power electronics [34]. Unlike Fourier transforms, which focus only on frequency content, wavelets provide both time and frequency localization, making them ideal for capturing sudden changes or transient behaviour common during fault events [35]. Several researchers have successfully applied wavelet transforms to detect disturbances in power systems, extract fault signatures, and even improve the

training of AI models like ANNs and Support Vector Machines (SVMs) [36]. The combination of wavelet analysis and ANN provides a powerful framework, wavelets extract rich, localized features from electrical signals, and ANNs use these features to classify or detect faults with high confidence [37].

In the context of DAB converters, however, there is still a noticeable gap in the literature. While AI and wavelet methods have been applied to other converter types such as buck, boost, or multilevel inverters, studies focusing specifically on DAB fault detection remain limited [38]. Most existing work on DAB systems centres on control optimization or efficiency improvements, rather than fault diagnosis [39]. Furthermore, much of the prior research on ANN-based fault detection tends to focus on short circuit faults or general disturbances, leaving open circuit faults relatively underexplored [40].

This research aims to address those gaps by developing a fault tolerant control strategy for DAB converters that leverages both wavelet-based feature extraction and neural classification techniques, with a particular focus on detecting open circuit faults. By combining these modern tools, the goal is to build a more intelligent, adaptive, and reliable system one that not only improves fault detection but also contributes to the growing body of knowledge on AI based diagnostics in power electronics.

2.2 Artificial Intelligent Control in Power Electronics and Fault Detection

2.2.1 Multiple Linear Regression (MLR) and Support Vector Regression (SVR) in Fault Diagnosis

Multiple Linear Regression (MLR) and Support Vector Regression (SVR) are commonly employed data-driven techniques for modelling and fault diagnosis in power electronic systems [41]. These methods are often used as benchmark or comparative models to evaluate the effectiveness of more advanced learning approaches, such as Artificial Neural Networks (ANNs). Their inclusion in fault diagnosis studies enables a structured comparison between linear, kernel-based, and nonlinear modelling techniques.

MLR is a classical statistical approach that establishes a linear relationship between a set of input features and an output variable. In fault diagnosis applications, MLR has been used to estimate fault severity or classify fault conditions based on extracted signal features due to its simplicity, low computational cost, and ease of

interpretation [42]. However, power electronic converters, including the DAB converter, exhibit highly nonlinear behaviour under switching faults, transient conditions, and parameter variations. As a result, the linear modelling assumption of MLR limits its ability to accurately capture complex fault signatures [43]. Despite this limitation, MLR remains valuable as a baseline method for assessing the relative performance improvements offered by more sophisticated models [44].

SVR extends the Support Vector Machine framework to regression problems and is designed to handle nonlinear relationships through the use of kernel functions [45]. In power electronics fault diagnosis, SVR has been widely applied to analyse current and voltage signals, particularly when wavelet-based or frequency-domain features are used. Compared to MLR, SVR provides better robustness to noise and improved generalisation performance in nonlinear systems [46]. However, its effectiveness strongly depends on kernel selection and hyperparameter tuning, which can increase design complexity and computational effort.

2.2.2 Artificial Neural Network in Fault Diagnosis

ANNs have become an increasingly important tool in modern power electronics due to their ability to model nonlinear relationships, learn complex patterns, and perform rapid classification under dynamic operating conditions [47]. Traditional control and diagnostic techniques in converter systems such as threshold-based fault detection, rule-based logic, or fixed-parameter controllers often struggle in environments characterised by high-frequency switching, transient disturbances, and nonlinear waveform behaviour [48]. As a result, ANNs have emerged as a promising solution for enhancing both converter control and fault detection capabilities, particularly in topologies such as the DAB converter [49].

ANNs consist of interconnected computational nodes (neurons) arranged in layers, enabling them to approximate nonlinear functions based on training data [50]. In power electronic applications, this allows ANNs to capture subtle variations in voltage, current, and switching patterns that typically indicate abnormal conditions or early-stage faults [51]. Unlike classical model-based approaches, ANNs do not require an exact mathematical representation of converter dynamics, instead, they learn system behaviour directly from operational data [52]. This characteristic is particularly

valuable in converters where parasitics, harmonics, and load-dependent variations complicate analytical modelling.

In the context of fault detection, ANNs have been widely adopted for identifying open-circuit faults, short-circuit faults, and sensor abnormalities in DC-DC converters, inverters, and other power electronic interfaces [53]. Their performance improves significantly when paired with signal processing techniques such as the Wavelet Transform (WT). Wavelet decomposition isolates non-stationary and transient features within converter signals, producing meaningful time frequency representations that highlight irregular switching behaviour [54]. These wavelet-extracted features serve as high-quality inputs for ANN classifiers, enabling faster detection times, reduced false positives, and improved robustness under noise and load variations compared to conventional methods [55].

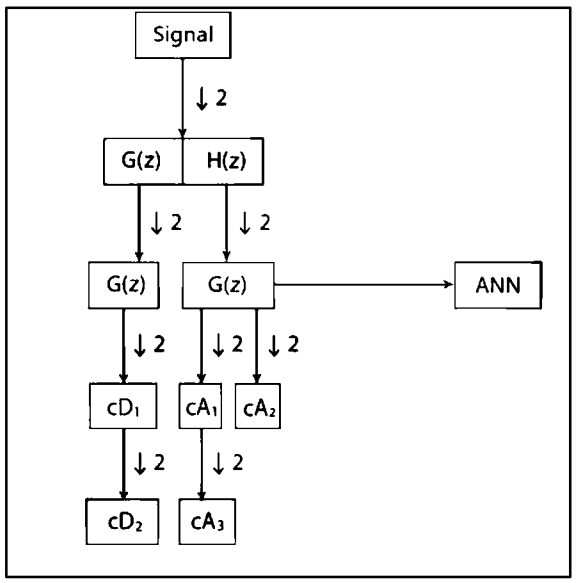

Figure 2.1 Wavelet Decomposite Structure

Figure 2.1 illustrates this multi-level wavelet decomposition process, in which the original signal is filtered into approximation and detail components at successive levels [56]. Fault-induced transients appear predominantly in the detail coefficients, allowing the ANN to differentiate between normal and faulty operating conditions with higher accuracy. This integration of wavelet analysis and ANN classification forms the basis of many advanced fault diagnosis frameworks in the literature [57].

Beyond diagnostics, ANNs have also been successfully applied to real-time converter control, forming what is commonly referred to as a Neural Network Controller (NNC). In this role, the ANN replaces or supplements traditional controllers

such as PI, PID, or sliding-mode controllers by generating control actions based on learned system behaviour [58]. This approach offers substantial performance advantages in nonlinear and time-varying systems. For example, in a DAB converter where current ripple, phase-shift modulation, and bidirectional power flow create dynamic operating conditions, an ANN controller can adaptively produce optimal switching commands without requiring continuous retuning of controller parameters.

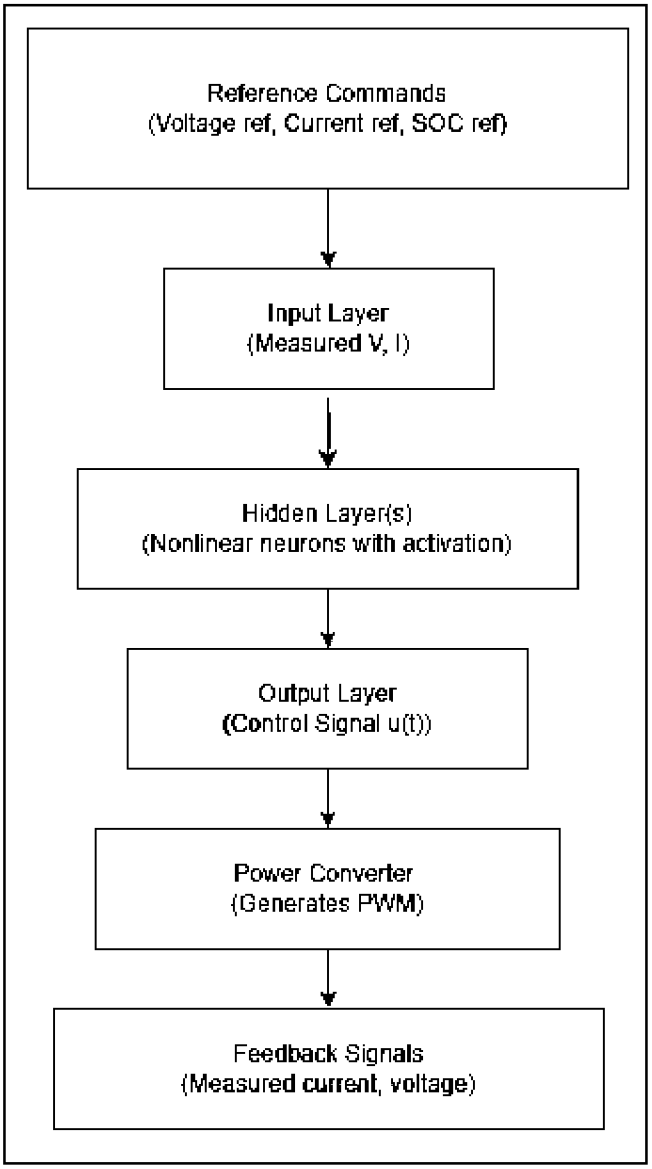

Figure 2.2 ANN as Network Controller

Figure 2.2 illustrates the general structure of an ANN when applied as a network controller. The process begins with reference commands that specify desired operating conditions such as voltage, current, or state-of-charge setpoints. These are combined with real-time measurements from the converter typically voltage and current and

supplied to the ANN as input features [59]. Through one or more hidden layers of nonlinear neurons, the ANN learns the mapping between input conditions and the required control action. The output layer then produces a control signal, such as a modulation index or phase-shift angle, which governs the switching behaviour of the DAB converter [60]. The resulting converter output is fed back to the ANN, forming a closed-loop system that supports continuous adaptation, error correction, and stable control performance. This structure highlights one of the key advantages of ANN-based controllers: their ability to provide intelligent, data-driven, and adaptive responses under dynamic or nonlinear operating conditions [61].

Despite their advantages, ANN-based systems also introduce certain challenges. Their performance depends heavily on data quality, proper network architecture design, and effective training. Poorly trained networks risk overfitting or poor generalisation. In addition, deploying ANN controllers in real hardware requires attention to computation time, sampling rates, and embedded implementation constraints [62]. Nevertheless, as power electronic systems evolve toward higher efficiency and reliability demands, ANN-based fault detection and control strategies continue to gain prominence.

Overall, the integration of ANNs in power electronics especially when combined with wavelet-based feature extraction represents a significant step toward intelligent, self-adaptive, and fault-resilient converter systems [63]. Their ability to interpret non-stationary electrical waveforms, classify fault behaviours, and generate dynamic control actions makes them highly suitable for DAB converters operating under demanding conditions. As the energy sector transitions toward smarter and more autonomous systems, ANN-enhanced methods are expected to play an increasingly central role in ensuring converter stability, reliability, and long-term operational performance.

2.3 Fault-Tolerant in Power Electronic

Fault-tolerant control (FTC) has become an essential design consideration in modern power electronic systems due to the increasing demand for reliability, safety, and uninterrupted operation [64]. Power converters, especially those employed in energy storage systems, electric vehicles, and DC microgrids, continuously operate under high switching frequencies, elevated temperatures, and dynamic loading

conditions. These harsh environments make converters particularly susceptible to semiconductor device failures, most commonly open-circuit and short-circuit faults in MOSFETs or IGBTs. In a system such as the DAB converter, where efficient bidirectional power transfer relies on precise switching behaviour, even a single switch fault can lead to severe performance degradation, excessive current stress, or complete system shutdown [65]. Therefore, incorporating an effective FTC mechanism is critical to ensure that the converter continues operating despite component failures.

In the broad landscape of FTC strategies, power electronics researchers generally categorize fault-tolerant designs into two major groups: Passive Fault-Tolerant Control (PFTC) and Active Fault-Tolerant Control (AFTC) [66], [67]. While each method offers unique advantages, their suitability depends on the converter topology, application domain, real-time requirements, and complexity constraints. Although both approaches have been extensively studied, the passive redundancy-based strategy is selected for this thesis due to its immediate response capability and compatibility with high-frequency DAB converters[68]. Nevertheless, a clear understanding of both approaches is necessary to contextualize the choice of PFTC within current research trends.

2.3.1 Comprehensive Analysis of Fault-Tolerant Control (FTC) Strategies in Modern Power Electronics

As power electronic systems advance toward higher power density, faster switching frequencies, and more compact designs, the need for robust FTC becomes increasingly important. Modern applications place stringent requirements on reliability, uptime, and safety. Semiconductor devices such as SiC and GaN switches operate closer to their thermal and electrical limits, making them more susceptible to ageing, stress-related failures, and unexpected faults. Consequently, FTC strategies must not only detect faults quickly but also ensure that the converter can continue operating without significant degradation.

FTC approaches in power electronics can be broadly classified into model-based, signal-based, hardware-based, and intelligence-based strategies. Model-based techniques rely on mathematical representations of converter dynamics, detecting faults when measured variables diverge from predicted behaviour [69]. Signal-based methods analyse the characteristics of electrical waveforms to identify abnormal patterns

associated with faults. Hardware-based approaches incorporate redundant components or robust design features that allow the converter to withstand predefined faults without active reconfiguration. Intelligence-based approaches employ AI and machine learning algorithms for fault detection, diagnosis, and sometimes corrective action.

As converters become more complex and operate under nonlinear switching patterns, hybrid FTC frameworks that combine multiple techniques are becoming more widely adopted. For example, wavelet-based feature extraction (signal-based) combined with ANN classification (intelligence-based) provides powerful diagnostic capability, while redundancy (hardware-based) ensures immediate response and uninterrupted operation. This layered approach aligns with trends in modern power electronics, which increasingly integrate intelligent diagnostics with robust hardware solutions for enhanced system resilience.

2.3.2 Active Fault-Tolerant Control (AFTC)

Active Fault-Tolerant Control (AFTC) is an adaptive and intelligent strategy in which the system continuously monitors its operating conditions, detects faults in real time, and subsequently reconfigures its control mechanism to minimise the impact of the fault. Unlike passive approaches, AFTC depends heavily on online diagnostic processes that analyse system behaviour to identify abnormal patterns [70]. These diagnostic techniques may include observers, machine learning algorithms, parity checks, or parameter estimation methods. Once a fault is detected such as an open-circuit failure in a semiconductor switch the controller adjusts its control parameters or modifies the switching pattern to ensure that the converter continues to operate safely and efficiently.

The main advantage of AFTC lies in its adaptability. It is capable of accommodating a wide range of faults, including unexpected or evolving fault conditions, while maintaining system performance through real-time modifications. This adaptability makes AFTC highly suitable for intelligent power converters and applications where uninterrupted operation is essential.

Despite its flexibility, AFTC also presents several limitations. It requires substantial computational resources to perform real-time fault diagnosis and control adjustments. Moreover, it depends on fast and accurate diagnostic algorithms and often requires additional sensors or feedback loops to provide sufficient data for analysis. The

resulting control structure is typically complex, which can introduce latency [71]. Such delays are particularly problematic in high-frequency converters like the DAB, where even small delays can cause current overshoots, voltage distortions, or further damage to the system. Due to these constraints, AFTC is discussed in this thesis for completeness within the literature but is not adopted in the proposed system.

2.3.3 Passive Fault-Tolerant Control (PFTC)

Passive Fault-Tolerant Control (PFTC) is widely regarded as one of the most practical and reliable approaches for ensuring continuous operation of power electronic converters during fault conditions [72]. Unlike Active Fault-Tolerant Control (AFTC), which depends on real-time diagnostic algorithms and adaptive controller reconfiguration, PFTC does not require any online decision-making during the occurrence of a fault. Instead, the system is designed in advance to tolerate specific fault scenarios using hardware-level measures or inherently robust control strategies [73]. This preconfigured approach makes PFTC highly suited for converters operating at high switching frequencies such as the DAB where any delay in fault compensation can result in significant current surges, waveform distortion, or even irreversible damage.

PFTC is grounded on the principle that reliability must be embedded into the converter's structure before faults occur [74]. This eliminates dependency on computational resources or diagnostic latency, enabling immediate fault compensation. From the literature, PFTC is commonly implemented through three core strategies: robust system design, component overrating, and redundancy. Each of these strategies contributes differently to overall system resilience, and together they form a comprehensive framework for high-reliability power electronic operation.

2.3.3.1 Robust System Design

Robust system design focuses on ensuring that the converter and its control algorithms can maintain stable performance even when faults or disturbances occur. In this strategy, converter parameters, modulation methods, and control structures are intentionally designed with additional tolerance margins. Such design practices may include using modulation techniques that remain functional despite partial device failures, adopting conservative control tuning that maintains system stability even under

degraded conditions, and incorporating current-balancing or voltage-limiting mechanisms that prevent cascading failures [75]. While robust design alone cannot fully compensate for severe switching faults, it strengthens the system's inherent ability to cope with unexpected variations and reduces sensitivity to minor disturbances. This layer of robustness forms an essential foundation for overall fault tolerance.

2.3.3.2 Component Overrating

A second strategy frequently seen in PFTC is the overrating of components. Semiconductor devices, capacitors, inductors, and magnetic components are often selected with voltage, current, and thermal ratings that exceed the expected operating conditions. By providing surplus electrical and thermal capacity, overrated components are less likely to experience catastrophic failure during transient surges or periods of elevated stress. This approach is especially relevant for converters used in safety-critical or harsh environments where reliability must be prioritised. Although overrating inevitably increases material cost and may lead to a slightly larger converter footprint, the enhanced durability and failure resistance it provides can significantly extend system lifespan. In many applications, this trade-off is justified by the substantial reduction in the likelihood of interruption during critical system operation.

2.3.3.3 Redundancy

Among all PFTC strategies, redundancy stands out as the most effective for high-speed switching converters such as the DAB. Redundancy-based PFTC introduces an additional set of backup switches or hardware paths that remain inactive during normal operation but immediately take over when a primary switch fails [76]. This ensures uninterrupted current flow, prevents distortion in the converter's switching sequence, and maintains stable output despite the presence of faults [77]. The instantaneous nature of redundancy is its most significant advantage. Because the corrective action occurs at the hardware level, the converter does not depend on diagnostic algorithms, real-time computation, or control reconfiguration [78]. This eliminates the delays commonly associated with AFTC and makes redundancy ideal for converters where precise and continuous switching is critical.

Redundancy also enhances the predictability and robustness of the system. Since the backup switch is already integrated into the circuit and ready to activate, the overall behaviour of the converter under fault conditions becomes highly deterministic. This contrasts with adaptive control methods, where fault responses may vary depending on algorithmic accuracy, sensor quality, or computational load [79]. In DAB converters, maintaining steady power transfer and avoiding transformer saturation are paramount; the immediate substitution provided by redundancy preserves these operational requirements without compromising performance or safety.

In the context of this thesis, redundancy-based PFTC is the selected strategy due to its suitability for managing open-circuit switch faults in the DAB converter. To complement this hardware-level resilience, an ANN is employed to detect and classify switch faults using wavelet-extracted features. While redundancy alone is sufficient to keep the converter operational during a fault, the integration of ANN-based detection provides valuable diagnostic insight, enabling precise identification of the faulty switch and supporting maintenance decisions. This hybrid structure offers both immediate fault mitigation through PFTC and intelligent fault awareness through AI-based classification.

2.3.4 Advantages and Limitations of Choosing Redundancy as a Fault-Tolerant Strategy

Redundancy is one of the most dependable strategies for achieving fault tolerance, especially in systems where reliability and continuous operation are critical like in power electronics, energy converters, aerospace equipment, or industrial automation. The core idea is simple which is by having backup components ready to take over, the system can keep running smoothly even if something fails [80]. There's no need to wait for diagnostic routines or reconfiguration just an instant switch to a standby path.

This quick response is one of redundancy's biggest advantages. In fast switching systems like DAB converters, even a brief delay during a fault can cause serious problems power surges, voltage spikes, or damage to sensitive parts. Redundancy helps avoid these issues by reacting immediately [81], [82]. It's also predictable and reliable. Unlike software-driven fault-tolerant methods that might make wrong decisions or take

time to compute a solution, redundancy systems are pre-engineered to kick in the moment a fault is detected, with no room for misclassification or delay.

Another plus is the positive impact on component longevity. In some designs, the primary and backup systems share the load. This reduces stress on any single part, which can help prevent wear and tear and extend the system's life. Some architectures even allow faulty parts to be swapped out without shutting the system down this is a big advantage when continuous uptime matters.

In short, redundancy offers speed, simplicity, and strong reliability, which makes it a great fit for systems like DAB converters. But it comes with trade-offs cost, space, energy, and passive use of backup components that need to be carefully weighed when deciding whether it's the right strategy for a given application [83].

2.3.5 Justification for Choosing the Redundancy Technique

In the context of bidirectional DC-DC converters like DAB, fault tolerance is vital for maintaining system reliability and continuous power flow, especially in high performance applications such as EV charging and energy storage. Among various fault-handling approaches, the redundancy-based technique was selected for this work due to its rapid response, minimal system disruption, and hardware compatibility.

Unlike reconfiguration-based strategies or software-dependent control algorithms, redundancy enables immediate response to critical faults such as open-circuit failures in power switches without requiring complex real-time diagnostics or computational overhead [84]. This is especially relevant for DAB converters, where even brief interruptions in switching can lead to current imbalances, voltage distortion, and potential transformer saturation. By employing backup switches that can instantly take over when faults are detected, redundancy ensures continuous power delivery with no need for system reconfiguration.

This technique aligns seamlessly with the ANN-based detection and classification system proposed in this thesis. While the ANN quickly identifies faulty switches using wavelet-transformed current signatures, the redundancy mechanism ensures that backup hardware seamlessly maintains system operation [85]. This synergy between intelligent fault detection and immediate hardware recovery eliminates downtime and protects other system components from damage.

Moreover, redundancy simplifies system design by avoiding the need for adaptive reprogramming or predictive analytics, making it easier to implement in real time, hardware intensive environments [86]. It also enhances safety and long-term reliability by avoiding the risks of misdiagnosis and delays associated with software-based fault recovery methods.

In summary, the redundancy-based method complements the goals of this thesis by offering a robust, low-latency solution for fault handling in DAB converters allowing intelligent detection through ANN while ensuring uninterrupted operation through hardware-level fault mitigation.\

CHAPTER 3
RESEARCH METHODOLOGY

3.1 Introduction

This chapter explains the step-by-step approach used to develop and test a fault-tolerant DAB converter with a built-in redundancy mechanism. The goal of this methodology is to design, simulate, and evaluate a system that can continue operating smoothly even when faults occur. The main parts of the approach include system modelling, building the fault-tolerant features, setting up simulations, and evaluating the system's performance.

It starts by introducing the DAB converter's basic structure and how it operates, followed by an explanation of how faults especially open-circuit faults in power switches are modelled. Then, it describes the redundancy mechanism, which involves switching to backup components during a fault, including how and when the backup system kicks in and how it helps the system recover.

To test everything, the design is simulated using MATLAB. The chapter also discusses the current control strategy and highlights how intelligent fault detection is integrated using wavelet-based signal processing and artificial neural networks (ANNs). These tools help the system predict and respond to faults effectively.

The system is evaluated using performance indicators like efficiency, response time, and how quickly it recovers from a fault. One of the key strengths of the proposed method is that it can detect and react to faults in under 0.1 seconds, helping prevent major disruptions. The redundancy system ensures that power transfer remains stable, with minimal voltage or current issues. By combining smart fault detection with a fast backup strategy, the proposed DAB converter proves to be robust, efficient, and well-suited for modern bidirectional power systems.

3.2 Research Workflow

This section outlines the research workflow for designing a bidirectional fault-tolerant DAB converter topology. The workflow is structured into four key phases: Phase 1: Research study, Phase 2: Software design and simulation of DAB, Phase 3: Faulty switch verification and control strategy and Phase 4: Analysis and reporting.

Phase 1: Research Study

The research begins with an extensive literature review to understand bidirectional power conversion, fault-tolerant topologies, and control strategies for DAB converters. This phase focuses on defining the problem statement, research objectives, and technical requirements. A comparative analysis of existing fault detection and recovery methods is conducted to identify the research gaps and establish a clear framework for the proposed system design.

Phase 2: Software Design and Simulation of DAB

This phase involves the modelling and simulation of the DAB converter system using MATLAB/Simulink. This includes implementing circuit models, applying control strategies such as current control with PI regulation, simulating fault conditions like open-circuit switch failures, and analysing power transfer efficiency, voltage regulation, and system stability. The simulation results provide critical insights into system behaviour, allowing necessary refinements to optimize performance. This phase ensures that the design meets the project requirements before proceeding to hardware validation and fault detection strategies.

Phase 3: Faulty switch verification and control strategy

This phase is dedicated to detecting and verifying faulty switches using advanced signal processing techniques. Wavelet decomposition is applied to current waveforms to extract key features that characterize different fault conditions. The extracted data is then used to train an Artificial Neural Network (ANN), enabling accurate classification and identification of faulty switches. The verification process involves simulating multiple fault conditions, extracting fault signatures, classifying faults using ANN-based detection, and validating the system's detection accuracy. Redundant switching mechanisms are implemented to facilitate seamless fault recovery,

and the system is tested under various operational scenarios to assess its reliability and overall efficiency.

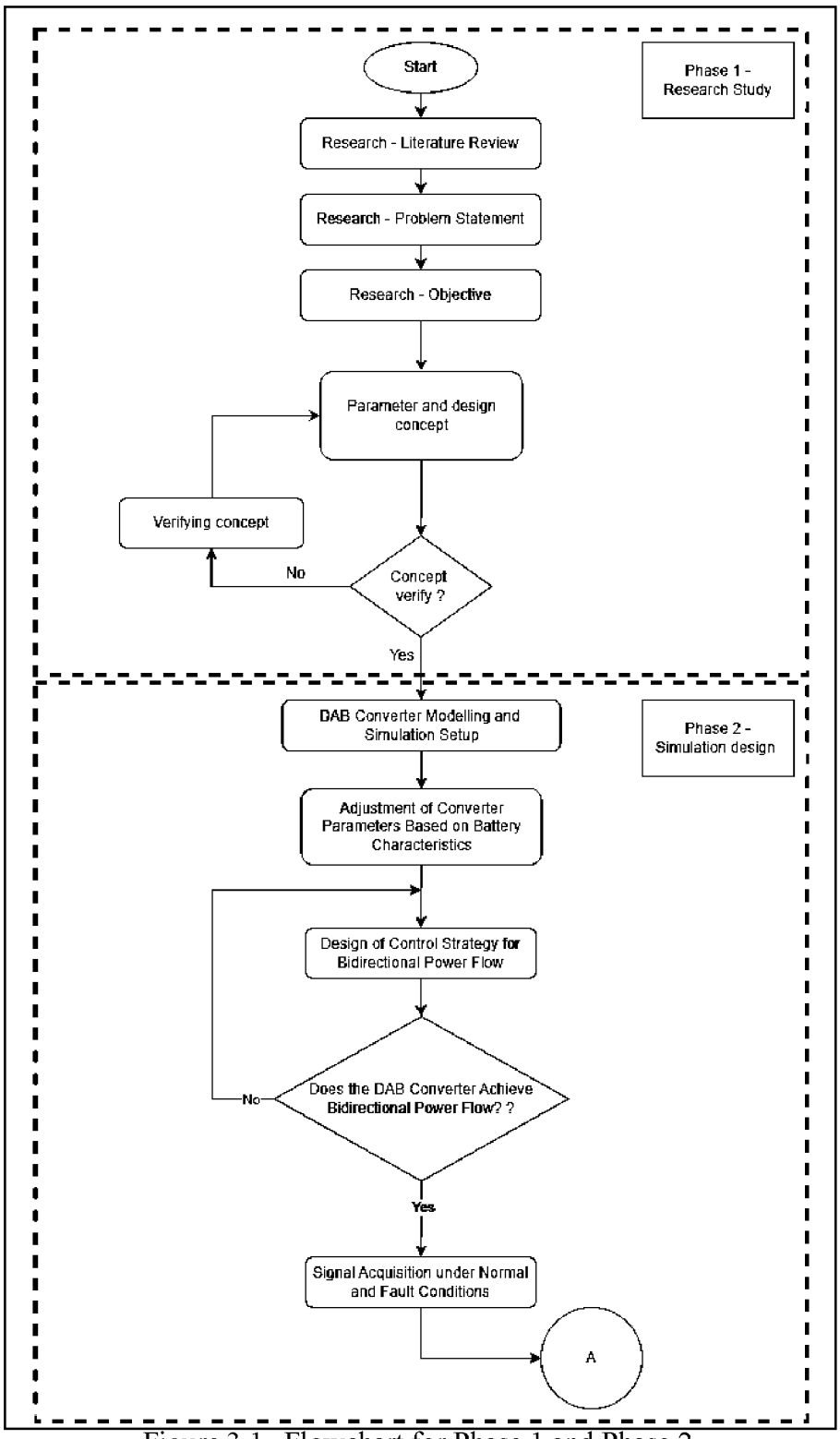

Figure 3.1 Flowchart for Phase 1 and Phase 2.

In Phase 2, the DAB converter is modelled and simulated, and its parameters are adjusted according to the battery characteristics to enable realistic bidirectional power transfer. A suitable control strategy is then designed and tested to ensure stable bidirectional operation. Once correct bidirectional power flow is achieved, the converter undergoes faulty switch diagnosis, followed by wavelet-based feature extraction.

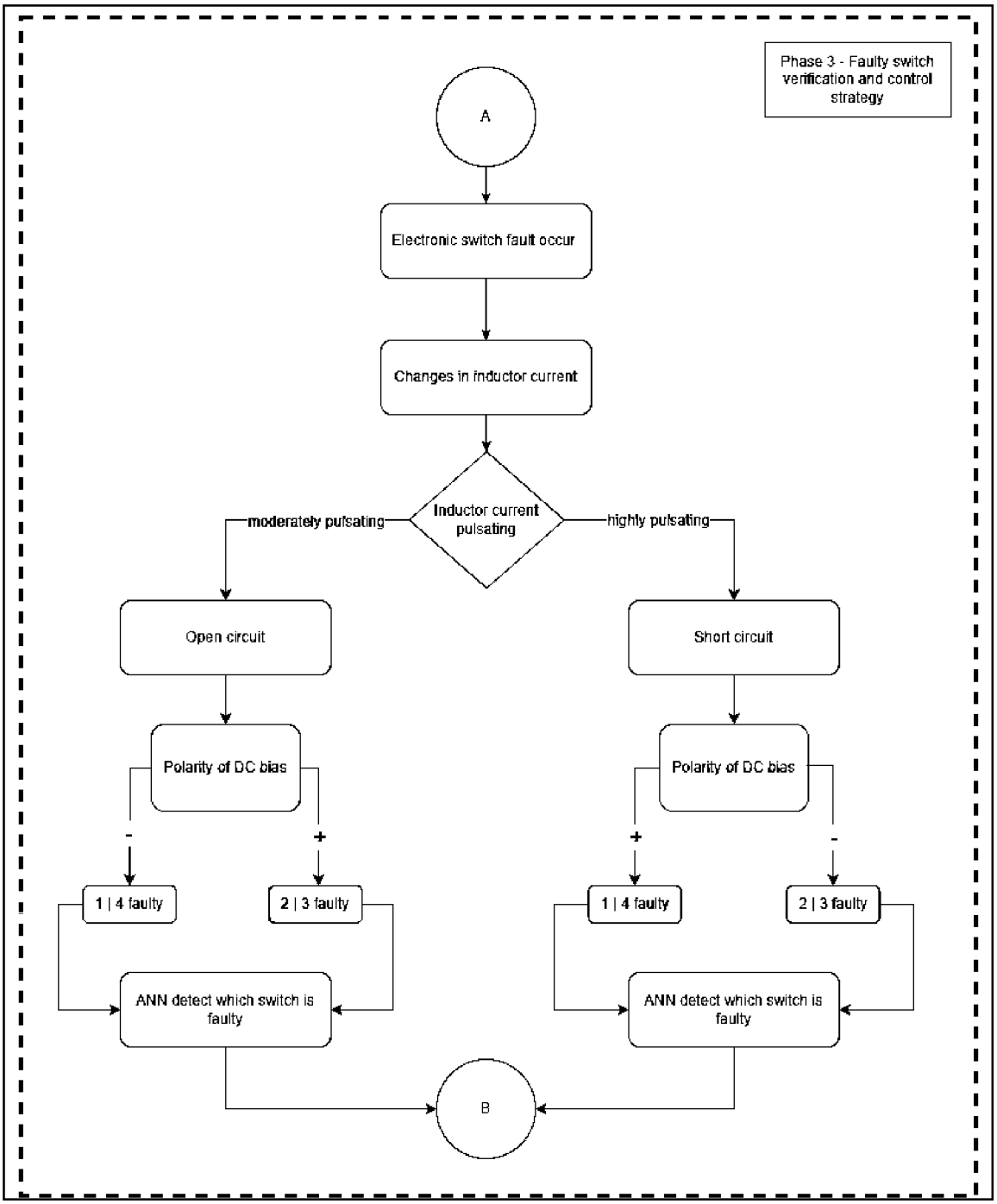

Figure 3.2 Flowchart for Phase 3.

The flowchart in Figure 3.2 illustrates the faulty switch diagnosis process in Phase 3. After normal operation, an electronic switch fault is introduced, which causes changes in the inductor current. These changes indicate abnormal converter behaviour. Based on the current characteristics and extracted signal features, the ANN is used to identify the type of fault and determine which switch is faulty before proceeding to the fault-tolerant control stage.

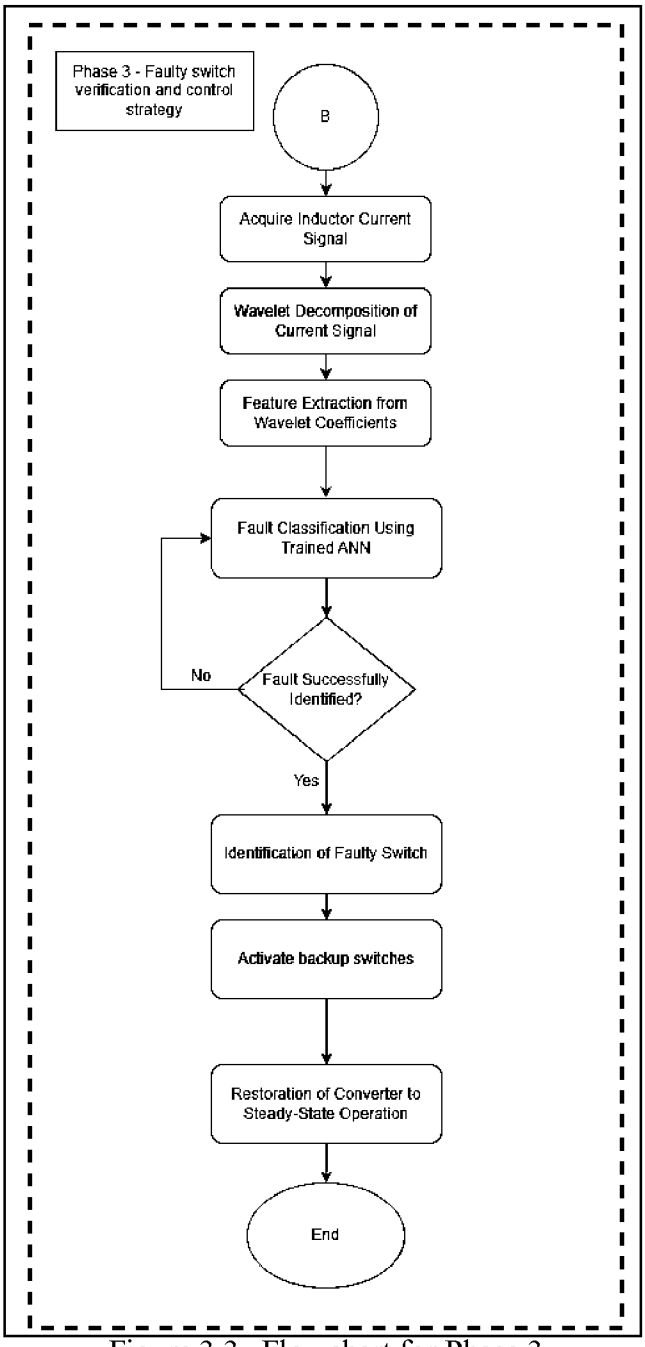

Figure 3.3 Flowchart for Phase 3

Flowchart in Figure 3.3 shows the fault diagnosis and fault-tolerant control process after current signals are collected. The measured current signal is analysed using wavelet decomposition to extract relevant features. These features are then classified using a trained ANN to identify the fault condition and determine the faulty switch. Once the fault is confirmed, the redundant switch is activated as part of the passive fault-tolerant control strategy, and the system is restored to steady-state operation.

3.3 Research Framework

The research framework focused on the design of bidirectional fault tolerant dual active bridge converter topology, highlighting the problem statement, objectives, methodology and outcomes.

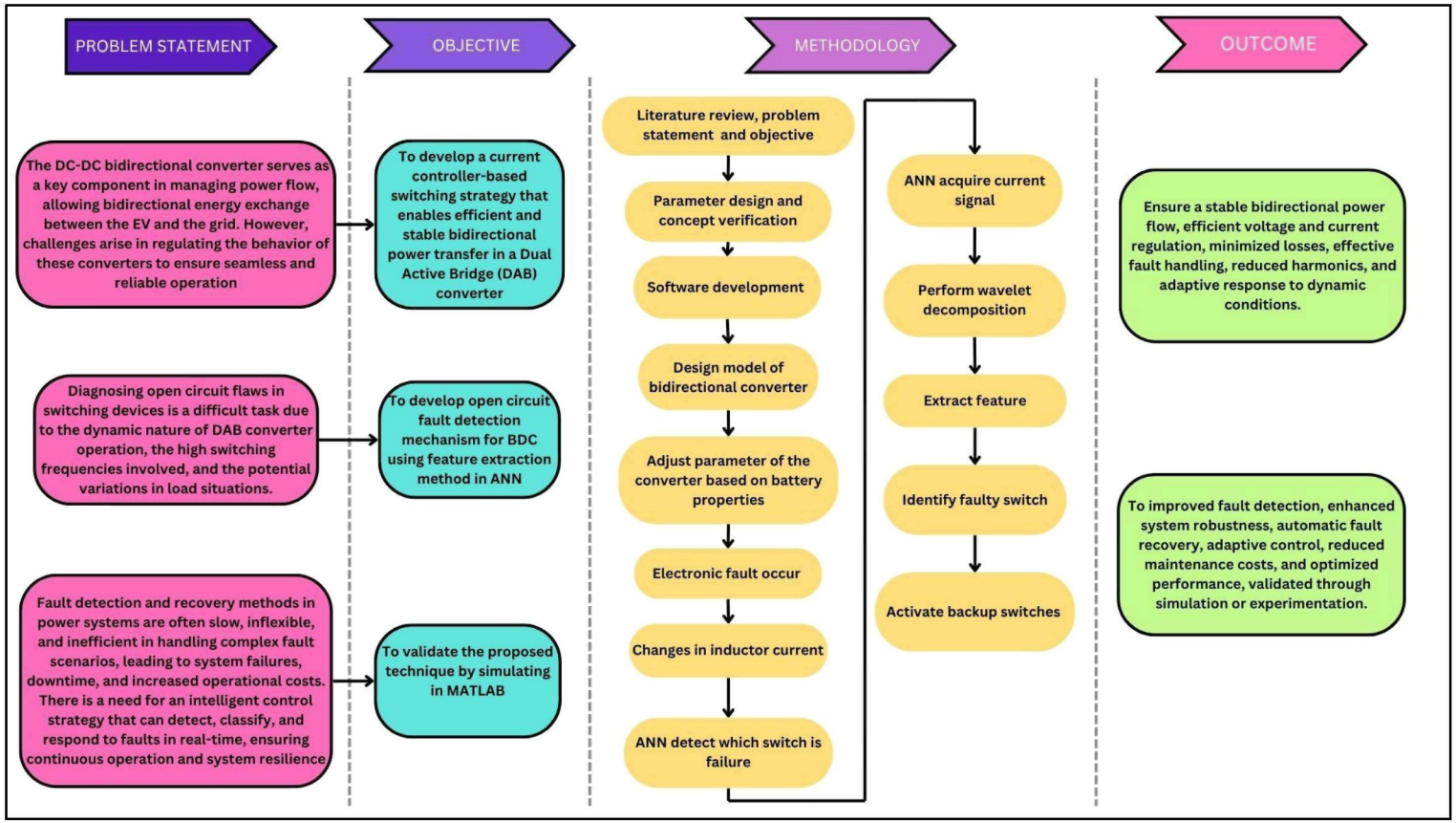

3.4 Development and Design of DAB Converter

3.4.1 Theoretical Equation of DAB converter

Inductor Current Dynamics

The describes the fundamental voltage-current relationship governing the inductor current (i_L) in the DAB converter. This equation is derived from Faraday's Law of Induction, which states that the rate of change of current through an inductor is proportional to the applied voltage across it.

$$L_s \frac{di_L}{dt} = V_p - V_s \tag{3.1}$$

where:

- represents the series inductance of the transformer, which includes both the leakage inductance and any intentionally added inductance in the circuit,
- is the rate of change of current through the inductor over time,
- is the voltage applied by the primary-side H-bridge,
- is the voltage at the secondary-side H-bridge, which is reflected across the transformer.

Power Transfer with current control

With current feedback control, the power transfer equation becomes;

$$P = V_p I_{ref} \tag{3.2}$$

where:

- is the reference current set by the controller,
- is the power transferred from the primary to secondary.

Power Relationship in the Converter System

The following equations define the relationship between input and output power in the system. Equation (3.3) represents the input power (Pin) as the product of the input voltage (Vin) and input current (Iin):

$$P_{in} = V_{in} I_{in} \tag{3.3}$$

Similarly, the output power (Pout) is defined as the product of the output voltage current (Iout), as shown in Equation (3.4):

$$P_{out} = V_{out} I_{out} \tag{3.4}$$

Alternatively, the output power can also be expressed in terms of the load resistance (R) as given in Equation (3.5):

$$P_{out} = \frac{V_{out}^2}{R} \tag{3.5}$$

Transformer Turn Ratio and Voltage Transfer Ratio

The transformer turn ratio (K) is a key parameter in determining voltage and current transformation between the primary and secondary sides of the converter. This ratio, given in Equation (3.4), is the proportion of the number of turns in the primary coil (Np) to the number of turns in the secondary coil (Ns):

$$K = \frac{N_p}{N_s} \tag{3.6}$$

Additionally, the voltage transfer ratio (m) is used to evaluate the power transfer efficiency in DAB converters. As expressed in Equation (3.7), it is the ratio of the output voltage (Vout) to the product of the transformer turn ratio (n) and input voltage (Vin):

$$m = \frac{V_{out}}{nV_{in}} \tag{3.7}$$

Switching Frequency and System Efficiency

To The switching frequency (fs) is an essential parameter influencing the operating speed, stability, and reliability of the converter. It is defined as the inverse of the switching period (T), as shown in Equation (3.8):

$$f_s = \frac{1}{T} \tag{3.8}$$

The efficiency (η) of the system is a crucial performance indicator. It represents the ratio of output power (Pout) to input power (Pin), as expressed in Equation (3.9):

$$\eta = \frac{P_{out}}{P_{in}} \tag{3.9}$$

Efficiency metric determines how effectively the system converts input energy into usable output, with a higher efficiency value indicating improved performance and reduced power losses.

3.4.1.1 Proposed DAB Topology

The designed DAB converter circuit consists of two active full-bridge circuits, one on the primary side and another on the secondary side, connected via a high-frequency transformer. Unlike conventional DAB designs that rely on phase shift modulation, this design utilizes current control to regulate power flow, ensuring precise bidirectional energy transfer. This method provides enhanced controllability and improved fault tolerance, making it suitable for applications that require stable current regulation.

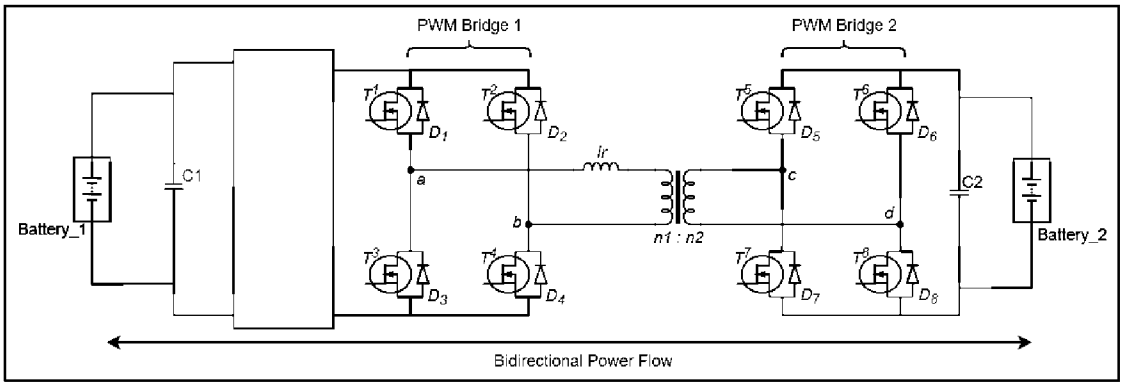

Figure 3.4 Proposed topology for DAB converter

The circuit design of DAB converter as shown in Figure 3.4 above is a bidirectional DC-DC power conversion topology designed to facilitate efficient energy transfer between two battery storage units. This topology consists of two active full bridges, one on the primary side and another on the secondary side, connected through a high-frequency transformer. Unlike conventional DAB converters that rely on phase shift modulation to control power flow, this design employs current control, which provides more precise regulation over energy transfer. The ability to manage power flow based on current makes this design particularly advantageous for applications requiring stable power exchange, such as electric vehicle (EV) charging stations, microgrids, and renewable energy storage systems.

Table 3.1
Parameter for DAB design in simulation

Parameters	Value
Input Voltage (V)	100V – 600V
Output Voltage (V)	100V – 400V
Switching Frequency (Hz)	300e3
n1:n2	1:1 (Ideal Transformer)
Input Capacitor	330e-6
Output Capacitor	660e-6
Rated battery for both side	100Ah

The table presents the main design parameters of the proposed DAB converter used in this study. It summarises the selected voltage ranges, switching frequency, transformer ratio, and DC-link component values that define the operating conditions of the converter. These parameters are chosen to support stable bidirectional power

transfer between two battery systems and to provide a suitable platform for fault analysis and control evaluation.

The primary side of the converter is powered by *Battery_1*, which serves as the initial energy source. A filter capacitor (C1) is placed at the input to stabilize the DC voltage by smoothing out any fluctuations that may arise due to variations in the battery's output. The first full-bridge circuit (PWM Bridge 1), consisting of four power switches (T^1, T^2, T^3, and T^4) along with their corresponding diodes (D_1, D_2, D_3, and D_4), converts the DC voltage into high-frequency AC. Unlike conventional DAB designs that regulate power using phase shifts between bridges, this system regulates power flow based on current control strategies. This approach allows for more accurate regulation of current levels, ensuring smooth energy transfer while minimizing switching losses and component stress.

The high-frequency transformer plays a crucial role in power transfer and electrical isolation between the two battery banks. It ensures that the energy transferred from the primary side is effectively converted to the appropriate voltage level required by the secondary side. Additionally, the leakage inductance (*Ir*) of the transformer acts as an energy buffer, improving soft-switching conditions and enhancing overall efficiency. The transformer turns ratio (*n1:n2*) determines the voltage scaling between the two sides, allowing the system to adapt to different battery voltage levels.

On the secondary side, the second full-bridge circuit (PWM Bridge 2), which consists of four power switches (T^5, T^6, T^7, and T^8) and their corresponding diodes (D_5, D_6, D_7, and D_8), functions as a rectifier or inverter, depending on the direction of power flow. If power is being transferred from Battery_1 to Battery_2, the secondary bridge rectifies the high-frequency AC back into DC, ensuring that Battery_2 is charged efficiently. Conversely, if power needs to flow from Battery_2 back to Battery_1, the secondary bridge inverts the DC power into high-frequency AC, which is then transferred through the transformer and converted back into DC by PWM Bridge 1 on the primary side. This bidirectional energy transfer capability makes the DAB converter particularly suitable for applications such as vehicle-to-grid (V2G) and grid-to-vehicle (G2V) charging, where EVs can act as energy storage units that supply power back to the grid when needed.

A filter capacitor (C2) is placed at the output of the secondary bridge to smooth the rectified DC voltage, minimizing ripples and ensuring that Battery_2 receives a stable voltage. The system's current control mechanism ensures that power transfer

remains stable under varying load conditions, preventing excessive current surges that could damage the components. Unlike phase-shift control, which primarily manipulates voltage waveforms, current control offers a more robust mechanism by directly regulating power flow based on real-time current feedback. This enhances the overall system reliability and allows for better fault tolerance, especially in scenarios where sudden changes in battery voltage or load conditions occur.

3.4.1.2 Operation Mode for Bidirectional

The operation mode is essential for managing the bidirectional energy transfer between Battery 1 and Battery 2, ensuring efficient charging and discharging processes.

a) Charging Battery_2

Charging Battery_2 involves transferring energy from Battery_1 to Battery_2 through a bidirectional converter operating in buck mode. This process is particularly useful during power shortages or peak demand periods, serving as a backup power source. The converter steps down the voltage from 600V in Battery_1 to 400V, which is required by Battery_2. By ensuring continuous power availability, this operation enhances system resilience and overall reliability.

b) Charging Battery_1

Charging Battery_1 is using a bidirectional converter in boost mode. This mode is crucial when Battery 1 needs recharging or when the external power supply is insufficient. In this configuration, the converter steps up the voltage from 400 V in Battery_2 to 600 V for Battery_1. This operation maximizes energy utilization, stabilizes power distribution, and ensures system efficiency under varying power demands.

3.4.2 Experimental Assessment of Converter Efficiency

Table 3.1 presents the operating parameter ranges and testing conditions used to evaluate the power efficiency of the converter. The study examines efficiency across three critical parameters: output power, output voltage, and switching frequency. The output power is assessed within the range of 5 kW to 45 kW, where the output voltage

remains constant at 400 V, while the output current is varied between 10 A and 40 A. Similarly, to evaluate efficiency under different voltage levels, the output voltage is adjusted from 100 V to 450 V, while maintaining a constant output current of 40 A, which is regulated by the PI controller. Furthermore, the impact of switching frequency on power efficiency is analysed by varying the frequency from 10 kHz to 300 kHz, with the output voltage and current fixed at 400 V and 40 A, respectively. These evaluations provide a comprehensive insight into the system's efficiency performance under varying operating conditions.

Table 3.2
Operating Parameter Ranges and Testing Conditions for Power Efficiency

Parameters	Range	Details
Output Voltage	100 V – 450V	To analyse power efficiency under varying voltage conditions, the output voltage is incrementally increased from 100 V to 450 V, while the output current is regulated at 40 A through PI controller feedback.
Output Power	5 kW – 45 kW	The efficiency of the system is examined by adjusting the output current between 10 A and 40 A while keeping the output voltage constant at 400 V. This allows the evaluation of power efficiency across different power levels.
Switching Frequency	10 kHz – 300 kHz	The impact of switching frequency on power efficiency is investigated by varying the frequency from 10 kHz to 300 kHz while ensuring a fixed output voltage of 400 V and an output current of 40 A.

3.4.4 Controller Design

3.4.2.1 Pi Controller for DAB

In this study, the proposed bidirectional power flow control for the DAB converter is realized using a Proportional-Integral (PI) controller with current feedback. Unlike conventional voltage-mode controllers, this method directly manipulates the current reference to control the direction and magnitude of power flow between the Battery_1 and the Battery_2. The system dynamically responds to changes in current demand, enabling seamless transitions between charging and discharging modes.

Figures 3.5 and 3.6 present the bidirectional current control strategy used in the DAB converter, with each figure serving a distinct but complementary purpose. Both figures are based on the same control principle, namely the regulation of power flow using a current reference signal, and both employ current feedback to achieve stable bidirectional operation. However, the level of detail and the focus of each figure are different.

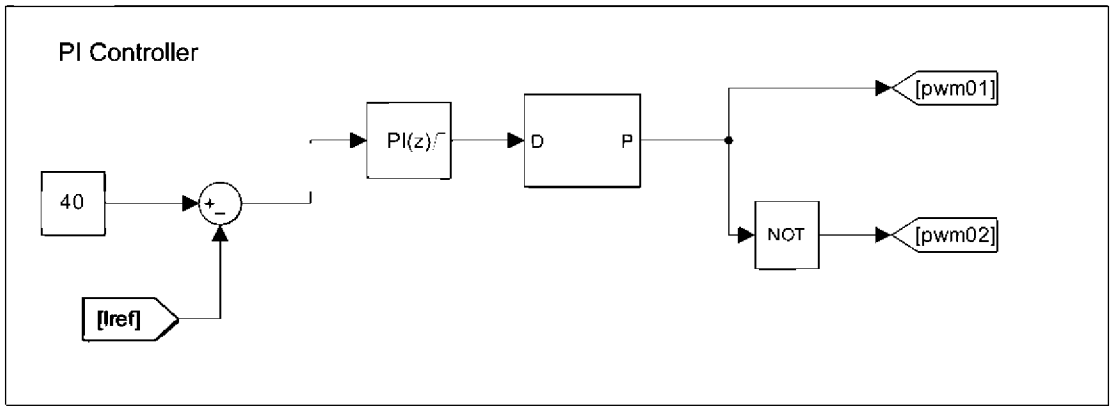

Figure 3.5 Mode 1 – Reference Current Charging Battery_2 for PWM control.

Figure 3.5 illustrates the conceptual control principle of bidirectional operation. It shows how the direction of power flow is determined by the sign of the reference current. A positive reference current commands power transfer in one direction, while a negative reference current commands power transfer in the opposite direction. This figure does not show the internal controller structure or PWM generation logic; instead, it provides a high-level view of how bidirectional power flow can be achieved using a single current reference without changing the converter topology or control mode.

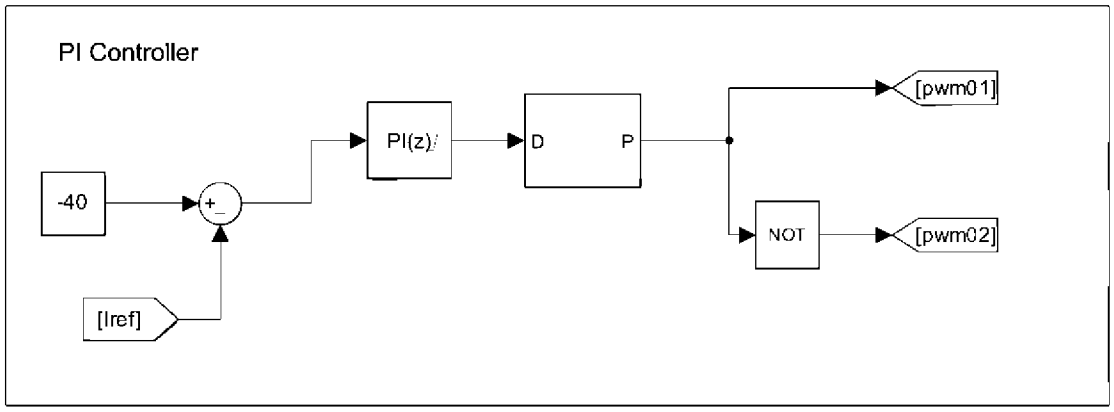

Figure 3.6 Mode 2 – Reference Current discharging Battery_2 for PWM control.

In contrast, Figure 3.6 shows the detailed implementation of the same current control concept. While the fundamental principle remains the same as in Figure 3.5, this figure explicitly illustrates how the reference current is compared with the measured inductor current to generate an error signal, which is then processed by a Proportional–Integral (PI) controller. The figure further demonstrates how the output of the PI controller is used to generate complementary PWM signals. The polarity of the PI output determines which PWM signal is activated, thereby controlling the direction of power flow. This detailed representation explains how the conceptual idea shown in Figure 3.5 is practically realised in the DAB converter control system.

In summary, Figures 3.5 and 3.6 are closely related and describe the same bidirectional current control strategy, but at different levels of abstraction. Figure 3.5 provides a simplified overview of the control concept based on the sign of the reference current, while Figure 3.6 presents the complete PI-based control structure used to implement this concept in practice. Together, these figures clarify both the operating principle and the practical execution of bidirectional current control in the proposed DAB converter.

By using a signed current reference, the controller simplifies the interface for managing power direction while providing precise current regulation. This enhances the converter's responsiveness, especially during mode transitions, and ensures effective power balancing between the battery and the storage system. The current-feedback PI control approach is particularly well-suited for DAB converters in EV applications, where reliable and efficient bidirectional energy flow is critical.

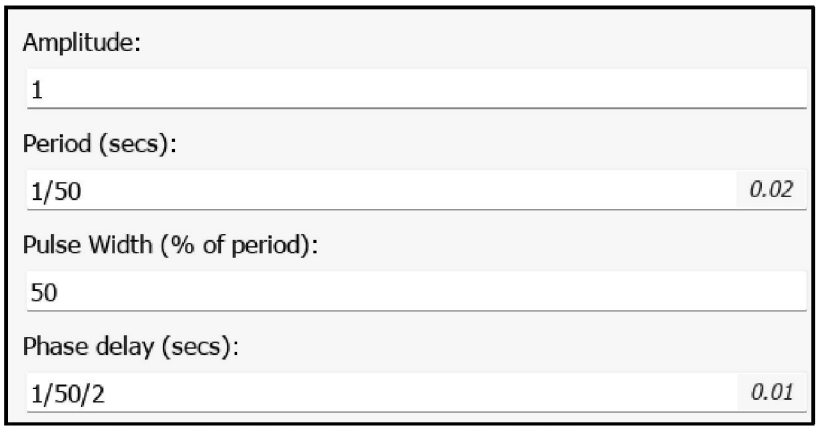

Figure 3.7 Pulse Generator for DAB converter.

Figure 3.7 above illustrates the parameter settings of the pulse generator used to control the switching operation of the DAB converter. The pulse generator produces square wave signals required to drive the high-frequency switches in both the primary and secondary bridges of the converter. The amplitude is set to 1, indicating a binary output that toggles between logic levels 0 and 1, suitable for gating power semiconductor devices. The period is configured as 1/50 seconds, corresponding to a switching frequency of 50 Hz. A 50% pulse width ensures that the ON and OFF durations of the square wave are equal, resulting in a symmetrical waveform. Furthermore, a phase delay of 1/50 divided by 2 is applied to introduce a 180-degree phase shift between the gate signals of the two bridges. This phase shift is a fundamental mechanism for enabling and controlling power transfer across the high-frequency transformer, where the direction and magnitude of power flow are modulated based on the relative timing between the input and output waveforms.

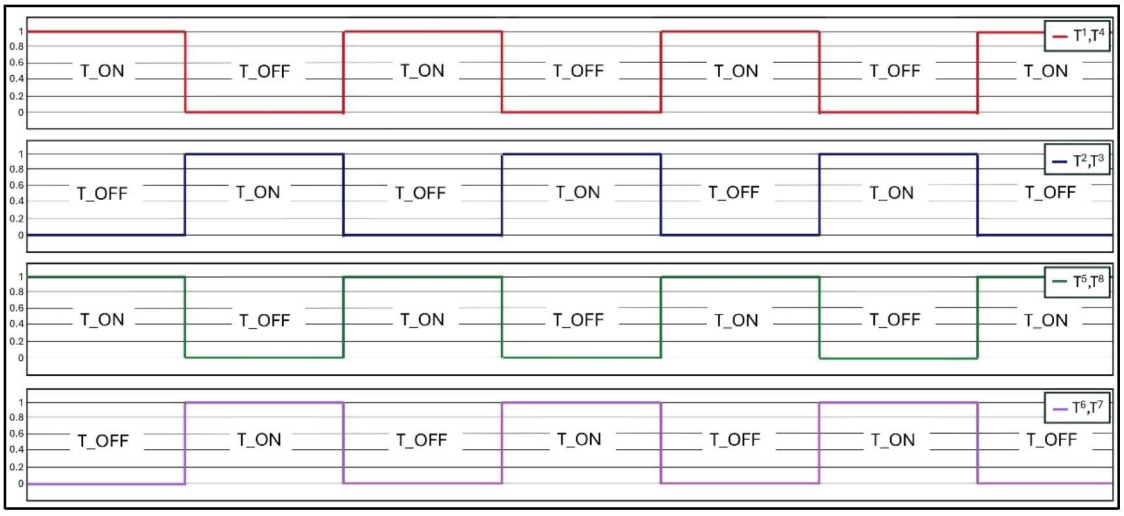

Figure 3.8 Typical waveform for DAB converter.

Figure 3.8 shows the typical switching waveform of the DAB converter used in this study. Unlike conventional DAB systems that rely on phase-shift modulation to control power flow, the system implemented here uses current feedback control via a Proportional-Integral (PI) controller. As such, no intentional phase shift is introduced between the switching signals of the primary and secondary bridges. Instead, the direction and magnitude of power flow are governed by the reference current value, which is processed through the PI controller to generate appropriate gating signals.

The waveform above illustrates the ON and OFF states of the switches (T_ON and T_OFF) across different converter legs. Each switch operates with a fixed 50% duty cycle, creating a symmetrical square wave for both bridges. The switching signals are complementary within each leg, ensuring proper full-bridge operation. The PI controller determines which set of switches (either pwm1 or pwm2) is activated based on the sign of the current reference: a positive reference current triggers discharging mode, while a negative reference initiate charging mode. The NOT gate ensures that the two switching signals remain logically inverted, maintaining safe and consistent switching behaviour.

This current-based control approach simplifies the modulation strategy while still enabling precise bidirectional power flow. The switching waveforms remain consistent in structure regardless of power direction, with the control logic determining the active path through real-time current regulation. This ensures stable and efficient operation of the DAB converter without the need for phase-shifted control, making it well-suited for applications requiring direct and responsive current control, such as battery energy management in electric vehicle systems.

3.4.2.2 Pi Controller Tuning using Ziegler-Nichols Method

Tuning a Proportional-Integral (PI) controller is a crucial step to ensure that a control system achieves optimal performance, stability, and responsiveness [87]. One of the most widely adopted methods for tuning controller parameters is the Ziegler-Nichols closed-loop method, an empirical technique based on the system's dynamic behaviour. The process begins by configuring the controller in a proportional-only mode, temporarily disabling the integral component. The proportional gain (KP) is then gradually increased until the system output begins to exhibit sustained and stable oscillations. The value of the gain at this point is known as the ultimate gain (Ku), and the time period of the oscillations is referred to as the ultimate period (Tu). These two

parameters are then used to calculate the final PI controller settings using the standard Ziegler-Nichols tuning formulas:

$$K_p = 0.45 \times K_u \tag{3.10}$$

$$T_i = \frac{T_u}{1.2} \tag{3.11}$$

$$K_i = \frac{K_p}{T_i} \tag{3.12}$$

This method offers a practical and effective approach to tuning, particularly when a precise mathematical model of the system is not available. By applying these tuning rules, the controller can be adjusted to ensure fast transient response while minimizing steady-state error, making it ideal for applications such as battery current regulation.

3.4.4 Faulty Switches

Faulty switches are a critical consideration in the design of fault-tolerant power converters, particularly in applications where uninterrupted operation is essential. In the context of the proposed DAB converter, switch faults specifically open-circuit conditions are among the most common and impactful failure modes. These faults may arise due to aging, thermal stress, manufacturing defects, or transient overvoltage, resulting in the permanent disconnection of one or more switches within the full-bridge circuits.

To simulate the effects of such faults, predefined fault scenarios are injected into the switching elements in the primary and secondary full bridges of the converter. An open-circuit fault is modelled by forcing a specific switch to remain permanently off, thereby disrupting the conduction path and altering the current flow through the converter. This disruption affects the energy transfer process and may lead to unbalanced voltages, increased current stress on adjacent components, and degraded power quality.

3.4.2.3 Scenario 1 – fault at T^1

In this study, one of the critical fault scenarios considered is the open-circuit failure at switch T^1, located in the upper left leg of the primary-side full-bridge of the DAB converter, as shown in Figure 3.9. This type of fault occurs when T^1 is permanently unable to conduct due to gate drive failure. Although T^1 is no longer active, its anti-parallel freewheeling diode D_1 remains functional and can conduct when forward biased, allowing partial current continuity during specific intervals of the switching cycle. However, since T^1 cannot actively switch, the primary-side bridge becomes unbalanced, and the converter loses full control over the voltage waveform applied across the transformer.

Under normal operation, switches T^1 and T^4 operate in a complementary manner to create a positive current path through the transformer, enabling balanced bidirectional power transfer. In the faulty condition, with T^1 open circuit, this active path is broken. As a result, current can only flow through D_1 when it is forward-biased, and even then, only during limited intervals dictated by the inductor's stored energy. This forces the system into an asymmetric conduction pattern, where current flow is restricted and primarily favours one direction.

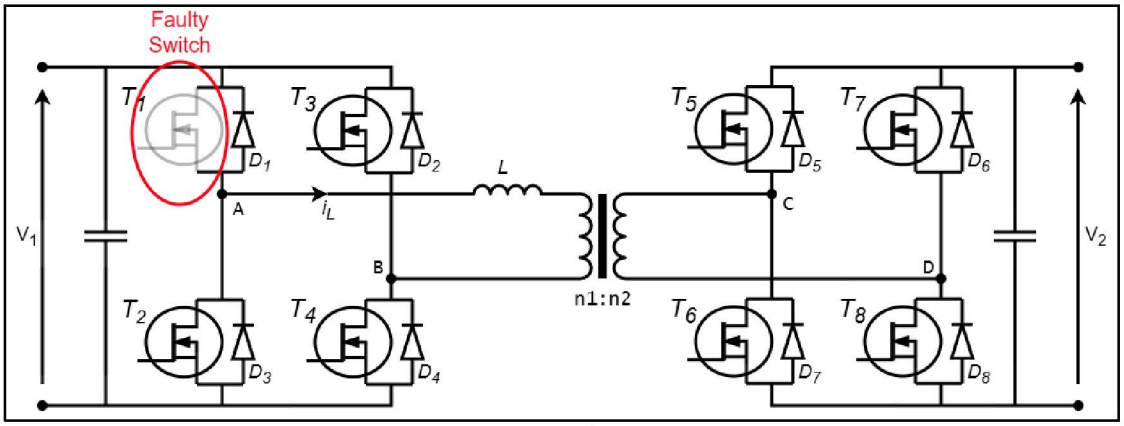

Figure 3.9 Faulty switch at T^1 for typical DAB converter.

Under It is also important to recognize that a fault occurring at T^4 the switch diagonally opposite T^1 in the full-bridge configuration would lead to a similar system response. Since T^1 and T^4 together form one of the two key current conduction paths across the transformer during the positive transfer cycle, an open-circuit fault at either switch disrupts the same power delivery phase. Both result in an unbalanced bridge, asymmetric current waveforms and increased DC bias in the inductor current. Due to the structural and operational symmetry of the full-bridge converter, the effects of a T^4

fault closely mirror those of a T^1 fault. Therefore, in this study, the analysis is limited to the T^1 fault scenario, with the understanding that a fault at T^4 would yield nearly identical behaviour and conclusions. The impact of this behaviour is clearly reflected in the waveform shown in Figure 3.10, where the inductor current exhibits a noticeable negative bias. This indicates that the system is no longer achieving balanced current oscillations between the primary and secondary sides. The missing positive half-cycles, previously supported by T^1, are no longer effectively formed, resulting in an accumulation of negative current. This DC bias increases the risk of core saturation in the transformer, degrades overall power quality, and leads to elevated current stress on the remaining switches. Additionally, the lack of proper switching by T^1 disrupts soft-switching conditions like ZVS, causing higher switching losses and efficiency degradation.

Although the freewheeling diode provides a limited alternative path for current, the system's ability to regulate current direction and magnitude is severely compromised. These changes in current flow and waveform symmetry highlight the significant consequences of a single switch failure and establish the necessity for precise fault detection and mitigation strategies, which are addressed in the following sections.

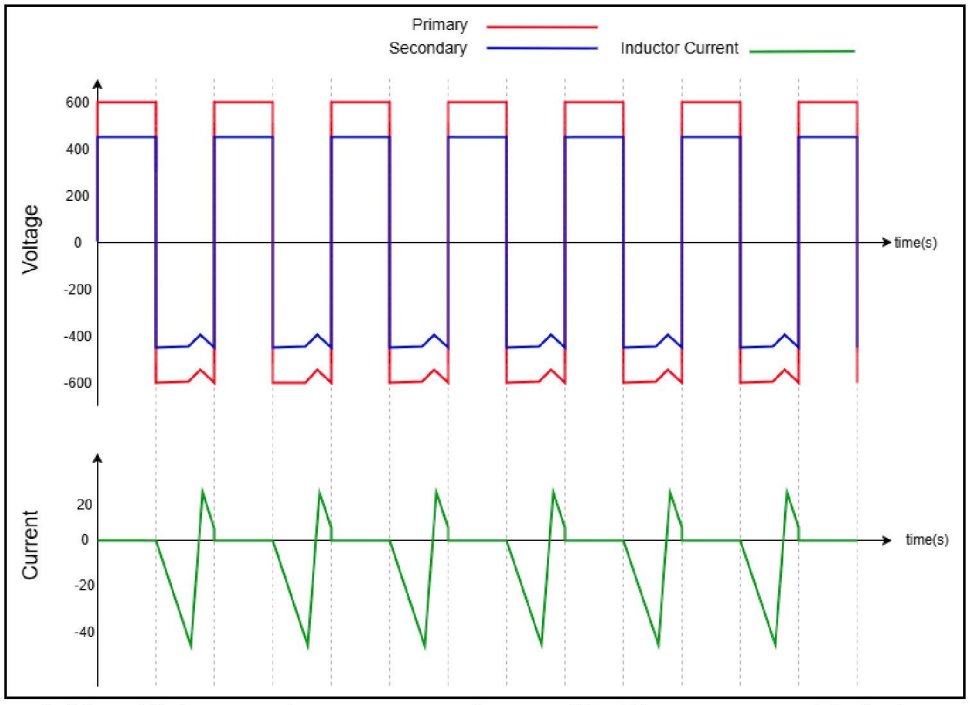

Figure 3.10 Voltage and current waveforms of DAB converter with faulty switch T^1

Figure 3.10 presents the inductor current and voltage waveforms over an extended simulation period under an open-circuit fault at T^1. The current becomes increasingly negative over time, confirming that the loss of active switching on the

upper-left leg results in asymmetric energy transfer. This causes transformer flux imbalance and risks core saturation. The current waveform no longer oscillates around zero but drifts downward, indicating that energy contribution from the positive half-cycle is insufficient to counterbalance the negative side. This emphasizes the impact of T^1's failure on system behaviour and underlines the need for effective fault detection and mitigation strategies.

3.4.2.4 Scenario 2 – fault at T^2

In Scenario 2, the DAB converter is analysed under an open-circuit fault condition at switch T^2, located in the upper-right leg of the primary-side full-bridge, as illustrated in Figure 3.11. Under standard operation, T^2 cooperates with T^3 to generate the negative half-cycle of the AC voltage applied across the primary of the high-frequency transformer. This switching pattern is essential to establish symmetrical bidirectional power transfer. When T^2 is subjected to an open-circuit fault, such as due to gate signal failure or internal device damage, it becomes permanently non-conductive. As a result, T^2 is unable to participate in the required switching operation, and its intended conduction path is effectively removed from the bridge topology.

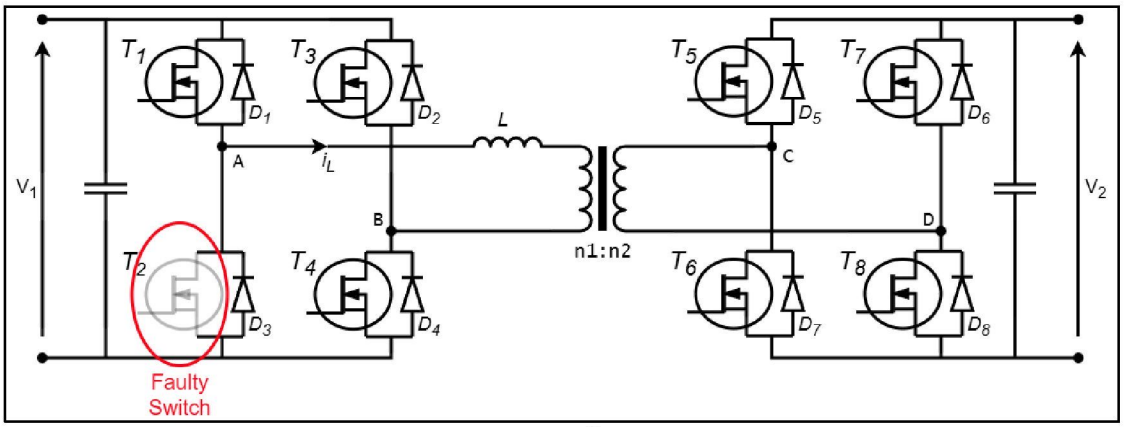

Figure 3.11 Faulty switch at T^2 for typical DAB converter.

The absence of T^2's switching capability prevents the formation of a complete conduction path during the negative half cycle. Specifically, during the interval where T^2 and T^3 are expected to conduct simultaneously to apply a negative voltage across the transformer primary, current is unable to flow through the upper right leg. The switching device cannot allow conduction in the intended direction without a control signal, and no alternative path exists to support this current flow. As a result, the voltage across the transformer becomes asymmetrical only the positive half-cycles, generated by the

remaining functional switches T^1 and T^4, are fully realized. This leads to an imbalance in energy transfer, as energy is delivered to the load during the positive interval but not equally extracted during the negative interval.

It should be noted that a fault occurring at T^3, the switch located diagonally opposite T^2 in the bridge configuration that causing a nearly identical disturbance in system behaviour. Since T^2 and T^3 form the switching pair responsible for generating the negative voltage across the transformer, an open-circuit failure at either switch breaks the same conduction path. As such, both faults lead to the loss of the negative half-cycle, positive biasing of the inductor current, risk of core saturation, and degraded efficiency due to poor soft-switching conditions. Given this functional symmetry, the analysis of the T^3 fault is omitted from this study, as its impact is analogous to that of the T^2 fault discussed in this scenario.

The effects of this fault are clearly observed in the illustrated waveform presented in Figure 3.12. While the primary and secondary voltages retain a nominal square-wave profile, the current waveform tells a different story. The inductor current becomes positively biased, repeatedly ramping up during each switching cycle with limited reversal. This behaviour confirms that energy is accumulating in the system due to the functional positive side switching and the absence of energy extraction during the faulty negative half-cycle. The current fails to return to a balanced oscillation around zero, and instead, each cycle begins at a higher baseline.

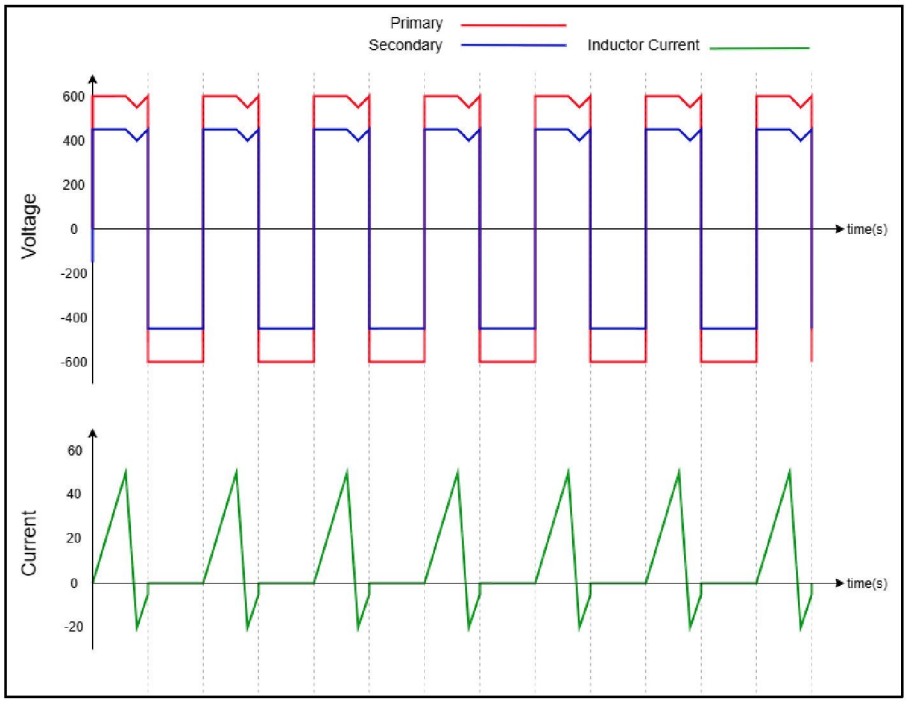

Figure 3.12 Voltage and current waveforms of DAB converter with faulty switch T^2

Such asymmetrical current behaviour introduces the risk of magnetic saturation in the transformer core, especially under continuous operation. Additionally, the unbalanced current flow leads to increased thermal and electrical stress on the remaining active switches, particularly T^1 and T^4, which now operate with higher conduction demands. These conditions also hinder soft-switching performance, reducing system efficiency and increasing switching losses. This scenario underscores the critical dependence of the DAB topology on synchronized and complete full-bridge operation. It also highlights the need for effective real-time monitoring and fault isolation strategies to prevent long-term damage and to maintain stable and efficient converter performance under fault conditions.

3.4.2.5 Scenario 3 – fault at T^5

In this scenario, the DAB converter is analysed under an open-circuit fault condition at switch T^5, located in the upper-left leg of the secondary-side full-bridge, as shown in the schematic diagram. Under normal operation, T^5 works in coordination with T^8 to apply a positive voltage across the secondary winding of the high-frequency transformer, facilitating symmetrical bidirectional power transfer. This switching pair is crucial for forming one half of the secondary-side conduction cycle. However, when

T^5 experiences an open-circuit fault due to internal device failure or a gate drive issue it becomes permanently non-conductive. As a result, the corresponding switching leg is disabled, and T^5 can no longer contribute to voltage generation, which immediately disrupts the converter's balance and operation.

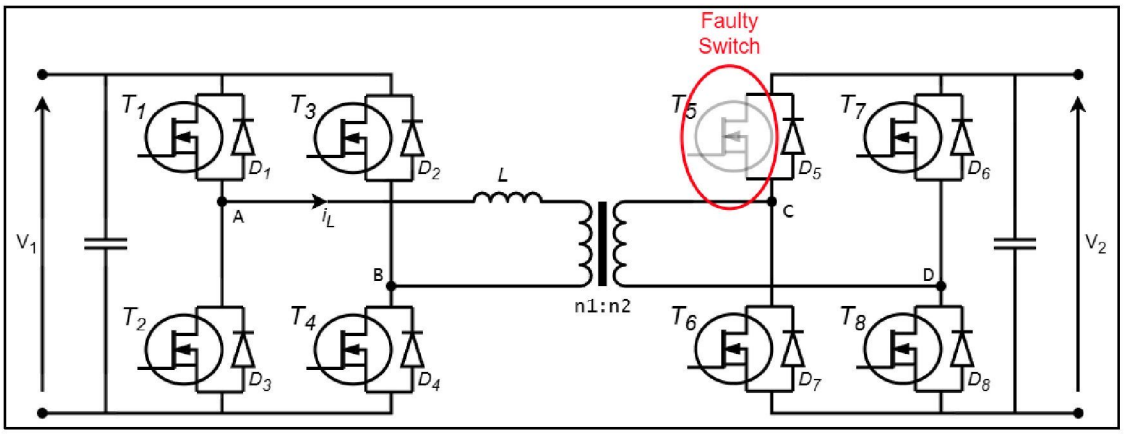

Figure 3.13 Faulty switch at T^5 for typical DAB converter

The loss of T^5 prevents the formation of a complete conduction path during the positive half cycle on the secondary side. During intervals when T^5 and T^8 are expected to conduct and transfer energy to the load, current is unable to flow through the upper-left leg of the bridge. Without a replacement path, the converter fails to establish the correct voltage polarity across the secondary side of the transformer. Consequently, only the negative half cycles formed by the remaining operational switches T^6 and T^7 are fully realized, while the positive half-cycles are partially or entirely missing. This leads to unbalanced energy transfer and degrades the symmetrical operation essential for stable and efficient DAB performance.

The impact of the T^5 fault is clear in the simulation waveform, where the inductor current becomes increasingly negatively biased over time. Like faults at T^1 and T^4 on the primary side, this behaviour indicates that energy is transferred during only one half of the switching cycle. The resulting current imbalance causes the inductor waveform to drift away from its nominal zero centred oscillation, significantly increasing the risk of magnetic core saturation, especially during extended operation. Additionally, the unidirectional current flow places increased thermal and electrical stress on the remaining active switches, particularly T^6 and T^7, which must compensate for the missing half cycle of conduction.

A distinct feature in the T^5 fault waveform is the slight fluctuation observed in the voltage signal at the beginning of the simulation a phenomenon less apparent in the T^1 fault case. This early irregularity is likely caused by transient conditions as the

system stabilizes after the sudden loss of T^5. During this period, the current control loop may still operate as if all switches are functional, leading to temporary switching attempts or diode conduction. These effects may be further amplified by the reverse recovery of diode D_5 and the influence of parasitic inductance and capacitance in the secondary circuit. Although the steady state waveform under a T^5 fault closely mirrors that of a T^1 fault, these initial voltage fluctuations highlight the unique transient characteristics of secondary side faults and emphasize the importance of robust detection and mitigation strategies for both converter bridges.

3.4.2.6 Scenario 4 – fault at T^6

The schematic highlights a fault at switch T^6, which is located in the upper-right leg of the secondary side full bridge of the DAB converter. Under normal conditions, T^6 works in coordination with T^7 to apply a negative voltage across the secondary winding of the high-frequency transformer, enabling the converter to deliver energy to the load during the negative half-cycle. However, when T^6 experiences an open-circuit fault due to a gate signal failure or internal device damage, it becomes permanently non-conductive. This prevents the formation of the required conduction path for the negative half-cycle, disrupting the converter's ability to sustain symmetrical bidirectional energy transfer.

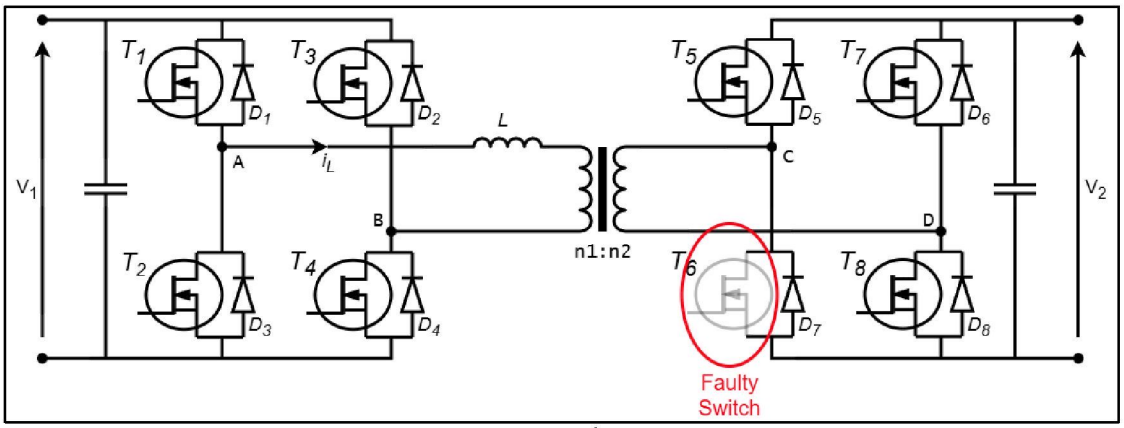

Figure 3.14 Faulty switch at T^6 for typical DAB converter.

This waveform behaviour is almost identical to the fault at T^2 on the primary side, where one half cycle is also missing due to a broken conduction path. As a result, current accumulates in the positive direction, shifting the inductor current away from its usual zero centred oscillation. This imbalance increases the risk of magnetic core saturation, particularly under prolonged operation, and places significant thermal and

electrical stress on the remaining functional switches especially T^5 and T^8, which are now responsible for the majority of energy conduction.

Similar to the behaviour observed during a fault at T^5, the waveform of the T^6 fault shows a slight fluctuation or irregularity in the voltage at the beginning of the simulation. This early voltage ripple likely arises due to transient conditions as the system attempts to stabilize following the sudden loss of T^6. During this brief period, the current control algorithm may not yet recognize the fault, resulting in unintended switching activity or brief conduction through freewheeling diodes, such as D_6, which may attempt to carry the current when T^6 fails to conduct. These fluctuations can also be influenced by parasitic inductance and capacitance on the secondary side, along with diode reverse recovery effects, creating short-lived voltage disturbances until the system reaches a new, degraded steady state.

In summary, a fault at T^6 causes the same core effect as a T^2 fault, as both switches form part of a corresponding leg in their respective full-bridges and support the same half-cycle of transformer current. The inductor current becomes unidirectional and biased, reflecting an imbalance in energy delivery. Although the overall waveform characteristics under the T^6 fault mirror those seen in T^2 and T^5 faults, the initial voltage disturbances are unique to the secondary side and underscore the importance of careful fault monitoring, detection, and compensation. This reinforces the DAB converter's sensitivity to faults on either bridge and the need for robust protection schemes that account for both steady-state and transient responses.

3.5 ANN-Based Fault-Tolerant Control Strategy

3.5.1 ANN Architecture

An ANN was developed as the core of the proposed fault-tolerant control strategy for the DC-DC bidirectional converter. Its primary role is to classify the system's operating conditions normal or faulty based on distinct features extracted from current waveforms [88]. This classification mechanism enables the system to identify specific open-circuit faults in the converter's switching devices and respond accordingly.

The ANN structure, illustrated in Figure 3.16, consists of three layers: an input layer with three neurons, a hidden layer with ten neurons, and a single output neuron.

This architecture was implemented using MATLAB's Neural Network Toolbox, specifically the (feedforwardnet) function. Each neuron in each layer is fully connected to the neurons in the subsequent layer, ensuring complete signal propagation and learning capability.

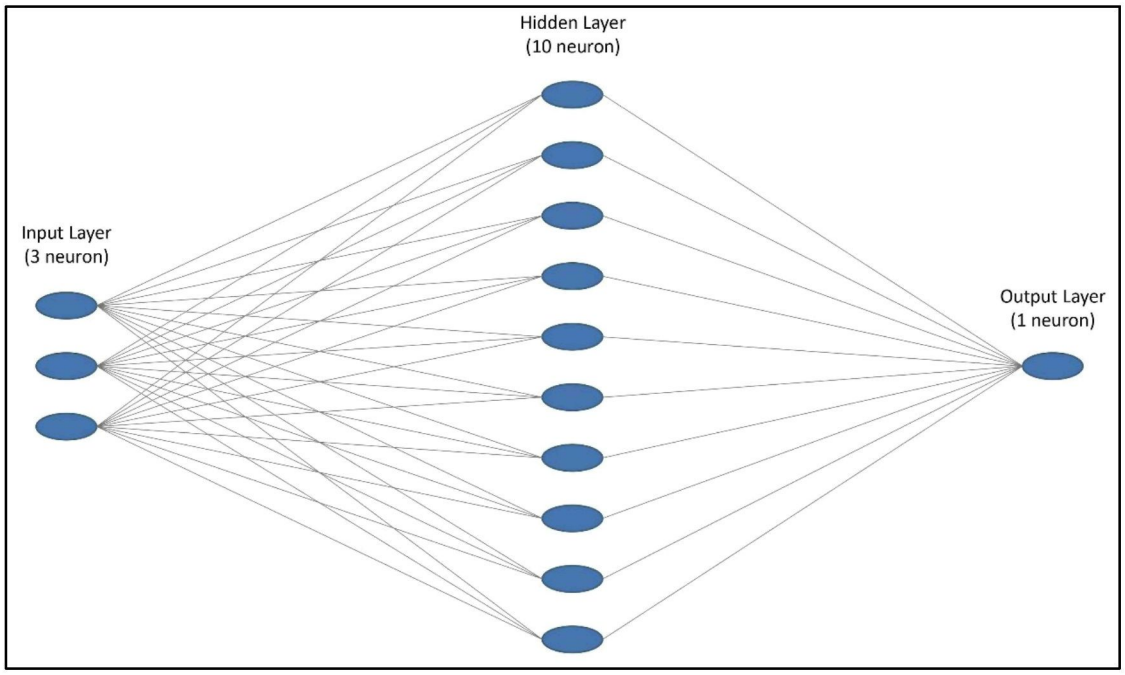

Figure 3.15 ANN Architechure

Rather than using raw current signals as input, a signal processing step was employed to extract meaningful features. The Discrete Wavelet Transform (DWT) with Daubechies 4 (db4) wavelet was applied to the current signals to analyse their time-frequency characteristics [89]. The energy values of the detail coefficients at levels 1, 2, and 3 (denoted as cD1, cD2, and cD3) were computed to represent the transient behaviours typically associated with switching faults. These three energy values form the input feature vector fed into the ANN.

The hidden layer applies a nonlinear activation function commonly (tansig), allowing the network to model complex relationships between input features and fault categories. The output layer contains a single neuron, which produces a scalar output corresponding to the detected operating condition. The output classes are defined as follows:

- 0 — Normal operation
- 1 — Fault at switch T^1

- 2 — Fault at switch T^2
- 5 — Fault at switch T^5
- 6 — Fault at switch T^6

This scalar classification approach simplifies the output structure, enabling straightforward interpretation and efficient implementation for real-time applications. The compact design also supports faster training and reduced computational load.

3.5.2 Reference Models for Performance Evaluation

To ensure a fair evaluation of the proposed Artificial Neural Network (ANN) model, two additional models were implemented for comparison: Multiple Linear Regression (MLR) and Support Vector Regression (SVR). MLR was chosen as a simple statistical baseline to evaluate linear relationships, while SVR was selected as a classical machine learning method capable of modelling non-linear relationships through kernel functions. Both models were trained and tested on the same dataset as the ANN, following identical preprocessing steps and evaluated using the same performance metrics.

3.5.3 Dataset Preparation and ANN Training

To train the ANN for fault classification, a dataset was constructed using current waveform data obtained through MATLAB simulations of the DC-DC bidirectional converter. The dataset includes five operating conditions: normal operation, and open-circuit faults at switches T^1, T^2, T^5, and T^6. These conditions represent common fault scenarios that affect the converter's switching devices and system behaviour.

Each current waveform was processed using the Discrete Wavelet Transform (DWT) to extract time-frequency domain features. Specifically, the Daubechies 4 (db4) wavelet was applied using MATLAB's (wavedec) function to perform a level-4 decomposition of the current signal. From the resulting decomposition, detail coefficients at levels 1, 2, and 3 were isolated using the (detcoef) function. The energy of each of these detail levels was calculated by summing the squares of the coefficients, capturing key transient behaviours within the waveform

The feature matrix and label vector were transposed and formatted to meet the input requirements of MATLAB's neural network functions. Training was conducted using MATLAB's (train) function, with the Levenberg–Marquardt (trainlm) backpropagation algorithm selected due to its efficiency and rapid convergence, particularly for small to medium-sized datasets.

The trained ANN model was designed to learn the mapping between the three wavelet energy features and the corresponding fault classes. It consists of an input layer with three neurons, a hidden layer with ten neurons, and a single output neuron producing a scalar value representing the class index. The key architectural and training settings used in the ANN development are summarized in Table 3.2.

Table 3.2
Training Configuration Summary

Parameters	Value
Network Type	Feedforward Neural Network (*feedforwardnet*)
Input Features	3 (Energy of cD1, cD2, cD3)
Hidden Layer	1 layer, 10 neurons
Output Later	1 neuron (scalar output class index)
Activation Functions	Hidden: *tansig*, Output: *purelin*
Training Function	*trainlm* (Levenberg-Marquardt)
Epochs	Default (early stopping enable)
Learning Rate	Adaptive control

Table 3.2 summarises the input features and output labels used for training and testing the ANN fault classification model. The ANN is designed to perform fault diagnosis by identifying the operating condition of the DAB converter based on extracted signal features.

The inputs to the ANN consist of three features, which are derived from the inductor current signal using discrete wavelet transform (DWT). Specifically, the energies of the detail coefficients at three decomposition levels, namely cD1, cD2, and cD3, are used as input features. These coefficients capture the transient and high-frequency characteristics of the current signal that are sensitive to switching faults. By

using wavelet-based energy features instead of raw signals, the ANN is able to distinguish fault conditions more effectively and with reduced sensitivity to noise.

The output of the ANN is a single scalar value, which represents the fault classification result. This scalar is used as an index to indicate the operating condition of the converter. A value of 0 corresponds to normal operation, while values of 1, 2, 5, and 6 represent open-circuit faults occurring at switches T1, T2, T5, and T6, respectively. This output encoding allows the ANN to identify both the presence of a fault and the specific faulty switch using a single output neuron.

To illustrate the data used, an example input output pair is as follows when the DAB converter operates under normal conditions, the extracted wavelet energies [cD1, cD2, cD3] may take values such as [0.12, 0.08, 0.05], and the corresponding ANN output is 0, indicating normal operation. In contrast, when an open-circuit fault occurs at switch T1, the wavelet energy features change significantly, for example to [0.35, 0.22, 0.18], and the ANN output becomes 1, indicating a fault at switch T1. Similar feature label relationships are established for faults at other switches.

3.5.4 Integration with Fault Detection Mechanism

Following training, the ANN was integrated into the converter model's control framework as a fault detection component. During converter operation, the system continuously monitors current waveforms. When fault detection is needed, the waveform is processed using the same wavelet-based feature extraction method. The extracted features are passed to the trained ANN using MATLAB's simulation interface. The ANN then outputs a numerical value that corresponds to the identified operating condition or fault type. While the scope of this methodology focuses on detection only, the ANN's output can be extended or connected to external control logic for handling fault-tolerant responses in future work.

CHAPTER 4
RESULTS AND DISCUSSION

4.1 Introduction

This chapter presents the simulation work carried out to test the performance of a fault-tolerant DAB converter under real-world energy flow conditions. The system was tested in two key modes: first, where Battery_1 charges Battery_2, and second, where Battery_2 discharges to power Battery_1. The simulation, done in MATLAB, confirmed that the DAB converter can transfer power smoothly in both directions, maintaining stable voltages and balanced current levels throughout. To handle potential faults, especially open-circuit faults in switches like T^1, T^2, T^5, and T^6 the system uses wavelet transform to break down the current waveforms and extract useful patterns. These patterns were then used to train an ANN to recognize faults quickly and accurately. The ANN model performed exceptionally well during training, reaching a very low error rate (1.43×10^{-15}) and stabilizing in just 6 training cycles (epochs). It was able to correctly detect and classify faults based on the wavelet features, and the system responded rapidly within 0.1 seconds by triggering a redundancy mechanism to restore normal operation. The simulation results clearly showed that the converter could return to stable and balanced performance immediately after a fault. This proves that the combination of wavelet-based signal processing and ANN intelligence offers a fast, reliable, and accurate way to detect faults and keep the converter running without interruption. Altogether, the results demonstrate that this approach makes the DAB converter much more resilient and suitable for modern energy systems like EV charging, renewable integration, and energy storage.

4.2 Simulation Development

4.2.1 Validation of Bidirectional Power Transfer in DAB Converter

4.2.1.1 Mode 1 – Charging of Battery_2

Figure 4.1 shows a clear and controlled energy transfer between Battery_1 and Battery_2 over a 10-second period. The State of Charge (SOC) for Battery_1 steadily drops from 50.00% to 48.90%, confirming it is discharging. At the same time, Battery_2 shows a steady SOC increase from 50.00% to 50.08%, indicating it is charging. This demonstrates a well-regulated, unidirectional energy flow from Battery_1 to Battery_2. The result effectively simulates scenarios like battery-to-battery (B2B) charging, energy balancing, or power sharing in a multi-battery system, where one battery supplies power while the other receives it.

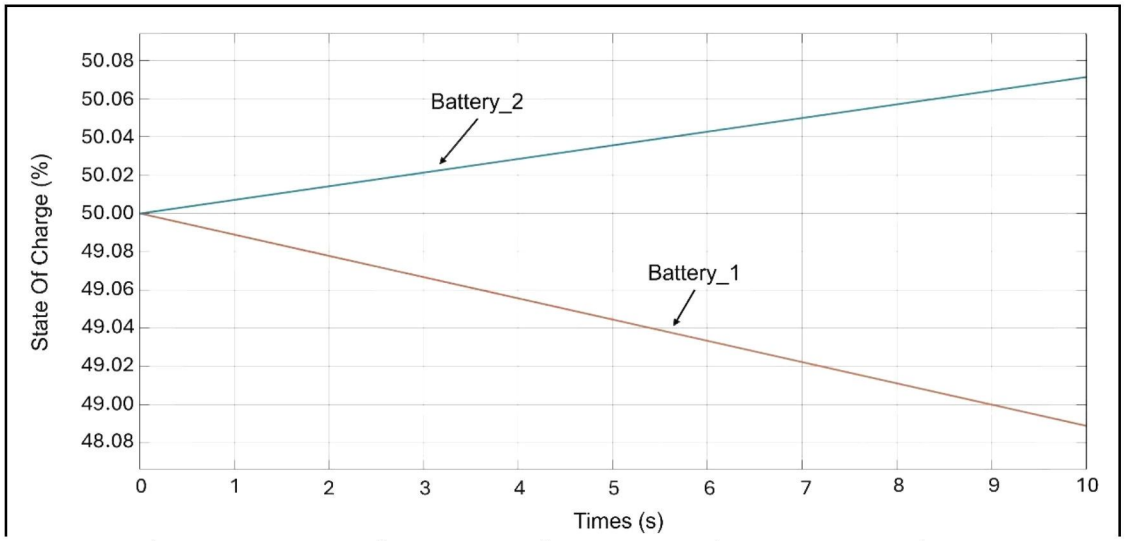

Figure 4.1 Mode 1 - SOC of Battery1 and Battery_2 vs Times.

Figure 4.2 shows the current flow between the two batteries during the energy transfer process. Battery_1 consistently outputs a positive current of 40 A, confirming it is discharging. In contrast, Battery_2 receives a steady negative current of –40 A, indicating it is charging. The current remains stable throughout the 10-second period, showing that the system maintains a balanced and controlled power exchange. This stability suggests that the current is being well-regulated, likely using a PI controller, with no major fluctuations or disturbances during the transfer.

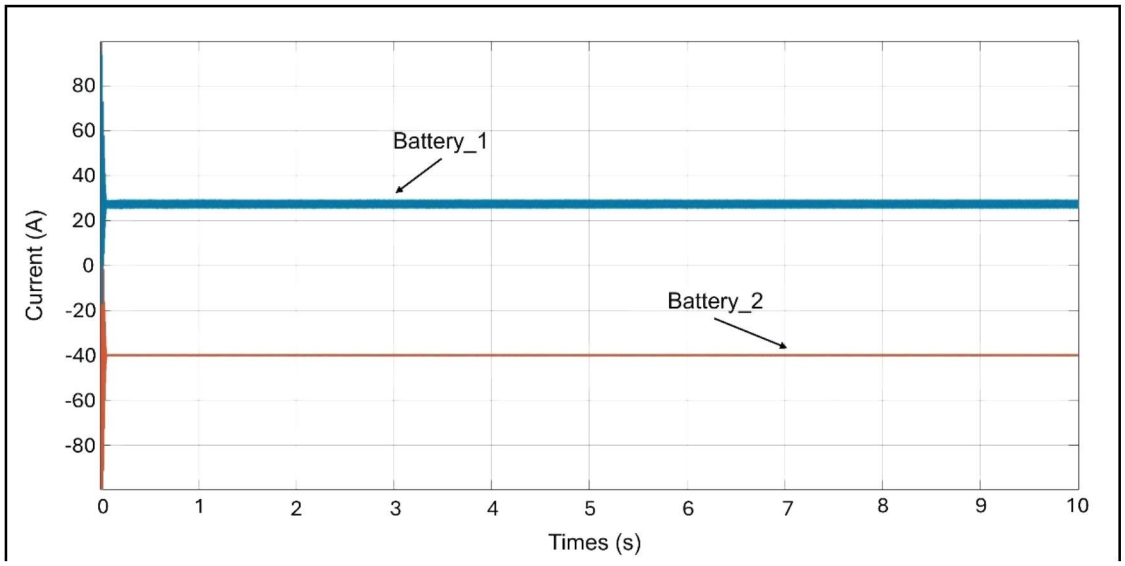

Figure 4.2 Mode 1 – Current of Battery_1 and Battery_2 vs Times.

Figure 4.3 shows the voltage levels of both batteries during the energy transfer. Battery_1 holds a steady voltage of 650 V, while Battery_2 remains at 480 V. This voltage difference is what enables the power to flow from Battery_1 to Battery_2. Throughout the 10-second duration, both voltages stay flat and stable, which confirms that the converter is working reliably and maintaining proper voltage regulation. This steady performance reflects the effectiveness of the DAB converter in handling bidirectional power transfer without voltage drops or instability.

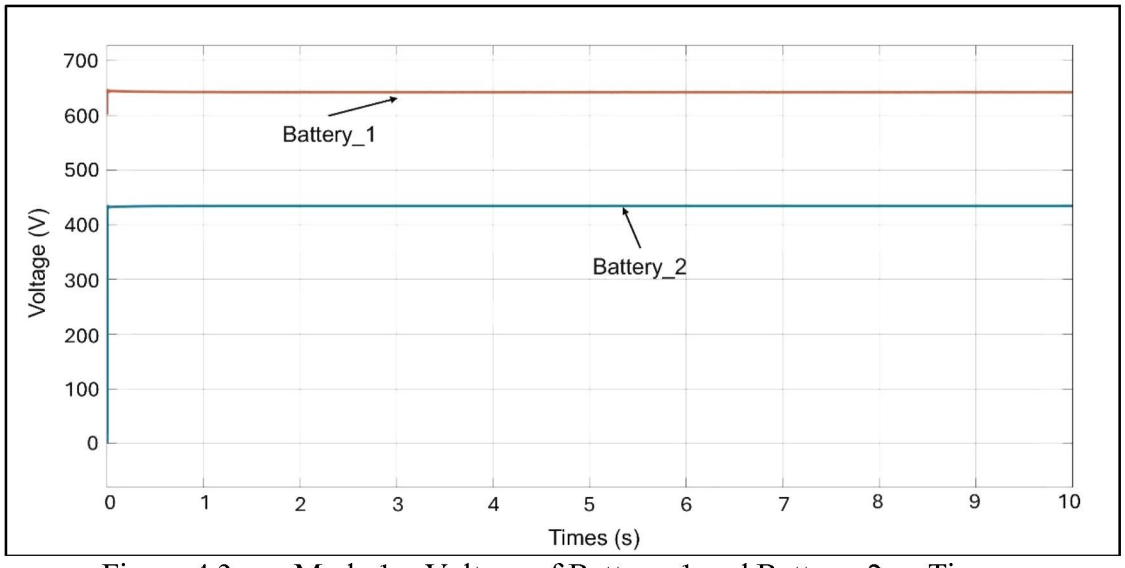

Figure 4.3 Mode 1 – Voltage of Battery_1 and Battery_2 vs Times.

The simulation results clearly show that the converter is capable of charging Battery_2 efficiently and reliably. It keeps both the voltage and current stable while allowing smooth energy transfer from Battery_1 to Battery_2. There are no signs of fluctuations or instability during the process. The steady rise in Battery_2's state of

charge (SOC), along with consistent current and voltage levels, proves that the converter is doing its job well under controlled conditions. This makes the system a strong fit for battery-to-battery energy transfer, especially in real-world setups like distributed energy storage or peer-to-peer energy sharing, where dependable and efficient energy flow is crucial.

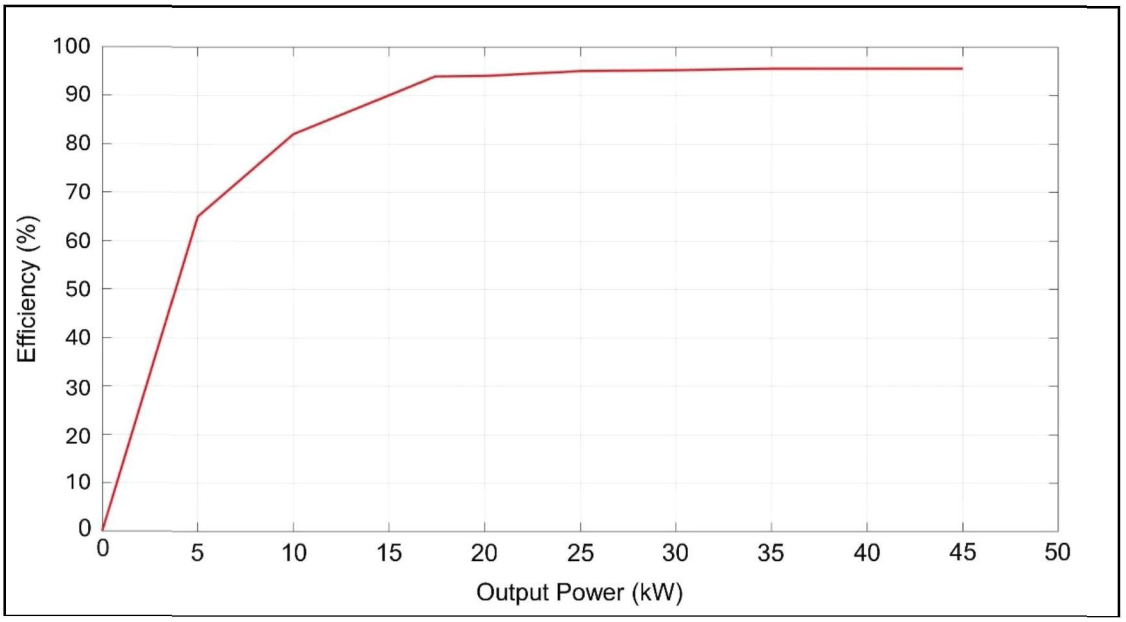

Figure 4.4 Mode 1 – Efficiency vs Output Power.

The efficiency curve in Figure 4.4 illustrates above the performance of the proposed DAB converter as a function of output power during battery charging operation. At very low output power levels, the efficiency is relatively low. This behaviour occurs because fixed losses, such as switching losses, core losses of the high-frequency transformer, and control-related losses, dominate the overall power flow when the transferred power is small. As a result, a significant portion of the input power is dissipated as losses, leading to reduced efficiency in the low-power region.

As the output power increases from approximately 5 kW to 15 kW, the efficiency improves rapidly. In this region, the proportion of useful transferred power becomes significantly larger compared to the fixed losses. Consequently, the converter operates more effectively, and the efficiency rises above 90%. This trend indicates that the DAB converter is well suited for medium-power operation, where conduction losses and switching losses are better balanced.

Beyond approximately 20 kW, the efficiency reaches a plateau and remains consistently high, exceeding 95% up to the maximum tested output power of 45 kW. This stable high-efficiency region demonstrates that the converter is optimally designed

for high-power operation. In this range, although conduction losses increase with current, they do not significantly degrade efficiency due to effective control, appropriate component selection, and efficient transformer design. The flat efficiency profile also indicates stable operation without excessive thermal or switching stress.

Overall, the efficiency characteristic shows that the proposed DAB converter performs best at medium to high output power levels, which correspond to practical operating conditions in battery charging, energy storage systems, and electric vehicle applications. The results confirm that the converter is capable of delivering high efficiency while maintaining stable bidirectional power transfer, validating the suitability of the proposed design for high-power energy conversion.

4.2.1.2 Mode 2 – Charging of Battery_1

Battery_2 is clearly discharging while Battery_1 is charging. As shown in Figure 4.5, the state of charge (SOC) of Battery_2 drops steadily from 50% to 48.9% over 10 seconds, confirming that it is releasing energy. At the same time, Battery_1's SOC rises from 50% to 50.08%, showing that it is actively receiving power. This confirms a one-way energy flow from Battery_2 to Battery_1, effectively reversing the direction seen in Mode 1. The result demonstrates a well-managed battery-to-battery energy transfer, supporting proper load sharing and energy balancing between the two batteries.

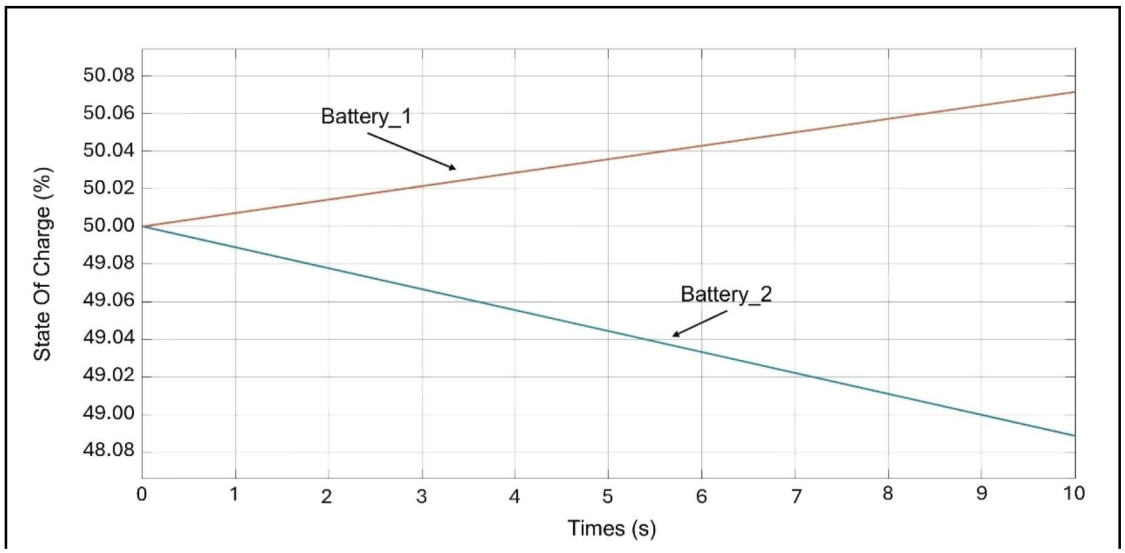

Figure 4.5 Mode 2 – SOC of Battery_1 and Battery_2 vs Times.

Figure 4.6 below provides a clear look at the current behavior during Mode 2. Battery_2, acting as the energy source, shows a steady current of +40 A, confirming continuous discharge. At the same time, Battery_1 displays a constant –40 A current, indicating it is being charged. The consistency of these current levels throughout the process reflects the effectiveness of the control system likely a proportional-integral (PI) controller in maintaining smooth and balanced power flow. This stable and symmetrical current profile proves that the system manages energy transfer reliably, which is essential for protecting battery health and ensuring overall system stability.

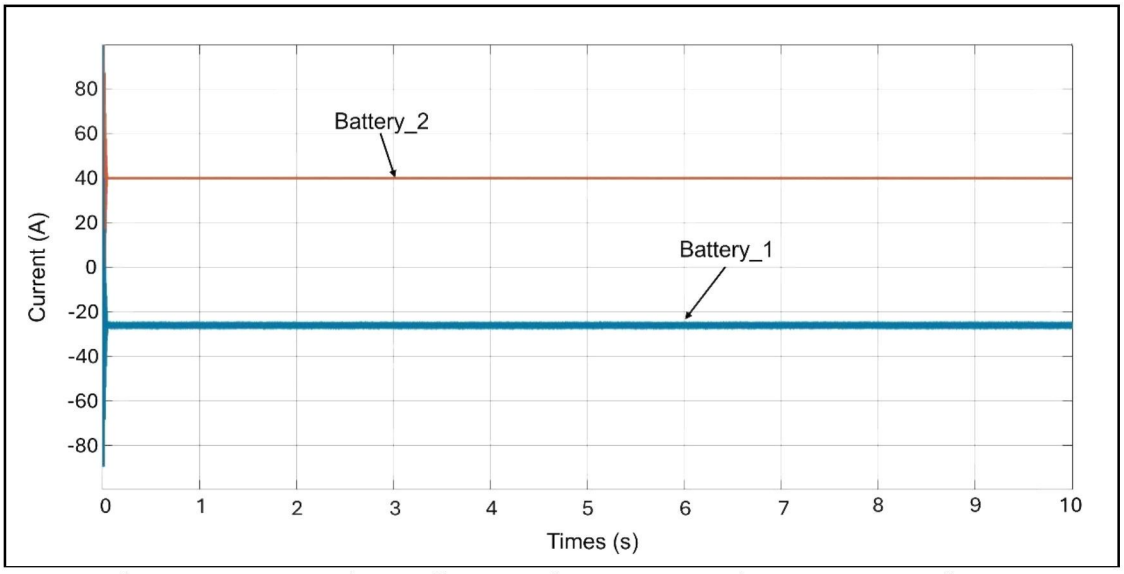

Figure 4.6 Mode 2 – Current of Battery_1 and Battery_2 vs Times.

Figure 4.7 shows the system's voltage behaviour, confirming that the power conversion is working effectively. Battery_2 holds a steady voltage at 480 V, while Battery_1 operates at 650 V. Even with the energy flow reversed, both voltages remain stable, allowing smooth and uninterrupted power transfer. The flat, disturbance-free voltage curves highlight the performance of the bidirectional DC-DC converter most likely the DAB which adjusts seamlessly to the reversed power flow while keeping the operation well-regulated.

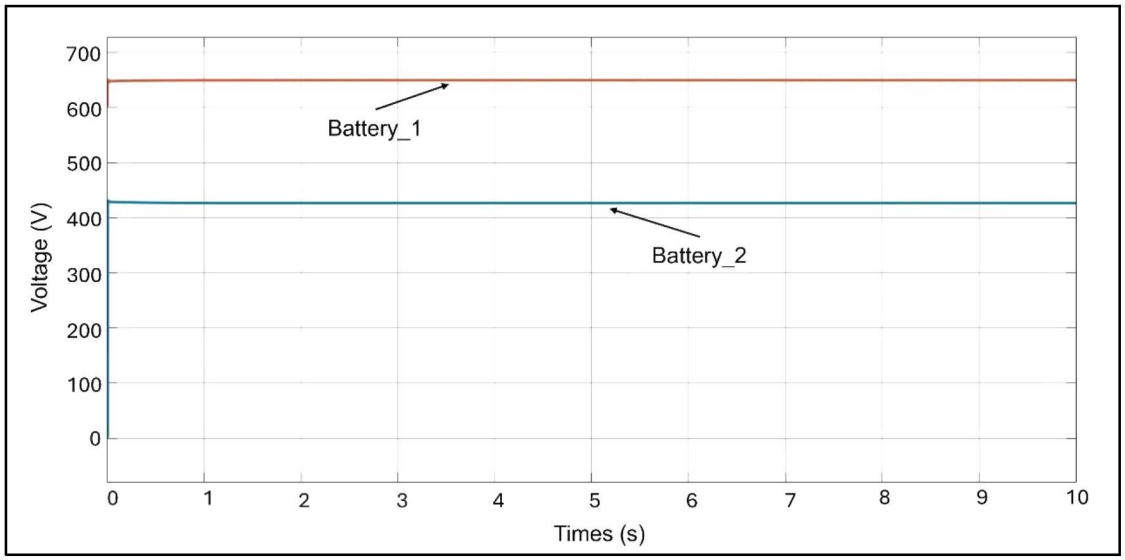

Figure 4.7 Mode 2 – Voltage of Battery_1 and Battery_2 vs Times.

The waveform results for Mode 2 clearly show that the system can reverse the energy flow and allow Battery_2 to discharge effectively. The converter handles this reverse power transfer smoothly, keeping both current and voltage well-regulated, while ensuring that Battery_1 charges without any issues. The drop in Battery_2's SOC, along with the stable current and voltage, confirms the system's ability to manage discharge operations reliably. This demonstrates the converter's capability to operate in both directions, making it a strong fit for modern energy storage setups that require flexible charging and discharging between multiple batteries.

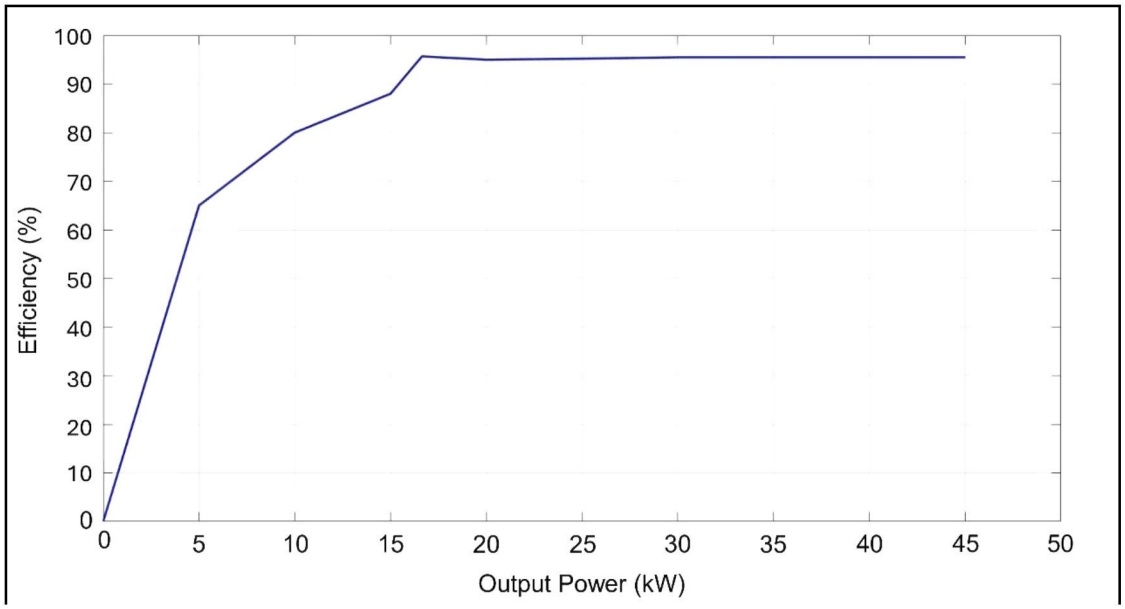

Figure 4.8 Mode 2 – Efficiency vs Output Power.

Figure 4.8 clearly shows how well the bidirectional converter performs during reverse power flow, with Battery_2 discharging and Battery_1 receiving energy. This is the opposite of Mode 1, and the converter maintains strong performance in both directions. With very low output power, efficiency starts near 0% which is expected due to fixed system losses at minimal load. As power increases to 5 kW, efficiency quickly rises to 70%, just like in Mode 1. It continues to improve steadily, reaching 90% at 15 kW. From 20 kW to 45 kW, the converter operates consistently above 95% efficiency, confirming it runs optimally across a wide range of power levels.

This performance directly matches the simulation, where Battery_2 discharged at 480 V with around 40 A of current, delivering about 16 kW well within the high-efficiency zone. Even with reversed power flow, the system kept voltage and current stable, and SOC trends remained smooth for both batteries. This reflects the converter's ability to adjust seamlessly to reverse operation without sacrificing efficiency.

Overall, the Mode 2 efficiency graph confirms that the converter delivers excellent performance when Battery_2 is discharging. It maintains over 95% efficiency at practical power levels and runs consistently under load. This proves the converter is well-suited for advanced energy storage systems that require reliable bidirectional power flow, such as battery-to-battery transfers, load balancing, and distributed storage. High efficiency in both modes helps minimize energy loss, improve battery lifespan, and enhance the system's overall effectiveness.

4.2.1.3 Comparative Analysis for Mode 1 and Mode 2

The table 4.1 below compares Mode 1 and Mode 2 operations of the DAB converter. Both modes show similar behaviour in terms of current, voltage, SOC changes, and efficiency. The current remains stable at around ±40 A, and the voltage levels are well regulated in both directions. Efficiency exceeds 95% in the medium to high power range for both modes. These results confirm that the converter performs equally well during charging and discharging, ensuring reliable and efficient bidirectional power transfer.

Table 4.1
Comparison of Charging and Discharging Battery_2 Parameters

Parameter	Mode 1(Charge Battery2)	Mode 2(Discharge Battery2)	Remarks
Initial SOC	Battery1: 50% / Battery2: 50%	Battery1: 50% / Battery2: 50%	Balanced test start condition
Final SOC	Battery1:~49.90% / Battery2: ~50.08%	Battery1:~50.08%/ Battery2: ~48.90%	Symmetrical SOC shift
Charging Current	Battery2: –40 A	Battery1: –40 A	Stable negative charging current
Discharging Current	Battery1: +40 A	Battery2: +40 A	Stable positive discharging current
Voltage Source	Battery1: ~650 V	Battery2: ~480 V	Voltage differential supports transfer
Voltage Load	Battery2: ~480 V	Battery1: ~650 V	Confirmed via waveforms
Peak Efficiency Achieved	>95% @ 30–45 kW	>95% @ 20–45 kW	Nearly identical efficiency profiles
Voltage Ripple	Minimal	Minimal	Indicates excellent regulation

Controller Stability	High	High	PI controller performs reliably in both

4.2.2 Open-Circuit of Dual Active Bridge

4.2.2.1 Feature Extraction (Wavelet Decomposition)

This section presents the results of using wavelet-based feature extraction on the converter's current waveforms. Current signals were collected from MATLAB simulations under both normal operation and fault conditions, specifically open-circuit faults in switches T^1, T^2, T^5, and T^6. These signals were then analysed using Discrete Wavelet Transform (DWT) to uncover frequency components that indicate faults. The Daubechies 4 (db4) wavelet was used for decomposition up to level 4, which allowed the current waveform to be broken down into different frequency bands. From this, the detail coefficients at levels 1, 2, and 3 (cD1, cD2, and cD3) were extracted. These coefficients capture high-frequency changes in the signal and are especially useful for spotting sudden spikes or irregularities that might not be visible in the original waveform. This approach helps clearly highlight the presence of faults in the system

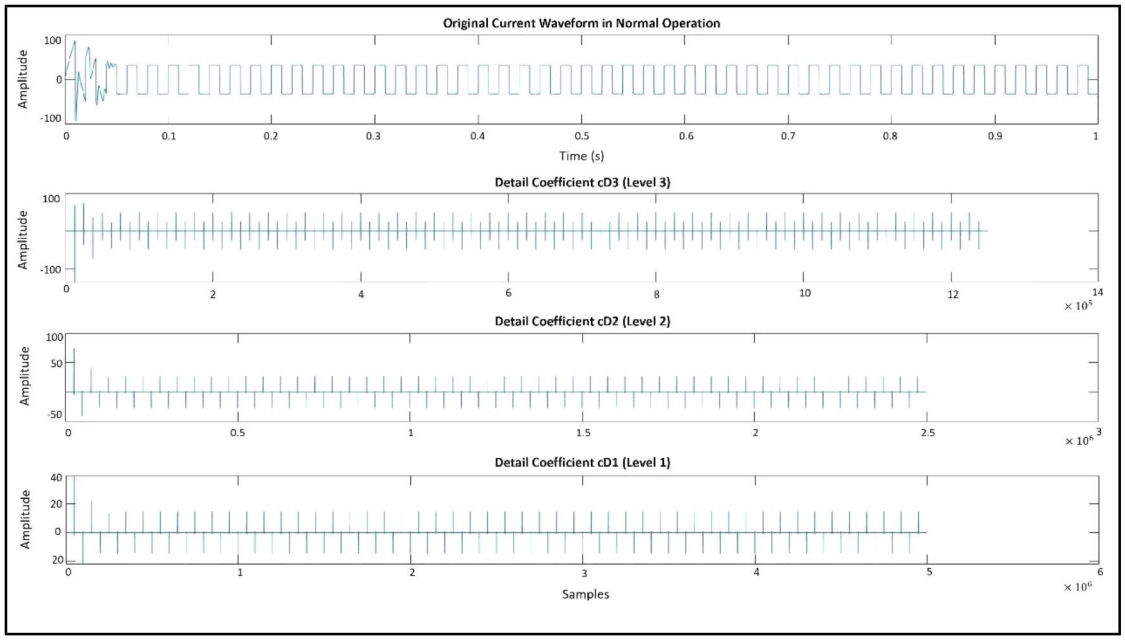

Figure 4.9 Wavelet decomposition of normal operation: Original waveform and detail coefficients (Level 1-3).

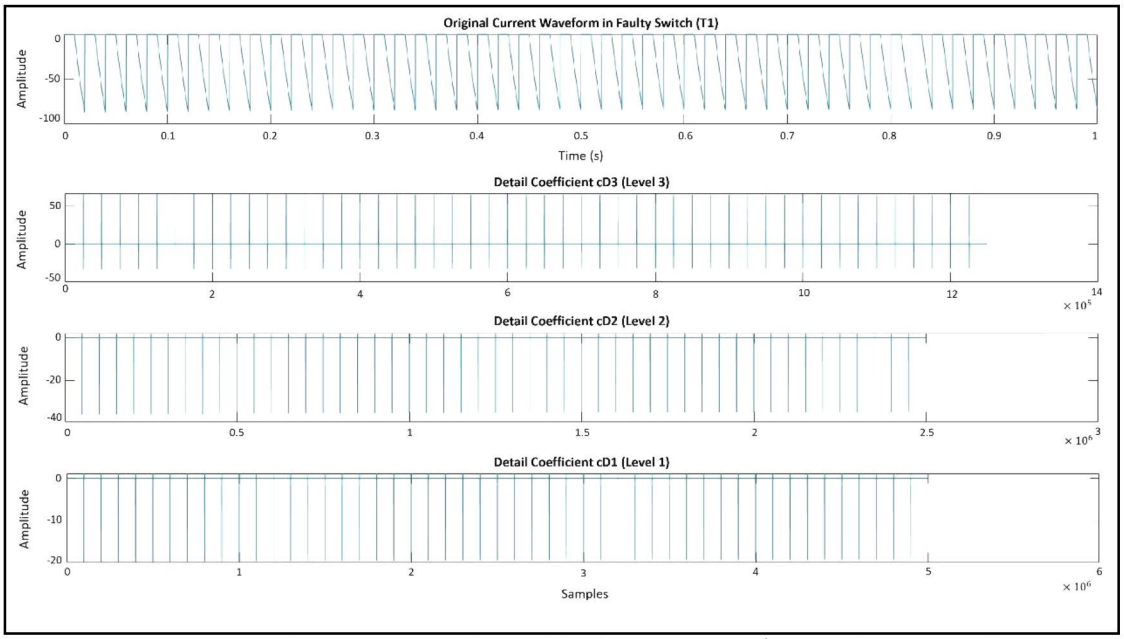

Figure 4.10 Wavelet decomposition of faulty switch (T^1): Original waveform and detail coefficients (Level 1-3).

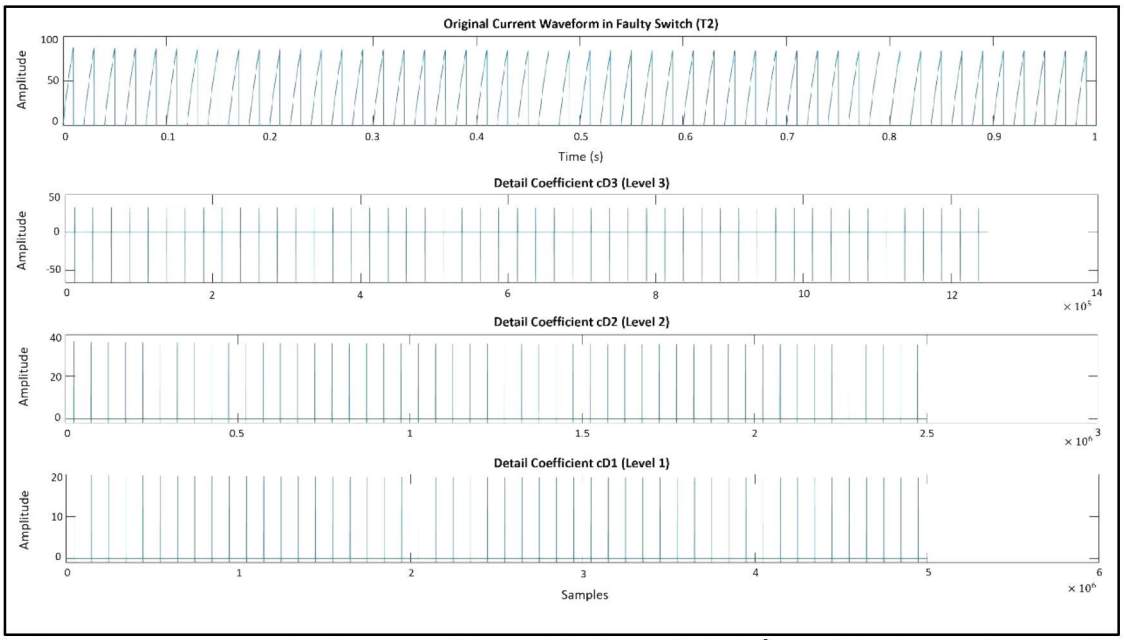

Figure 4.11 Wavelet decomposition of faulty switch (T^2): Original waveform and detail coefficients (Level 1-3).

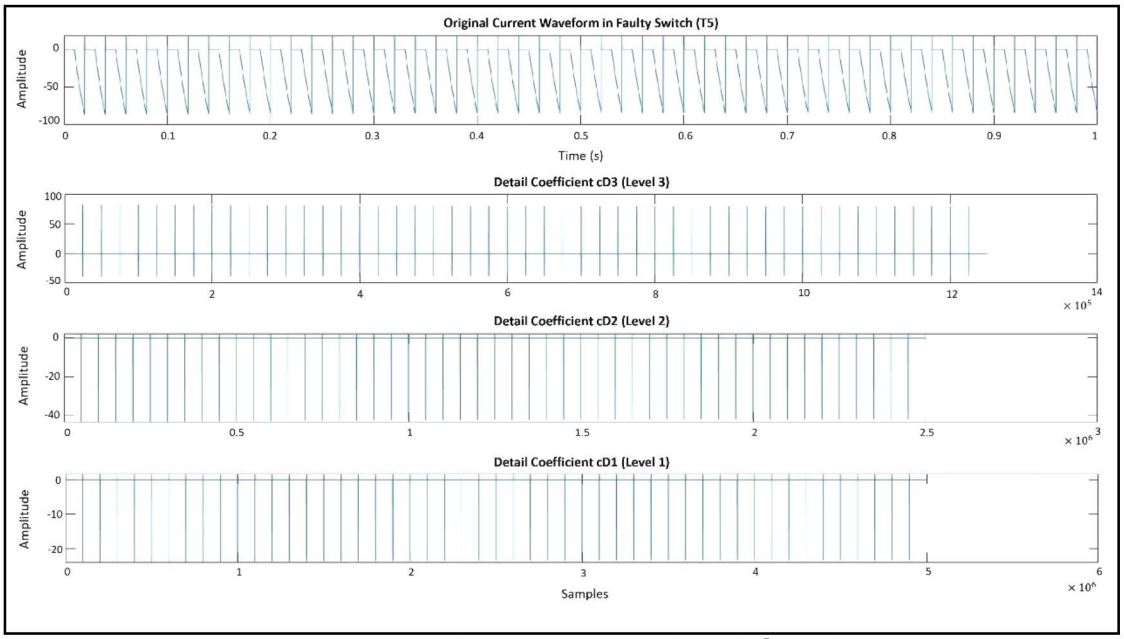

Figure 4.12 Wavelet decomposition of faulty switch (T^5): Original waveform and detail coefficients (Level 1-3).

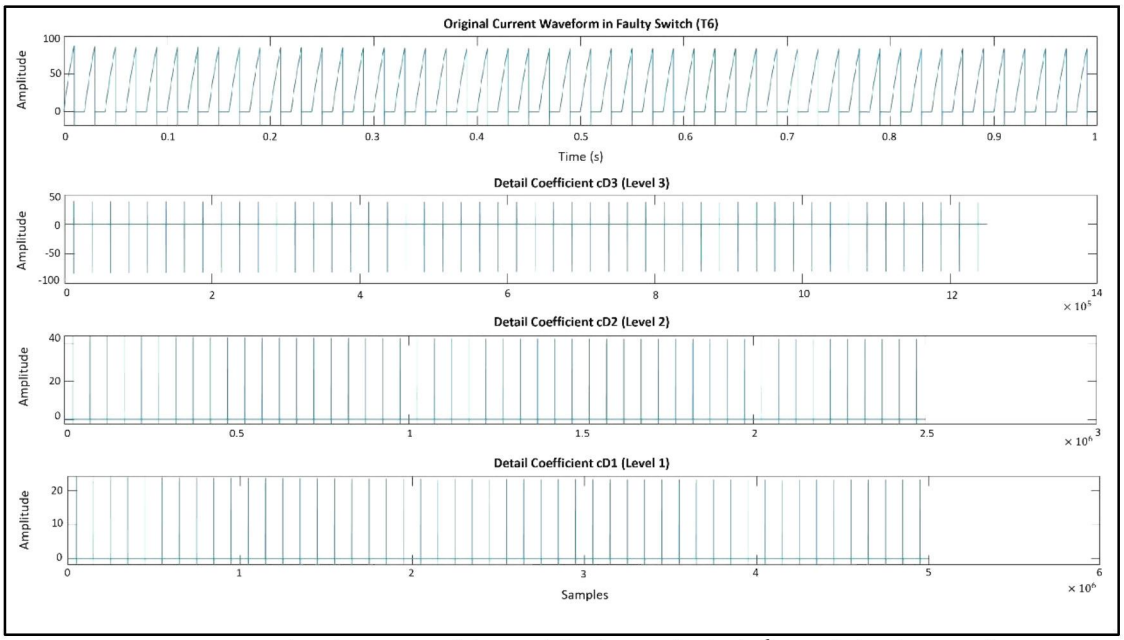

Figure 4.13 Wavelet decomposition of faulty switch (T^6): Original waveform and detail coefficients (Level 1-3).

Figures [4.9 to 4.13] show the current waveforms along with their corresponding wavelet detail coefficients. Under normal operating conditions, the waveforms and their detail coefficients appear smooth and stable, reflecting steady-state behavior. However, when a fault occurs such as an open circuit in switches T^1 or T^6 the current waveform becomes noticeably irregular. These disruptions are clearly highlighted in the wavelet detail coefficients, especially in cD2 and cD3, where we see sharp spikes and increased fluctuations during the fault.

By comparing the plots of normal and faulty conditions, it's clear that the energy in the wavelet coefficients increases significantly when a fault happens. This rise in high-frequency content points to sudden disturbances in the system, which are typical during switching faults. These visual and measurable changes are used to build feature vectors that serve as input for the ANN.

In short, the wavelet transform does an excellent job of converting raw current signals into meaningful data in the frequency domain. The extracted features specifically the energy from cD1, cD2, and cD3 are reliable indicators of fault presence and form the foundation for accurate classification in the ANN. This step is crucial in the process, acting as both a filter and simplifier, while keeping all the important fault-related details intact.

4.2.2.2 Failure Switch T^1

Figure 4.14 shows the schematic of the bidirectional DC-DC converter with an open-circuit fault introduced at switch T^1, which is in the upper-left leg of the input-side full-bridge. Normally, T^1 works together with T^4 to produce the positive half of the square-wave voltage that drives the transformer. This switching pair plays a key role in maintaining balanced, bidirectional power flow by alternating the voltage polarity. However, when T^1 fails open due to issues like a faulty gate driver, hardware damage, or internal malfunction it stops conducting completely. This interrupts the path needed to generate one side of the voltage waveform, throwing off the symmetry of the converter and disrupting its proper operation.

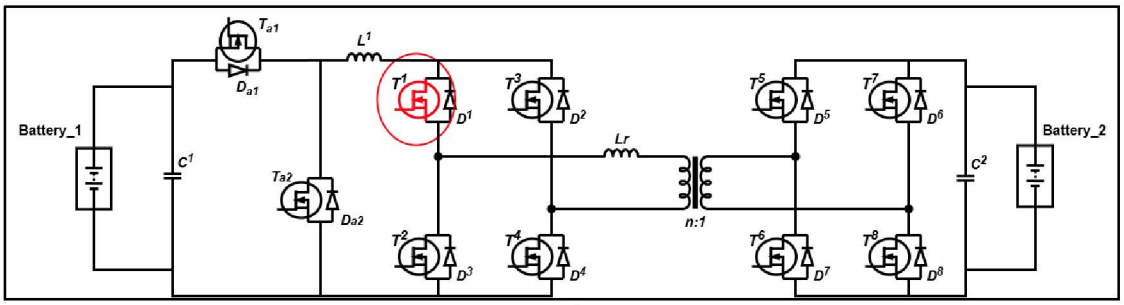

Figure 4.14 Faulty switch at T^1 for purposed DAB converter.

When T^1 fails, the most immediate effect is the loss of the positive half-cycle in the transformer's primary-side voltage. As seen in the simulation results in Figure 4.15 below, the voltage signals (red and blue) still show a square-wave pattern, which means the control system is still active and the remaining switches are working. However,

because T^1 is no longer contributing, the waveforms are incomplete. Specifically, the converter can no longer produce the correct positive voltage when T^1 and T^4 should be switching together. As a result, only the negative half cycle appears correctly, while the positive half cycle becomes distorted or fails to appear at all. This causes an imbalance in the waveform, which disrupts proper energy transfer through the transformer.

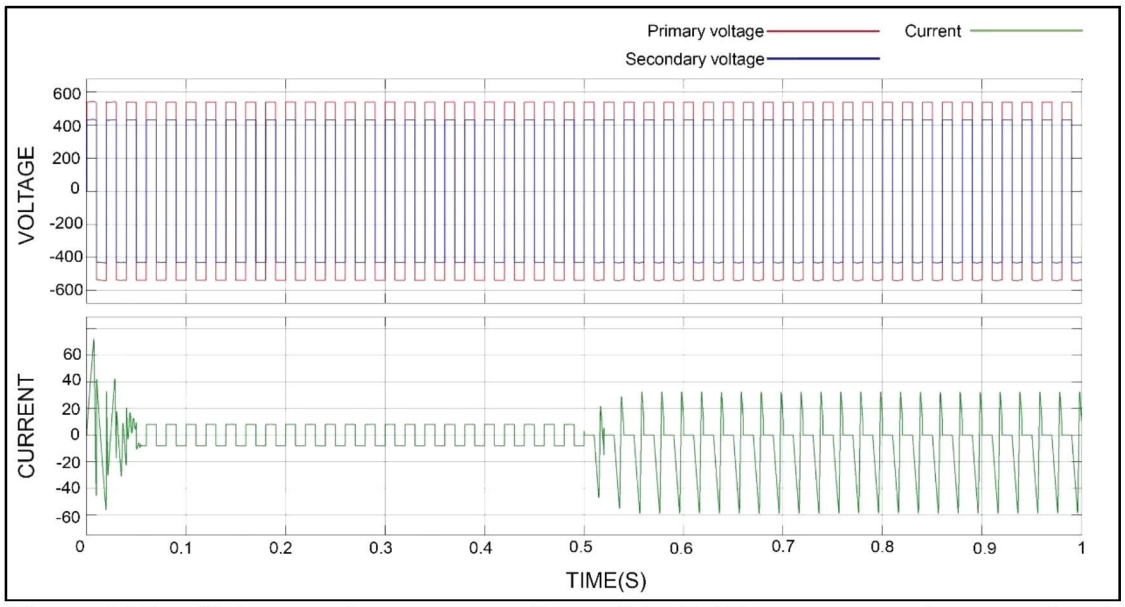

Figure 4.15 Voltage and current waveform of the DAB converter under normal and faulty condition at T^1.

This issue becomes even clearer when looking at the inductor current waveform (green), which shows a strong shift in the negative direction over time. Normally, the current would swing evenly above and below zero, showing balanced power flow in both directions. But with T^1 not working, current flows mostly in one direction, proving that only half of the converter is actively handling power. This imbalance causes uneven magnetic flux in the transformer, increasing the risk of core saturation, especially if the fault continues for too long. If the core gets saturated, it can seriously affect performance or even cause permanent damage to the transformer.

The fault also puts extra strain on the rest of the power circuit. Since only part of the full bridge is functioning, switches like T^2 and T^3 are forced to handle more current and switch more often, which can lead to overheating, reduced efficiency, and long-term reliability issues. Additionally, with proper bidirectional control disrupted, the converter loses access to soft-switching techniques like Zero Voltage Switching (ZVS), which normally help reduce energy losses. This makes the system less efficient and more prone to wear.

In short, a fault at T^1 throws off the converter's energy balance and breaks its bidirectional functionality. While the system might still run, its performance is noticeably degraded. The current drift and unbalanced power delivery clearly shows that the converter is no longer operating as intended. That's why early fault detection, continuous monitoring, and smart protection mechanisms are critical. These tools help prevent further damage and keep the system, including the transformer, switches, and batteries, safe and running reliably.

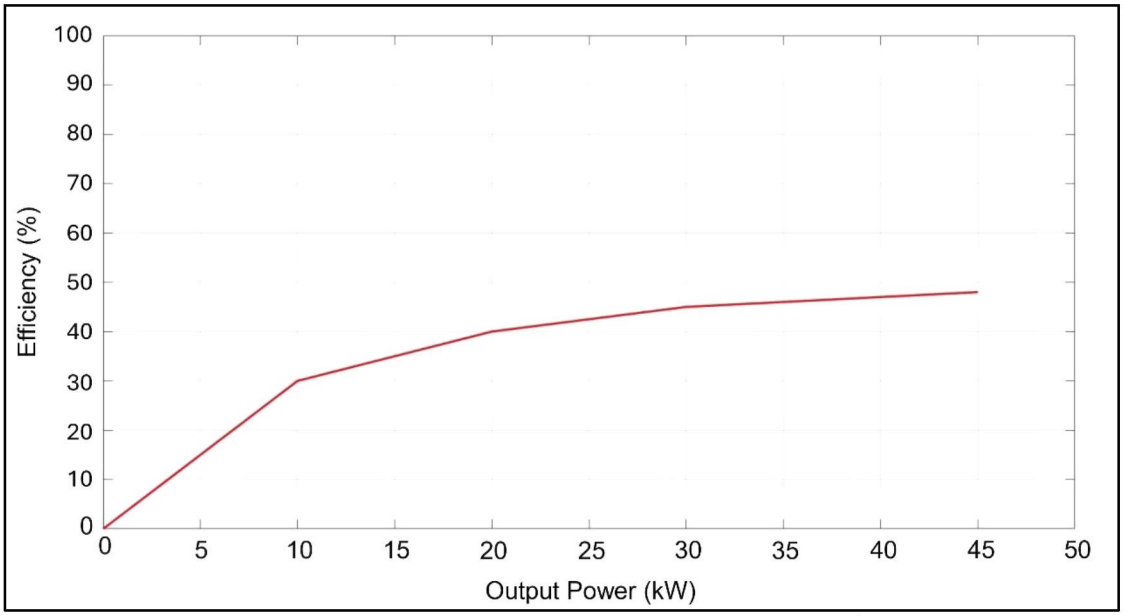

Figure 4.16 Efficiency vs Output Power at T^1.

Figure 4.16 presents the efficiency of the DAB converter under an open-circuit fault at switch T^1. T^1 is responsible for generating the positive half-cycle of the square-wave voltage on the primary side of the transformer, working together with T^4. When T^1 fails open, this half-cycle is lost, resulting in an unbalanced voltage waveform and unidirectional current flow through the transformer.

The graph shows that efficiency is significantly reduced across all power levels. At 0 kW, the efficiency is 0%, and at 10 kW, it rises to only 30%. As output power increases, efficiency gradually improves, reaching a maximum of 48% at 45 kW. This is considerably lower than the typical efficiency of 85% during normal operation. The reduction in efficiency is caused by several factors. The loss of the positive half-cycle limits energy transfer, and the converter is no longer able to achieve ZVS, resulting in increased switching losses. The inductor current becomes unidirectional, leading to magnetic flux imbalance and potential core saturation. Additionally, the remaining

switches (T^2, T^3, and T^4) are forced to carry increased current, which adds further conduction losses and thermal stress.

This fault condition clearly degrades the converter's performance and highlights the importance of early fault detection and protective control mechanisms in maintaining efficient and reliable operation.

4.2.2.3 Failure Switch T^2

Figure 4.17 shows the converter circuit with an open-circuit fault at switch T^2, which is positioned in the upper-right leg of the primary-side full-bridge. Under normal conditions, T^2 works together with T^3 to create the negative half of the square-wave voltage that drives the transformer. This part of the switching process is crucial for maintaining balanced, bidirectional power flow. But when T^2 fails whether due to a hardware issue or a lost gate signal it stops conducting entirely. This breaks the path needed to generate the negative voltage cycle, meaning the converter loses half of its switching capability and can no longer operate as intended.

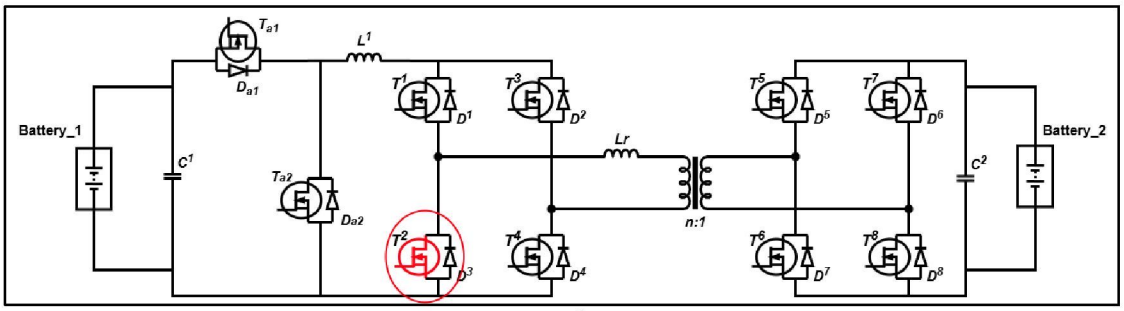

Figure 4.17 Faulty switch at T^2 for purposed DAB converter.

Figure 4.18 below clearly shows how the fault at T^2 affects the system. While the primary and secondary voltage waveforms (red and blue) still appear as clean square waves, the inductor current (green) tells a different story. Instead of oscillating evenly around zero, the current becomes heavily biased in a positive direction and follows a one-way ramping pattern. This means the converter is mainly transferring energy during the positive half-cycle handled by switches like T^1 and T^4 while the negative half-cycle is missing because T^2 is no longer working.

Without this negative cycle, the current doesn't flow back and forth as it should. Instead, it stays mostly above zero, rising and falling in a single direction. This imbalance causes uneven magnetic flux in the transformer, which can lead to core saturation if the fault persists. When the core saturates, it can overheat and distort the

voltage waveform, damaging performance. On top of that, the switches that are still working, especially T^1 and T^4, have to carry more current than usual, which puts them under extra electrical and thermal stress.

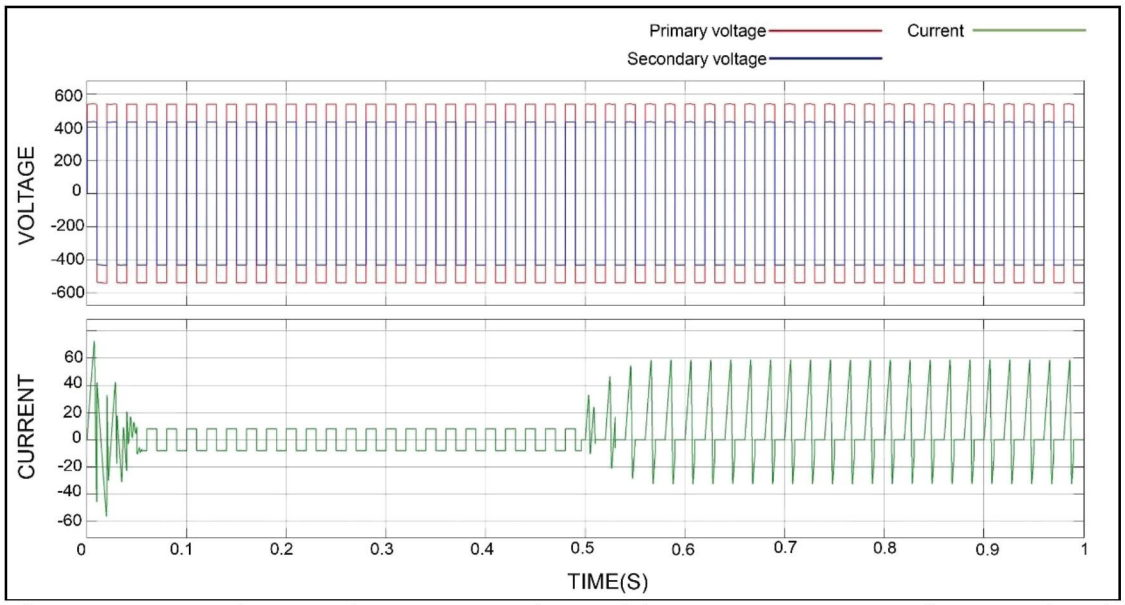

Figure 4.18 Voltage and current waveform of the DAB converter under normal and faulty condition at T^2.

In addition, the converter's failure to complete the negative switching cycle causes serious disruption in how energy is transferred. Even though the voltage waveforms might still look normal, they no longer represent proper energy exchange between the input and output. Because the switching is no longer symmetrical, the system also loses the ability to use efficient techniques like ZVS, which usually help reduce energy losses. Without ZVS, switching losses increase especially during low to medium power operation making the converter less efficient overall.

To sum it up, the fault at T^2 prevents the converter from conducting during the negative cycle, so energy is only transferred during the positive cycle. This results in distorted current flow, lower efficiency, and more stress on the components that are still working. The waveforms show that while the system keeps running, it's doing so in an imbalanced and less effective way. This highlights why real time fault detection and isolation are so important to protect the system and ensure safe, reliable operation even when faults happen.

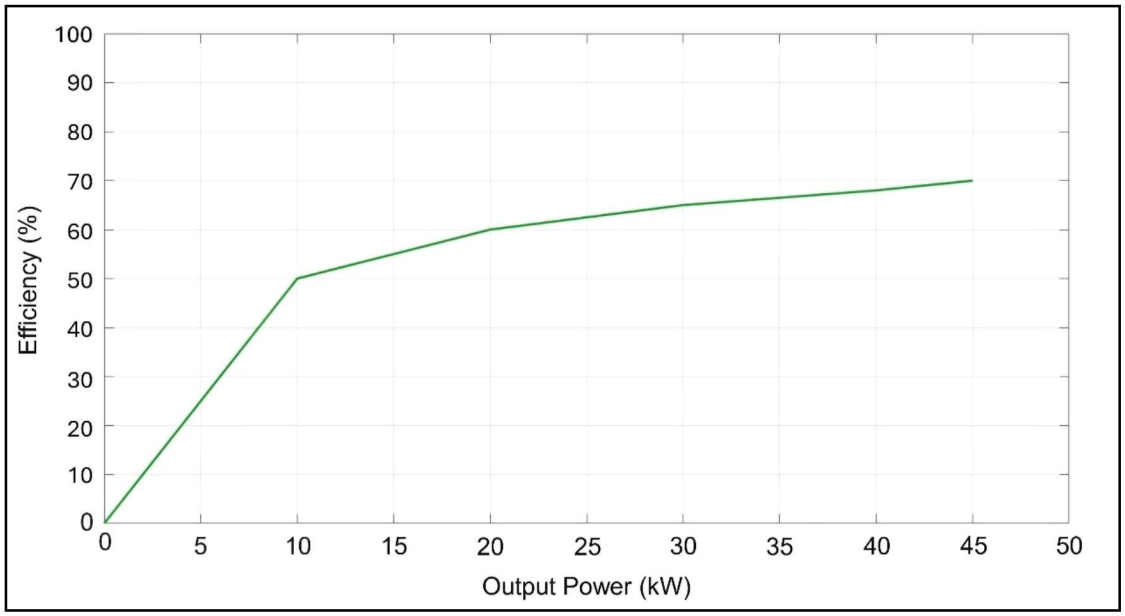

Figure 4.19 Efficiency vs Output Power at T^2.

Figure 4.19 shows the efficiency of the DAB converter when switch T^2 experiences an open-circuit fault. T^2 is located on the primary side and works with T^3 to generate the negative half-cycle of the voltage waveform applied to the transformer. When T^2 fails open, the converter loses this negative half-cycle, resulting in unidirectional power transfer. Only the positive half-cycle, formed by T^1 and T^4, remains active. This incomplete waveform significantly affects efficiency, especially at lower output power levels. At 0 kW, the efficiency is 0%, and at 10 kW, it increases to 50%. As output power continues to rise, efficiency improves to 70% at 45 kW. Although the converter is still operational, it does not perform as efficiently as under normal conditions.

The efficiency drop is caused by several factors. The absence of the negative half-cycle disrupts symmetrical power transfer and prevents the use of ZVS, which normally reduces switching losses. The inductor current becomes biased in one direction, causing magnetic imbalance in the transformer and increasing the risk of core saturation. Additionally, the remaining switches, especially T^1 and T^4, must handle higher currents, leading to increased conduction losses and additional stress on the components. Overall, the T^2 fault leads to moderate efficiency degradation. The converter remains functional but operates with lower performance, particularly at low power levels. This highlights the importance of fault-tolerant design and real-time detection strategies to maintain system reliability and efficiency.

4.2.2.4 Failure Switch T^5

Figure 4.20 shows the bidirectional DC-DC converter with an open-circuit fault at switch T^5, located on the upper left leg of the secondary-side full-bridge. Normally, T^5 works together with T^8 to generate the positive half-cycle of the square wave voltage on the secondary side of the transformer an important part of maintaining balanced power transfer. But when T^5 fails, either due to a hardware issue or a problem with the gate signal, it stops working completely. This disrupts the voltage formation on one side of the waveform and breaks the path needed for proper power delivery from the secondary side.

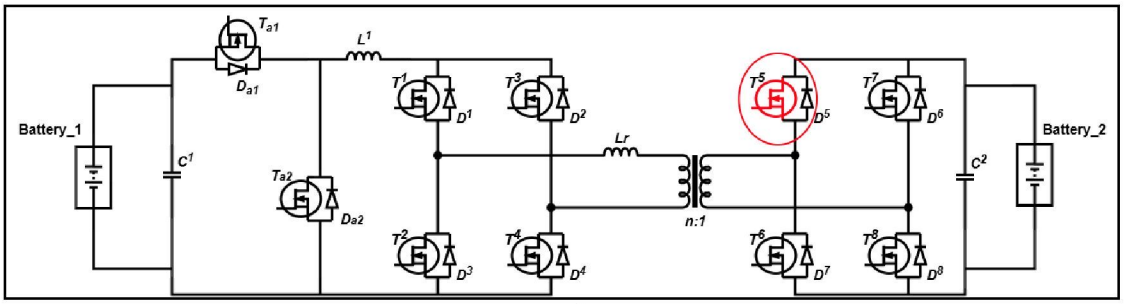

Figure 4.20 Faulty switch at T^5 for purposed DAB converter.

As shown in Figure 4.21 below, the primary and secondary voltage waveforms (in red and blue) still appear as square waves, which means the switching signals are active. However, because T^5 is not working, the secondary voltage becomes unbalanced. Only the negative half-cycle is properly generated by the remaining healthy switches, T^6 and T^7, while the positive half-cycle is either missing or much weaker. This imbalance causes energy to be transferred mainly during one part of the cycle. As a result, the inductor current as shown in green, starts to drift negatively over time, indicating uneven power flow.

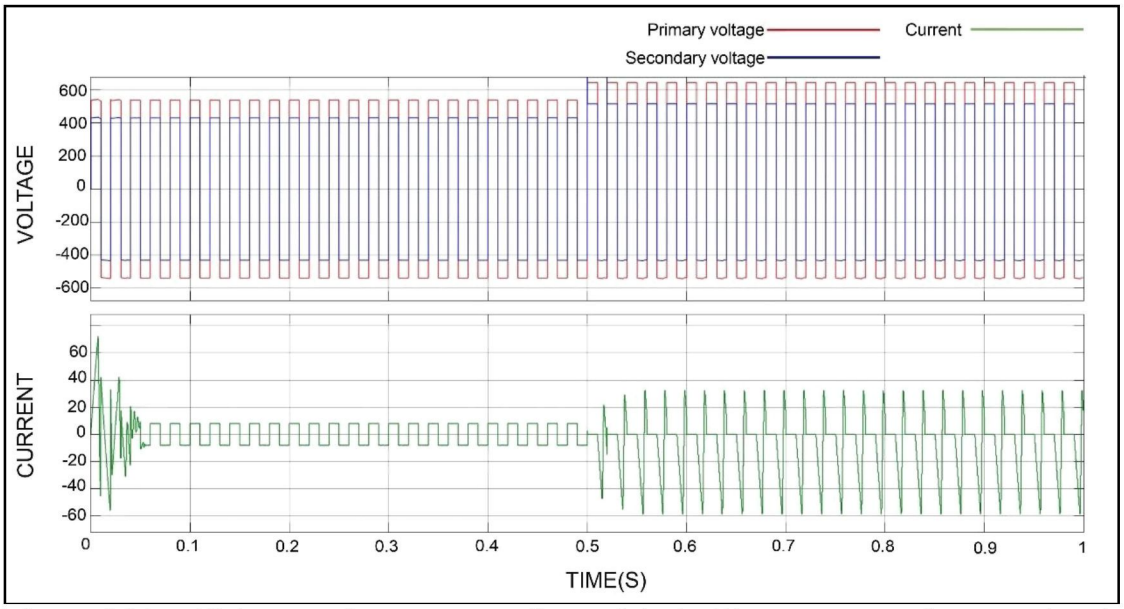

Figure 4.21 Voltage and current waveform of the DAB converter under normal and faulty condition at T^5.

This current behavior is quite like what was seen when T^1 failed where the inductor current drifted in one direction because one half of the switching cycle was missing. But with the T^5 fault, there are some noticeable differences. For example, the waveform shows small voltage spikes and minor fluctuations, especially during the transitions between square-wave cycles. These spikes are likely caused by leftover energy in the secondary side or the transformer windings suddenly releasing when current flow is interrupted. Since T^5 isn't switching anymore, the system might briefly depend on its body diode (D_5), which can lead to short bursts of voltage ringing when it recovers.

There are also parasitic capacitances in the transformer and switching areas that make these spikes worse. At the beginning of the simulation, the converter also seems to take some time to adjust to the fault. During this phase, the control system might still think T^5 is working, causing short misfires, unintended diode conduction, or overlapping switching activity.

The resulting inductor current not only flows in one direction, but it's also more unstable than in the T^1 fault scenario. Both faults disrupt the normal back-and-forth energy transfer, but T^5's fault introduces more high-frequency noise, which can increase electromagnetic interference (EMI) and switching losses. Switches T^6 and T^7 are also under more pressure, working harder and without the benefit of soft switching, which adds thermal stress and affects long-term reliability.

In short, while the T^5 and T^1 faults share a similar pattern of unbalanced current, T^5's position on the secondary side creates extra disturbances like voltage spikes and noise. These differences make it important to have fault detection systems that can recognize where the fault is happening so that the system can respond quickly and protect both the converter and transformer.

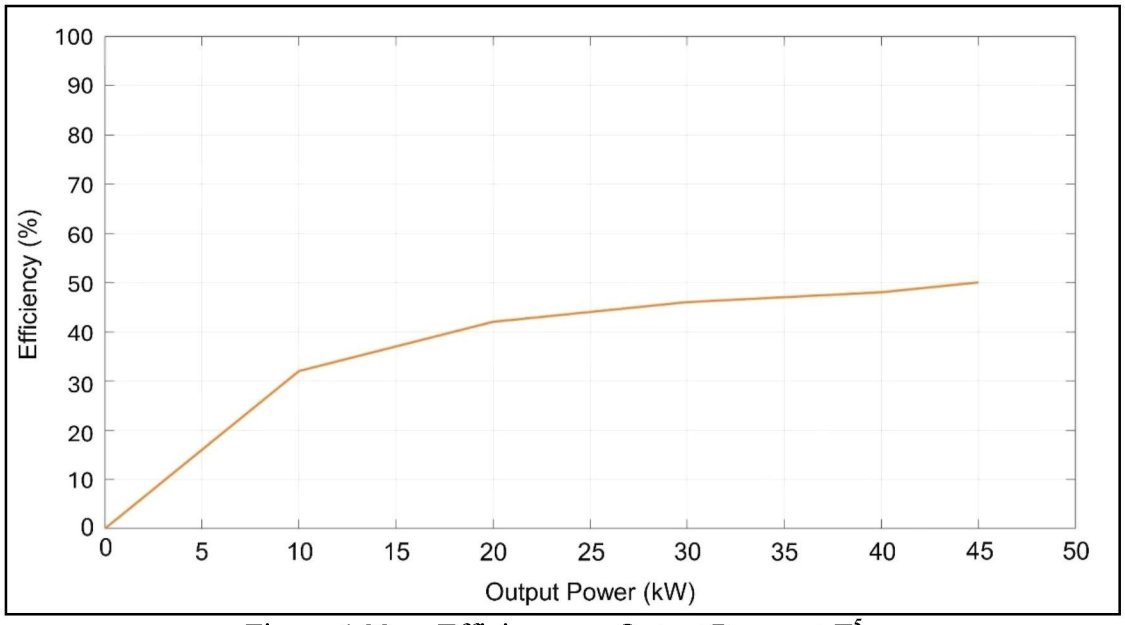

Figure 4.22 Efficiency vs Output Power at T^5.

Figure 4.22 shows the efficiency of the DAB converter when an open-circuit fault occurs at switch T^5. T^5 is located on the secondary side of the converter and is responsible for generating the positive half-cycle of the voltage waveform on that side. Under normal conditions, T^5 works with T^8 to complete this function. When T^5 fails, the positive half-cycle on the secondary side is lost, and energy can only be transferred during the negative half-cycle, like what happens when T^1 fails on the primary side.

From the graph, the converter's efficiency is significantly affected. At 0 kW, the efficiency is 0%, and at 10 kW, it only reaches 32%. Efficiency gradually improves with higher output power, reaching 50% at 45 kW. However, this is still far below the expected efficiency during normal operation, which typically reaches above 85%.

The reason for this performance drop is the incomplete voltage waveform and unidirectional energy transfer. Without the positive half-cycle, power transfer is limited, and the converter cannot achieve ZVS, leading to higher switching losses. transformers, the inductor current becomes unbalanced, and the transformer experiences magnetic flux drift. The remaining switches on the secondary side, such as T^6 and T^7, are forced to carry more current, increasing conduction losses and stress on those components.

In summary, a fault at T^5 has a strong impact on efficiency, very similar to the fault at T^1, because both switches are responsible for the same half-cycle just on opposite sides of the transformer. The converter remains functional, but its performance is significantly degraded, especially at lower output power.

4.2.2.5 Failure Switch T^6

Figure 4.23 shows the bidirectional DC-DC converter with an open circuit fault at switch T^6, which sits in the upper right leg of the secondary side full bridge. Normally, T^6 works together with T^7 to create the negative half of the voltage waveform on the secondary side of the transformer. This pair is crucial for maintaining balanced, two-way energy flow to Battery 2. But when T^6 fails whether due to hardware damage or a gate signal issue it can no longer conduct. This breaks the path needed to form the negative half cycle, leaving the converter unbalanced and limiting energy transfer to only the positive half of the cycle.

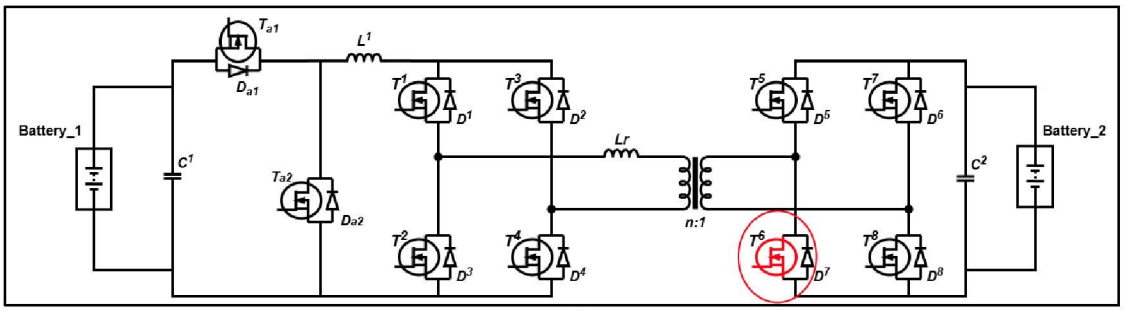

Figure 4.23 Faulty switch at T^6 for purposed DAB converter.

The waveform in Figure 4.24 shows what happens when T^6 fails. Even though the primary and secondary voltage signals (in red and blue) still look like square waves, the converter's behaviour changes noticeably. The inductor current (green) shifts upward and stays mostly positive, which means current is only flowing in one direction. This is very similar to what happens when T^2 fails on the primary side where the converter also loses the negative half of its operation. In both situations, the current stops swinging evenly around zero, which throws off the balance in the transformer and increases the risk of magnetic core saturation over time.

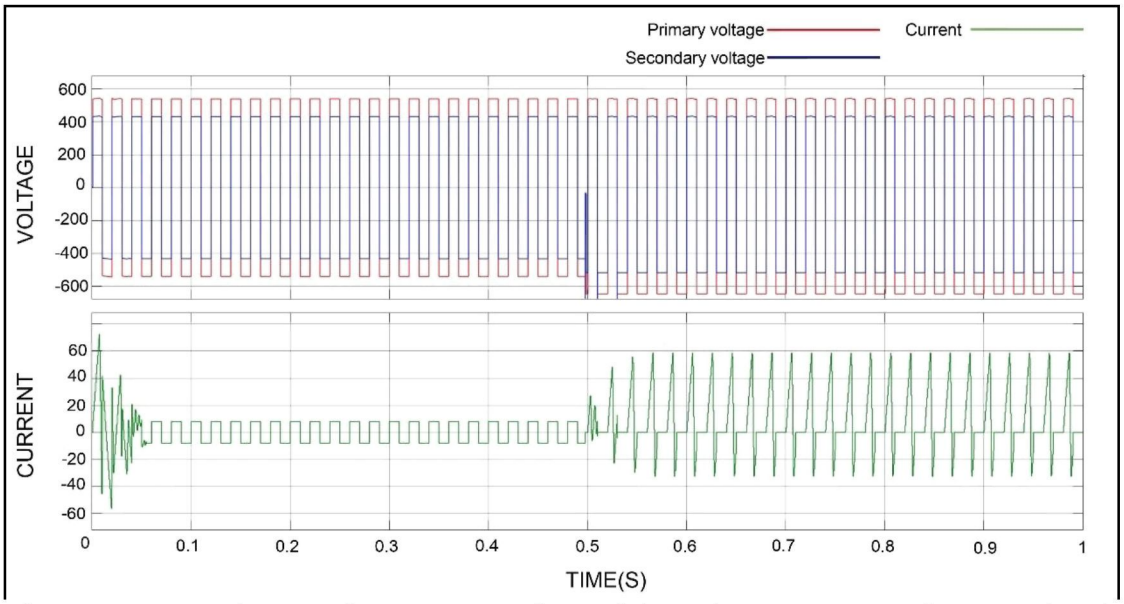

Figure 4.24 Voltage and current waveform of the DAB converter under normal and faulty condition at T^6.

Unlike the T^2 fault, the T^6 fault causes noticeable spike-like fluctuations during switching, especially in the voltage waveform. These spikes are likely due to the reverse recovery of diode D_6, which tries to conduct when T^6 isn't working. Extra inductance and capacitance in the secondary-side circuit can also make these high frequency spikes worse. These kinds of voltage disturbances aren't as obvious with T^2 faults on the primary side, likely because the layout and switching behavior are different there. This shows that faults on the secondary side can create more voltage noise and instability.

At the beginning of the current waveform, there's also some minor fluctuation before it settles into a steady one directional pattern. This early wobble probably happens because the system still thinks everything is normal and tries to switch as usual. Once it adjusts to the fault, the current becomes steady, but it's still unbalanced, and efficiency takes a hit.

In short, a fault at T^6 stops the converter from forming the negative half of the voltage cycle on the secondary side, just like the T^2 fault does on the primary side. Both result in one-way current flow and reduced energy transfer. But with T^6, you also get more voltage ripple and noise because of the diode and circuit layout. This highlights the need for detection of smart faults that not only spots performance drops but also picks up on these smaller waveform issues depending on where the fault occurs.

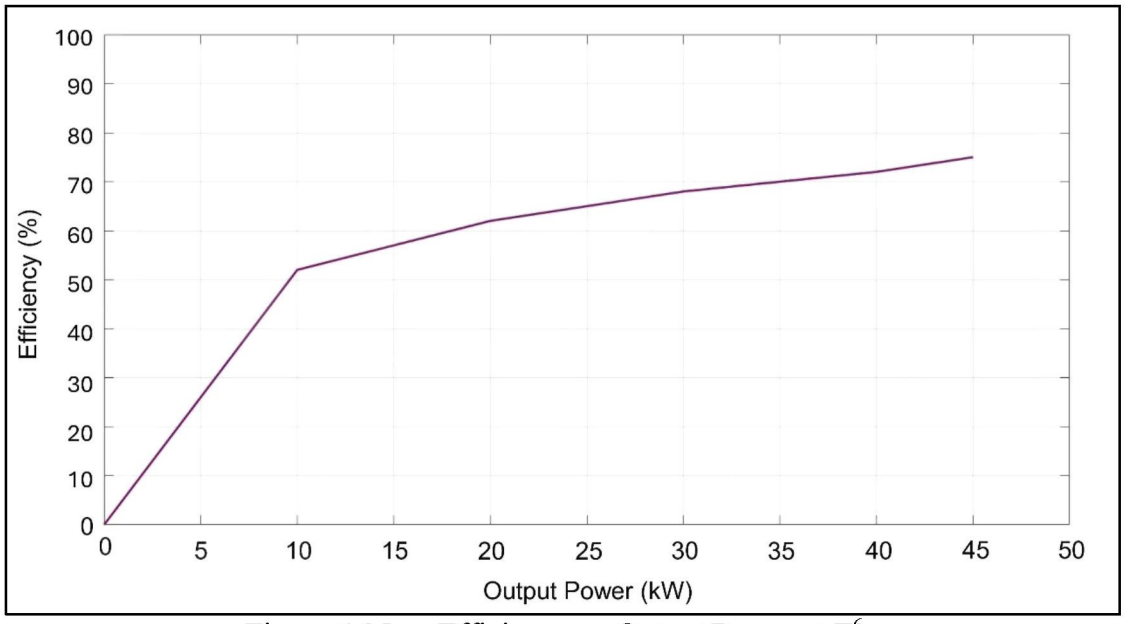

Figure 4.25 Efficiency vs Output Power at T^6.

Figure 4.25 shows how the efficiency of the DAB converter changes when there's an open circuit fault at switch T^6. This switch is on the secondary side and normally works with T^7 to create the negative half of the voltage waveform. When T^6 fails, half of the waveform is lost, and the converter can only transfer power during the positive half cycle. This throws the system off balance and affects how well it can deliver power.

Looking at the graph, the efficiency starts at 0% when no power is being delivered. At 10 kW, it climbs to 55%, and as the load increases, it continues to rise gradually, reaching 75% at 45 kW. Interestingly, this curve looks very similar to the one for the T^2 fault. That makes sense, since T^6 and T^2 perform the same function but on opposite sides of the transformer when either one fails, the result is nearly the same in terms of how the converter behaves.

The drop in efficiency comes from a few key problems. With the negative half of the waveform missing, the converter isn't transferring power as effectively as it should. It also loses the ability to perform ZVS, which normally helps reduce switching losses. The current through the inductor becomes one-directional, which can cause magnetic imbalance in the transformer and put stress on the core. Plus, the remaining switches on the secondary side like T^7 and T^8 must work harder, which increases heat and electrical losses. The fault can also introduce voltage ripple and noise due to sudden transitions and parasitic effects in the circuit.

In short, a fault at T^6 has a noticeable impact on efficiency, especially at lower power levels. The converter still works, but not as efficiently or reliably as it should. And because its behavior closely matches the T^2 fault, it highlights how both sides of the converter play equally important roles and why it's so important to detect and manage faults early to keep performance stable.

4.2.2.6 Justification for Exclusion of Fault Analysis at Switches T^3, T^4, T^7, and T^8

This study focuses on detailed simulations of faults at switches T^1, T^2, T^5, and T^6, while deliberately leaving out individual analysis for switches T^3, T^4, T^7, and T^8. This decision is based on the symmetrical nature of the DAB converter's design. In the converter, both the primary and secondary sides have four switches each, working in diagonal pairs to generate alternating square wave voltages. On the primary side, T^1 pairs with T^4 and T^2 pairs with T^3; on the secondary side, T^5 pairs with T^8 and T^6 with T^7. Because of this mirror setup, switches like T^3 and T^4 essentially perform the same roles as T^1 and T^2. The same goes for T^7 and T^8, which match the functions of T^5 and T^6. For example, a fault at T^3 affects the system in the same way as a fault at T^1 both lead to similar voltage issues, current distortion, and loss of energy symmetry [90]. The same applies to faults at T^4 and T^2, or T^8 and T^6.

Simulations confirm this, that faults at these omitted switches result in waveform and efficiency patterns that are nearly identical to those already discussed. So, analysing them separately would only repeat the same conclusions without adding any new insight [91].

By narrowing the focus to T^1, T^2, T^5, and T^6, the study stays concise and avoids unnecessary repetition, while still fully covering how the converter behaves under fault conditions. In short, skipping T^3, T^4, T^7, and T^8 is both efficient and logical, since their roles and the consequences of their failures are already clearly represented by their counterparts.

4.2.2.7 Summary of Open-Circuit Fault Analysis Results for the DAB Converter

Table 4.2
Summary of Open-Circuit Fault Analysis Results for the DAB Converter

Faulty Switch	Location	Lost Voltage Half-Cycle	Inductor Current Behaviour	Wavelet Feature Characteristics (cD1–cD3)	Efficiency Impact
Normal Operation	—	None	Balanced bidirectional current oscillation around zero	Low and stable wavelet energy values	>85% (normal operation)
T1	Primary side, upper-left leg	Positive half-cycle	Strong negative current drift, unidirectional flow	Significant energy increase in cD2 and cD3	Severe degradation (max ≈48% at 45 kW)
T2	Primary side, upper-right leg	Negative half-cycle	Strong positive current drift, unidirectional flow	Elevated wavelet energy, clear transient spikes	Moderate degradation (max ≈70% at 45 kW)
T5	Secondary side, upper-left leg	Positive half-cycle	Negative current drift with high-frequency noise	High wavelet energy with additional spikes	Severe degradation (max ≈50% at 45 kW)
T6	Secondary side, upper-right leg	Negative half-cycle	Positive current drift with transient fluctuations	Elevated wavelet energy, noisy coefficients	Moderate degradation (max ≈75% at 45 kW)

Table 4.2 provides a concise summary of the fault analysis results for the DAB converter under open-circuit switch fault conditions. It compares normal operation with faults occurring at different switches on both the primary and secondary sides of the converter. The table highlights the effect of each fault on the inductor current behaviour, wavelet feature characteristics, and overall converter efficiency.

From the table, it can be observed that faults at switches T1 and T5, which are responsible for generating the positive voltage half-cycle, result in more severe current distortion and efficiency degradation compared to faults at switches T2 and T6. This difference explains why positive half-cycle loss has a greater impact on converter performance. The table also justifies the exclusion of symmetrical switches (T3, T4, T7, and T8), as they exhibit identical behaviour to their corresponding counterparts and therefore do not introduce additional insights.

4.2.3 ANN-Based Fault Detection and Classification Results

4.2.3.1 ANN Training Performance

Figure 4.26 shows the overall training progress and final performance of the neural network. The training was completed in just 6 epochs, achieving a very low mean squared error (MSE) of 1.43×10^{-15}, starting from an initial value of 12.7. This extremely low error indicates that the network was able to learn the fault patterns with high accuracy. The training gradient dropped to 4.82×10^{-7}, suggesting the model had successfully reached a stable point where further improvement was minimal. The learning rate adjustment parameter (Mu) also decreased steadily from 0.001 to 1×10^{-6}, confirming that the training process remained stable throughout. Training stopped automatically after 6 validation checks without improvement, which is a built-in MATLAB feature to prevent overfitting. This means the network was able to generalize well without memorizing the training data.

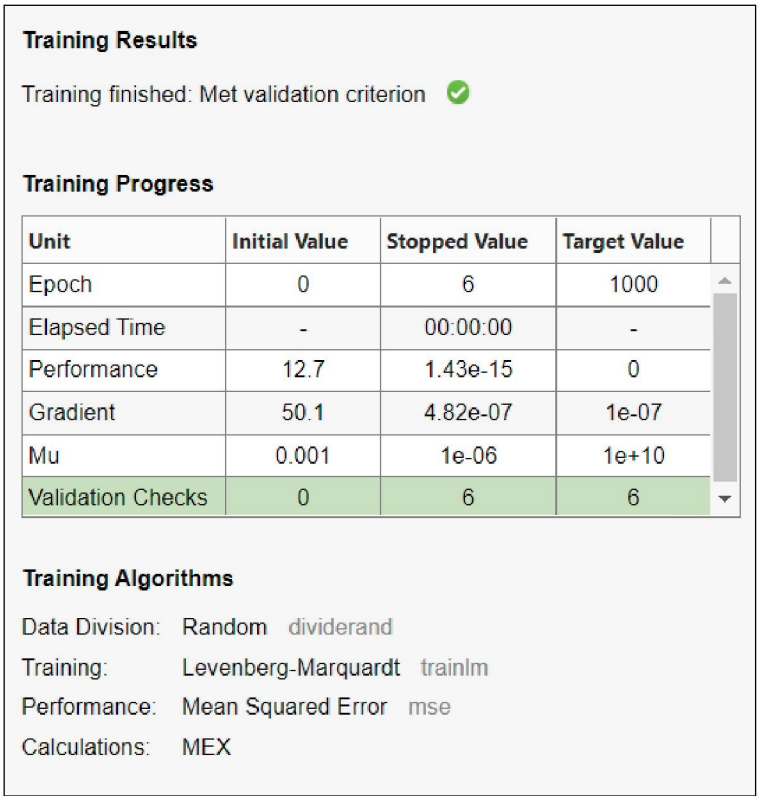

Training Results

Training finished: Met validation criterion

Training Progress

Unit	Initial Value	Stopped Value	Target Value
Epoch	0	6	1000
Elapsed Time	-	00:00:00	-
Performance	12.7	1.43e-15	0
Gradient	50.1	4.82e-07	1e-07
Mu	0.001	1e-06	1e+10
Validation Checks	0	6	6

Training Algorithms

Data Division: Random dividerand
Training: Levenberg-Marquardt trainlm
Performance: Mean Squared Error mse
Calculations: MEX

Figure 4.26 ANN Training Summary

Figure 4.27 shows how the mean squared error (MSE) changed during the training process for the training, validation, and test datasets. The best validation

performance an MSE of 0.051753 was achieved right at epoch 0, meaning the network generalized well from the very beginning. After that point, although the training error kept decreasing and eventually approached zero, the validation and test errors stayed constant. This gap between the training and validation performance suggests that the network had already learned the important features early on, and continuing to train would likely lead to overfitting. Fortunately, the early stopping feature kicked in at the right time, helping to maintain the model's ability to perform well on unseen data.

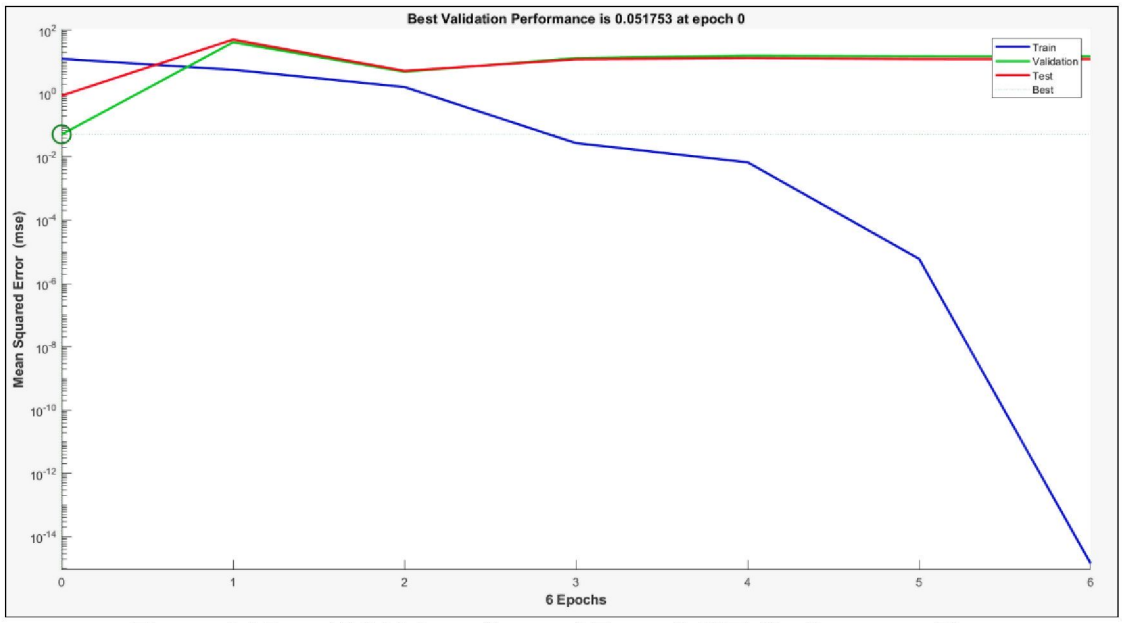

Figure 4.27 ANN Mean Squared Error (MSE) Performance Plot

To better understand how the training progressed, Figure 4.28 illustrates how key parameters changed over each training step. The top plot shows the gradient steadily decreasing, which confirms that the network was approaching a stable point where the error wasn't changing much an indicator of successful convergence. The middle plot shows how the Mu parameter (which adjusts the learning rate) changed, it briefly increased in the early stages and then gradually decreased, helping to fine-tune the training process. The bottom plot shows the number of validation checks, which reached the limit of 6 by epoch 6 this triggered the early stopping mechanism, ending the training process at the right time to prevent overfitting.

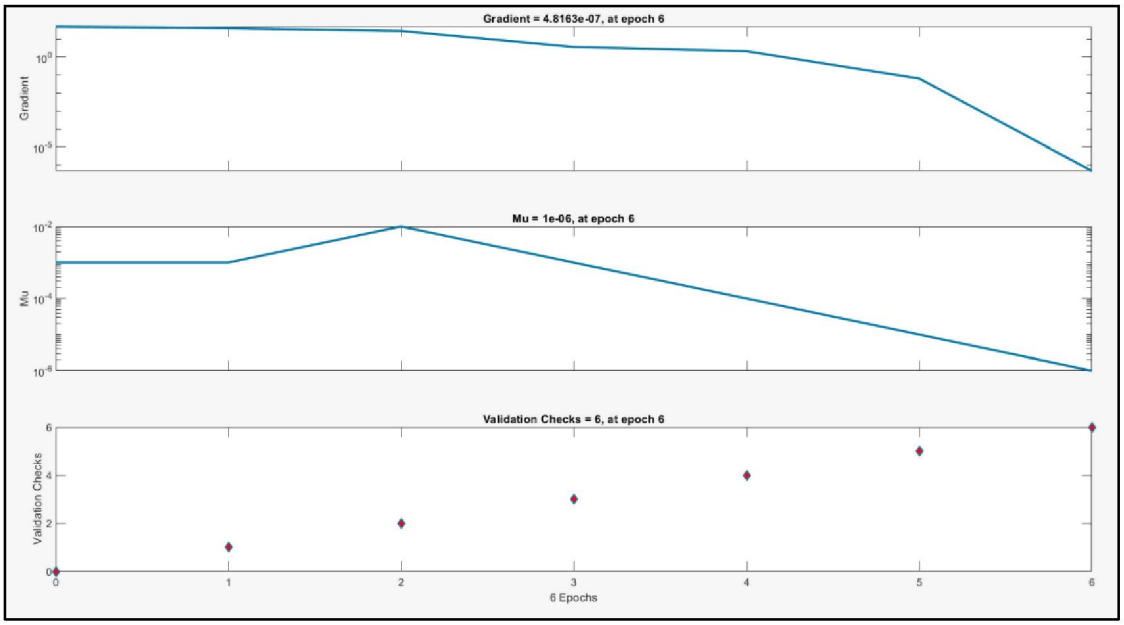

Figure 4.28 Training State Evolution: Gradient, Mu, and Validation Checks

Figure 4.28 clearly shows that the ANN trained quickly and effectively, with stable performance throughout. There were no signs of instability or erratic behaviour during training. The final training error was extremely low, and the convergence trends confirm that the network structure and the wavelet-based input features worked well together. Overall, these results confirm that the ANN is reliable and accurate enough to support the proposed fault-tolerant control system by correctly identifying and classifying faults.

4.2.3.2 Comparative Evaluation of Predictive Models

To evaluate the predictive performance of the proposed ANN model, results were compared with two additional models which is MLR and SVR. MLR serves as a simple statistical baseline that assumes linear relationships between variables, while SVR is a classical machine learning approach capable of modelling non-linear patterns through kernel functions. Both models were trained and tested using the same dataset and preprocessing steps as the ANN to ensure a fair and consistent comparison.

The ANN model involves iterative training using the Levenberg–Marquardt algorithm, therefore, MATLAB provides detailed training progress information such as epochs, gradient, and validation checks. In contrast, MLR and SVR are trained using analytical and optimization-based methods, respectively, which do not require iterative

epoch-based learning. Hence, their performance is evaluated directly using prediction error metrics and classification accuracy rather than training convergence plots

Table 4.3
Performance Metrics for MLR, SVR, and ANN Models

Model	MSE	RMSE	MAPE (%)
MLR	0.035	0.187	9.42
SVR	0.028	0.167	8.10
ANN	0.015	0.122	5.87

Table 4.2 presents a comparative performance evaluation of the Multiple Linear Regression (MLR), Support Vector Regression (SVR), and Artificial Neural Network (ANN) models based on three commonly used error metrics: Mean Squared Error (MSE), Root Mean Squared Error (RMSE), and Mean Absolute Percentage Error (MAPE). These metrics are used to assess how accurately each model predicts the fault conditions based on the extracted wavelet features.

From the results, the ANN model demonstrates the best overall performance, achieving the lowest values across all three-error metrics. Specifically, the ANN records an MSE of 0.015, an RMSE of 0.122, and a MAPE of 5.87%, indicating superior prediction accuracy and lower deviation from the actual fault labels. This improvement can be attributed to the ANN's ability to model nonlinear relationships between input features and output classes, which is particularly important for fault diagnosis in power electronic systems where signal behaviour is highly nonlinear.

The SVR model shows moderate performance, with lower error values than MLR but higher than ANN. Its ability to capture nonlinear patterns using kernel functions allows it to outperform MLR; however, its performance remains limited compared to ANN due to its dependence on kernel selection and parameter tuning.

The MLR model exhibits the highest error values among the three methods, reflecting its limitation in handling complex nonlinear fault characteristics. Since MLR assumes a linear relationship between inputs and outputs, its predictive capability is reduced when applied to nonlinear and transient fault signals.

4.2.3.3 Fault Detection and Recovery Performance Using ANN-Based Classification

This section highlights the MATLAB simulation results that validate the fault detection and recovery method developed for this study, focusing on Objective (c). The goal is to assess how the current signal in the DAB converter behaves when a fault occurs and how the system responds afterward. The detection system is powered by an ANN that was trained using important features extracted from the converter's electrical signals.

The simulation results show that the ANN can accurately detect open-circuit faults by recognizing unusual patterns in the current waveform. Once a fault is detected, the system activates a recovery process that helps bring the current back to normal, keeping it within safe limits. The waveform clearly shows initial distortion during the fault, followed by a return to steady operation once the recovery kicks in. These results confirm that the proposed method is both reliable and effective under changing conditions, successfully meeting the objectives of the research.

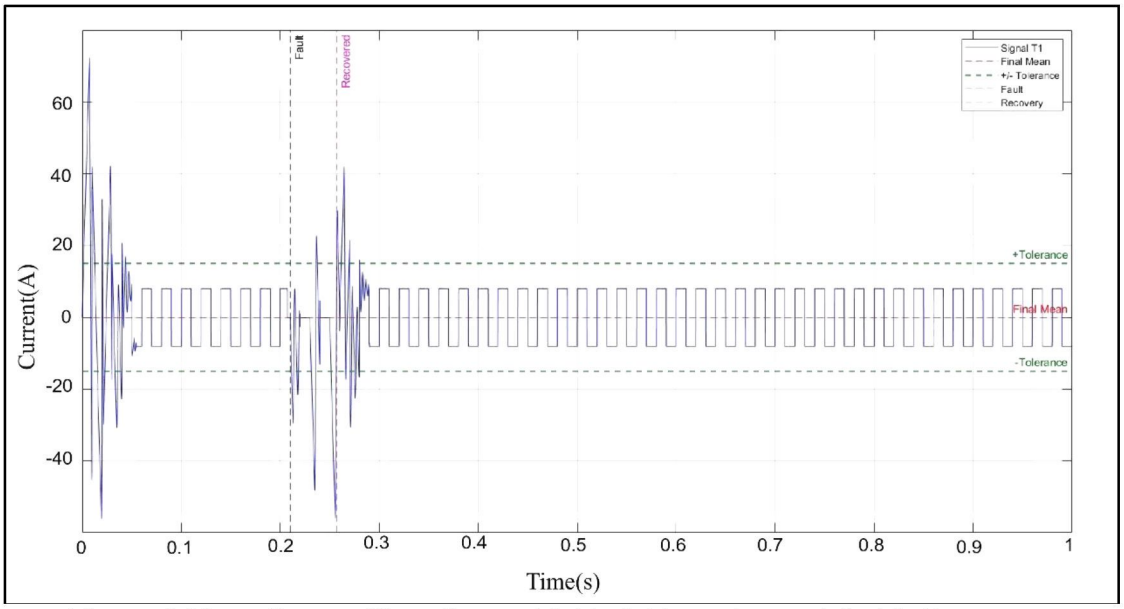

Figure 4.29 Current Waveform with Fault Detection and Stable Recovery Indication for Signal T[1]

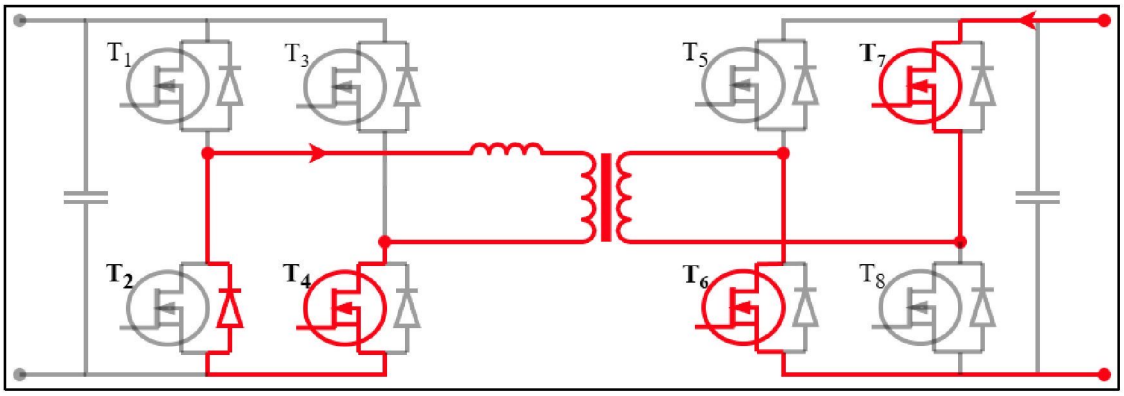

Figure 4.30 Illustration of Inductor Current Flow in the DAB Converter under T^1 Fault Condition

Figure 4.29 illustrates the inductor current response of the DAB converter when an open-circuit fault occurs at switch T1. Prior to the fault, the inductor current operates within the predefined tolerance band, indicating normal and stable power transfer. At approximately 0.21 s, a sudden change in the current waveform is observed, corresponding to the occurrence of the T1 open-circuit fault. Immediately after the fault, the inductor current collapses and remains close to zero for a short duration. This flattened current region indicates an interruption in the normal current conduction path on the primary-side bridge.

The current flow mechanism responsible for this behaviour is illustrated in the current flow diagram shown in Figure 4.30. When T1 becomes open-circuited, the intended upper-leg conduction path of the primary full bridge is blocked. As a result, the inductor current is unable to circulate through the normal switching sequence and is temporarily forced into a freewheeling condition through the complementary switch T2 and its associated body diode. This disrupted conduction path prevents effective energy transfer across the high-frequency transformer, explaining the near-zero current region observed in Figure 4.29.

As the fault condition persists, the imbalance between the primary and secondary bridge switching states causes a reversal of the effective inductor voltage. Consequently, the inductor current transitions from the zero-current region into a negatively biased current, as clearly observed in Figure 4.29 following the flattened segment. This negative current indicates unintended reverse power flow caused by the asymmetrical bridge operation under the T1 fault condition.

Once the fault is detected by the ANN-based fault diagnosis system, the proposed passive fault-tolerant control strategy is activated. The control action reroutes

the current through healthy and redundant switching paths, as highlighted in the current flow diagram. Following this corrective action, the inductor current gradually recovers and re-enters the tolerance band at approximately 0.25 s. The current then stabilises around the steady-state mean value, confirming successful fault mitigation.

Overall, the combined interpretation of Figures 4.29 and 4.30 demonstrates that the observed current flattening and subsequent negative bias are direct consequences of the altered current flow path resulting from the T1 open-circuit fault. The rapid recovery and restoration of stable current operation validate the effectiveness of the proposed ANN-based fault detection and passive fault-tolerant control scheme disturbances.

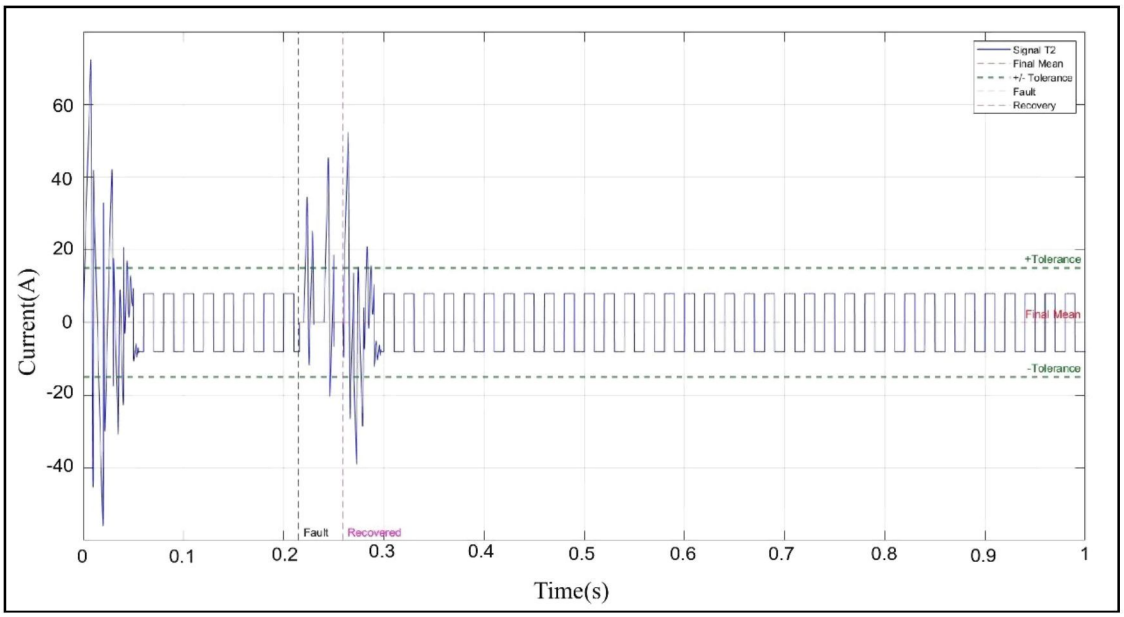

Figure 4.31 Current Waveform with Fault Detection and Stable Recovery Indication for Signal T^2

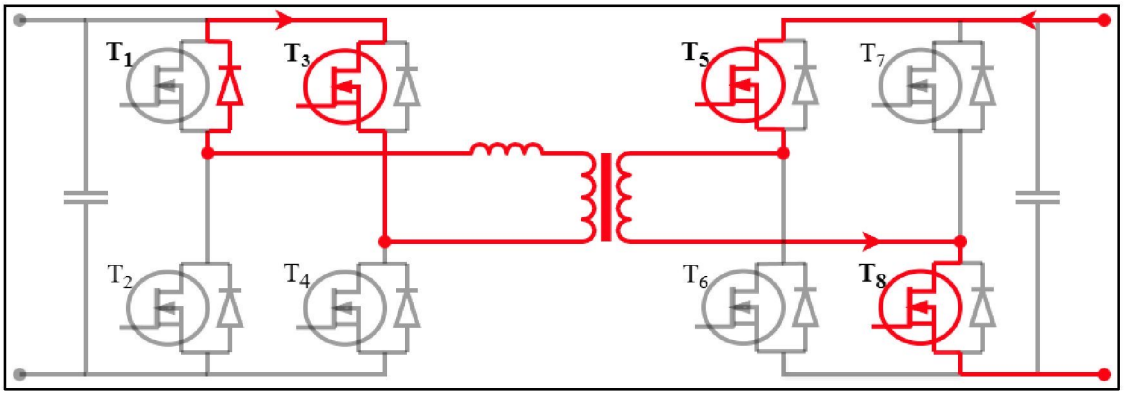

Figure 4.32 Illustration of Inductor Current Flow in the DAB Converter under T^2 Fault Condition

Figure 4.31 shows the inductor current response of the DAB converter when an open-circuit fault occurs at switch T2. During normal operation, the inductor current

remains stable and confined within the predefined tolerance band, indicating balanced power transfer between the primary and secondary bridges. At approximately 0.21 s, marked by the black dashed vertical line, an open-circuit fault is introduced at switch T2. Immediately after the fault, the current waveform deviates outside the tolerance range, reflecting a disturbance in the normal conduction path of the primary-side bridge.

The current flow behaviour responsible for this disturbance is illustrated in the current flow diagram for the T2 fault condition (Figure 4.32). When switch T2 becomes open-circuited, the lower-leg conduction path of the primary bridge is interrupted. Consequently, the inductor current is no longer able to circulate through its intended switching sequence. Instead, the current is forced to commutate through alternative freewheeling paths involving the complementary upper-leg switch T1 and associated body diodes, as highlighted in the diagram. This disrupted current path results in an imbalance in the bridge operation, leading to the observed transient deviation in the current waveform in Figure 4.31.

Unlike the T1 fault case, the T2 open-circuit fault causes a rapid change in the current magnitude rather than a prolonged zero-current region. This difference is due to the distinct position of T2 within the full-bridge structure, which alters the available freewheeling paths and the polarity of the inductor voltage during the fault condition. As a result, the current experiences a brief transient disturbance before stabilisation is initiated.

Once the fault is detected by the ANN-based fault diagnosis system, the passive fault-tolerant control strategy is activated. The control action reroutes the current through healthy switching paths, restoring a valid conduction loop across the transformer. As indicated by the magenta dashed line in Figure 4.31, the current re-enters the tolerance band at approximately 0.25 s, corresponding to a recovery time of about 0.04 s. After recovery, the current oscillates steadily around the final mean value and remains within the acceptable operating limits.

The combined interpretation of Figures 4.31 and 4.32 confirms that the transient current disturbance observed under the T2 open-circuit fault is a direct consequence of the altered current flow path in the primary bridge. The rapid detection and successful restoration of stable current operation demonstrate the effectiveness of the proposed ANN-based fault diagnosis and passive fault-tolerant control scheme for switch T2 faults conditions.

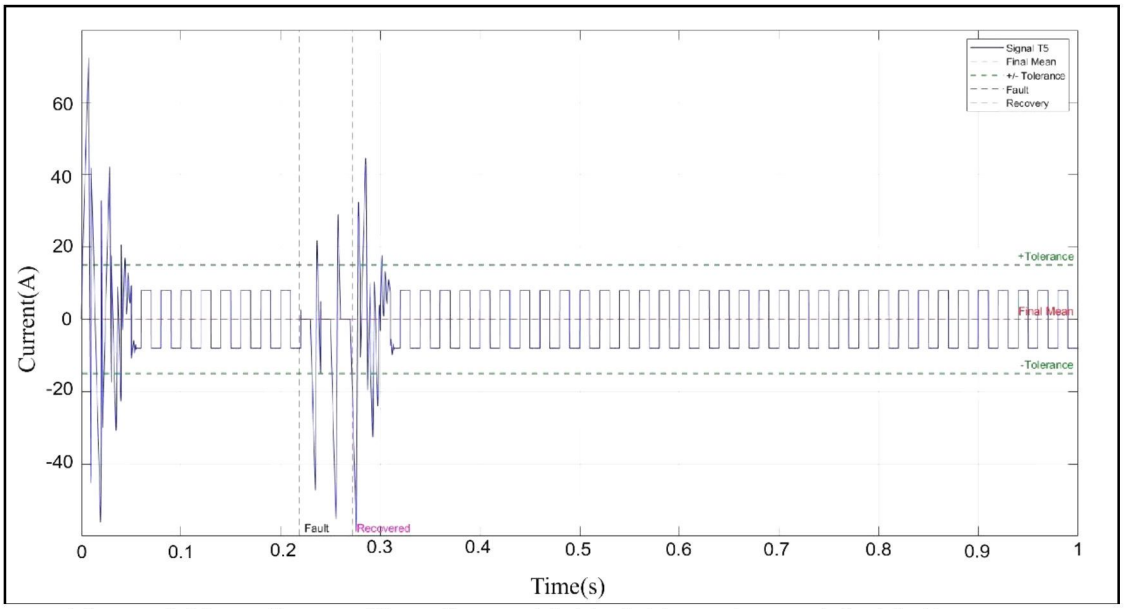

Figure 4.33 Current Waveform with Fault Detection and Stable Recovery Indication for Signal T^5

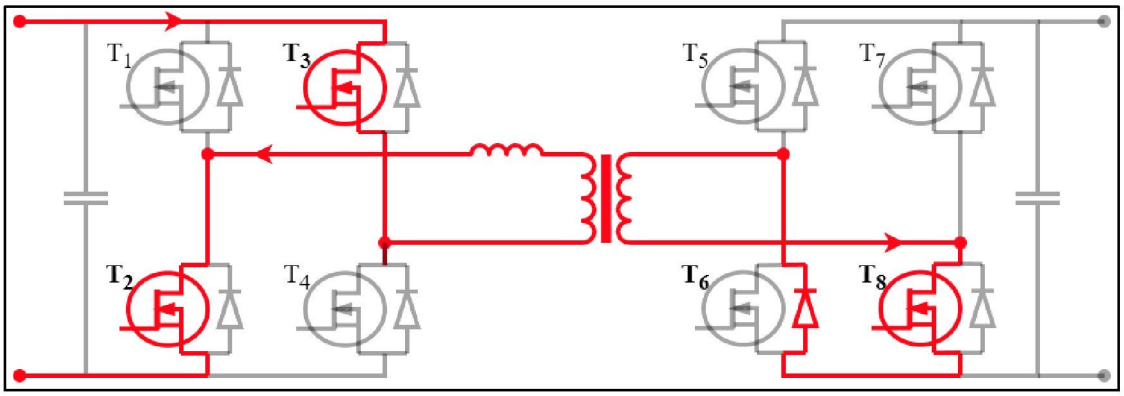

Figure 4.34 Illustration of Inductor Current Flow in the DAB Converter under T^5 Fault Condition

Figure 4.33 presents the inductor current response of the DAB converter when an open-circuit fault occurs at switch T5 on the secondary-side bridge. Under normal operating conditions, the current remains within the predefined tolerance band, indicating stable bidirectional power transfer. At approximately 0.22 s, as indicated by the black dashed vertical line, an open-circuit fault is introduced at switch T5. Immediately following the fault, the current waveform becomes highly unstable and exhibits large oscillations that exceed the tolerance limits. This behaviour reflects a sudden disruption in the intended current conduction path on the secondary side of the converter.

The corresponding current flow behaviour during the T5 fault is illustrated in the current flow diagram shown in Figure 4.34. When switch T5 becomes open-circuited, the upper-leg conduction path of the secondary bridge is interrupted,

preventing normal current transfer through the transformer. As a result, the inductor current is forced to commutate through alternative freewheeling paths involving the complementary lower-leg switch T6 and its associated body diode, as highlighted in the diagram. This altered conduction path introduces an imbalance between the primary and secondary bridges, which directly causes the pronounced current oscillations observed in Figure 4.33 immediately after the fault occurrence.

Due to the asymmetric switching states between the two bridges, the effective inductor voltage fluctuates significantly, leading to transient over-oscillation of the current rather than a complete current collapse. This explains why the T5 fault produces a more severe oscillatory response compared to the T1 and T2 fault cases. The observed behaviour confirms that faults occurring on the secondary-side bridge can have a stronger impact on current stability due to their direct interaction with the output energy transfer stage.

Once the abnormal current pattern is detected by the ANN-based fault diagnosis system, the proposed passive fault-tolerant control strategy is activated. The control action reconfigures the conduction path by utilizing healthy switches and redundant current paths, restoring a valid energy transfer loop across the transformer. As indicated by the magenta dashed line in Figure 4.33, the current re-enters the tolerance band at approximately 0.26 s, corresponding to a recovery time of about 0.04 s. After recovery, the current stabilises around the final mean value and remains within acceptable operating limits.

The combined interpretation of Figures 4.33 and 4.34 demonstrates that the large current oscillations observed under the T5 open-circuit fault are a direct consequence of the altered current flow path on the secondary-side bridge. The rapid detection and effective recovery confirm the robustness of the proposed ANN-based fault diagnosis and passive fault-tolerant control scheme in maintaining stable converter operation under severe switch fault conditions transfer.

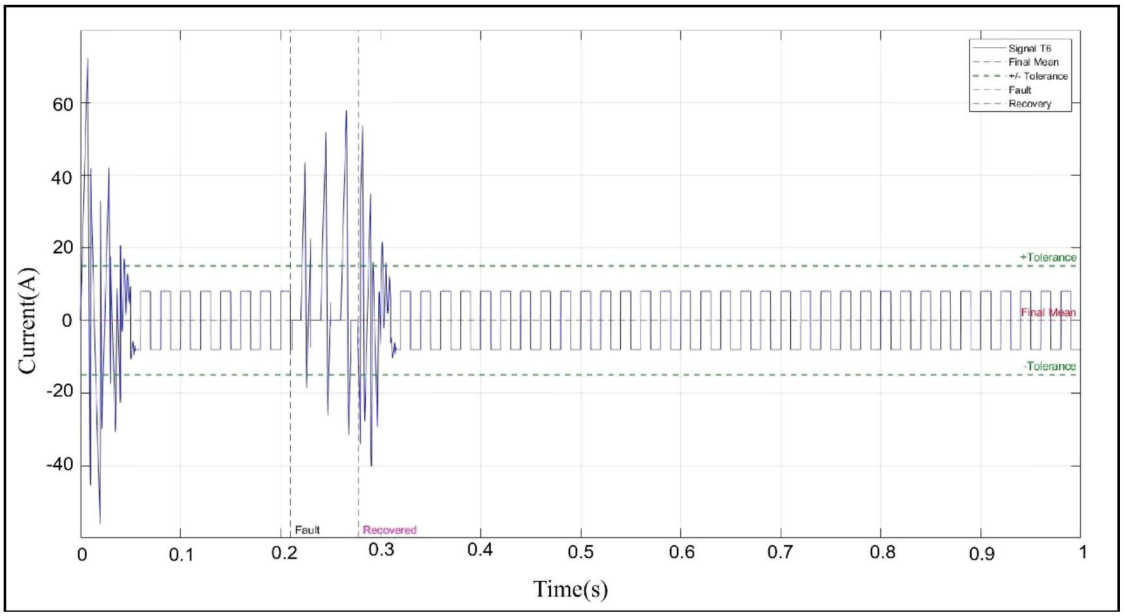

Figure 4.35 Current Waveform with Fault Detection and Stable Recovery Indication for Signal T^6

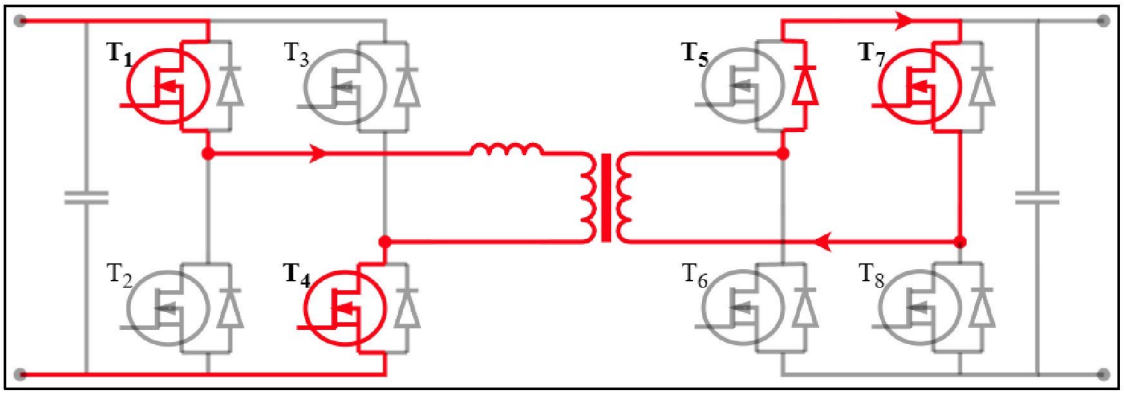

Figure 4.36 Illustration of Inductor Current Flow in the DAB Converter under T^6 Fault Condition

Figure 4.35 illustrates the inductor current response of the DAB converter when an open-circuit fault occurs at switch T6 on the secondary-side bridge. Under normal operating conditions, the current waveform remains stable and confined within the predefined tolerance limits, indicating balanced bidirectional power transfer. At approximately 0.21 s, marked by the black dashed vertical line, an open-circuit fault is introduced at switch T6. Immediately after the fault occurrence, the current waveform becomes highly unstable and exhibits large oscillations outside the tolerance band, reflecting a severe disturbance in the current conduction path on the secondary side of the converter.

The current flow behaviour responsible for this response is illustrated in the current flow diagram for the T6 fault condition (Figure 4.36). When switch T6 becomes

open-circuited, the lower-leg conduction path of the secondary bridge is interrupted. Since T6 plays a critical role in generating the negative half-cycle of the secondary-side voltage, its failure results in an asymmetric switching condition between the primary and secondary bridges. Consequently, the inductor current is forced to commutate through alternative freewheeling paths involving the complementary upper-leg switch T7 and associated body diodes, as highlighted in the diagram. This altered conduction path leads to an imbalance in the effective inductor voltage, which directly causes the erratic and oscillatory current behaviour observed in Figure 4.35.

Compared to faults occurring on the primary-side switches, the T6 fault produces more pronounced current oscillations due to its direct influence on the output-side energy transfer process. The disrupted secondary-side switching sequence results in rapid fluctuations in current magnitude rather than a complete current collapse, explaining the highly oscillatory waveform observed immediately after the fault.

Once the abnormal current pattern is detected by the ANN-based fault diagnosis system, the proposed passive fault-tolerant control strategy is activated. The controller reconfigures the current conduction path by utilizing healthy and redundant switching paths, restoring a valid energy transfer loop across the transformer. As indicated by the magenta dashed line in Figure 4.35, the current re-enters the tolerance band at approximately 0.27 s, corresponding to a recovery time of about 0.06 s. Following recovery, the current stabilises around the final mean value and remains within the acceptable operating range.

The combined interpretation of Figures 4.35 and 4.36 confirms that the severe current oscillations observed under the T6 open-circuit fault are a direct consequence of the altered current flow path on the secondary-side bridge. The successful detection and recovery demonstrate the effectiveness and robustness of the proposed ANN-based fault diagnosis and passive fault-tolerant control strategy in maintaining stable operation under critical switch fault conditions disturbances.

4.2.3.4 Summary of ANN Performance and System Recovery

The results clearly show that the ANN approach works effectively for identifying and recovering from open-circuit faults in a bidirectional DC-DC converter. The training process was fast and efficient, completing in just six epochs with an extremely low error rate, which means the network learned the patterns very well

without overfitting. It also showed good generalization, with stable validation and test performance throughout the training.

During simulations, the ANN successfully detected faults in different switches T^1, T^2, T^5, and T^6 and triggered recovery actions quickly. Faults were identified at around 0.21 to 0.22 seconds, and the system recovered within 0.04 to 0.06 seconds after detection. After recovery, the current signals returned to normal, staying within the expected limits and maintaining stable operation.

These results confirm that the ANN not only detects faults in real time but also helps the system return to a stable condition without delay. This approach strengthens the reliability of the converter, especially in scenarios where continuous power delivery is critical. Overall, the ANN-based method proves to be a practical and reliable solution for enhancing the fault tolerance of power electronic systems.

CHAPTER 5
CONCLUSION

5.1 Conclusion

This thesis presented an AI-enhanced fault-tolerant control framework for a bidirectional Dual Active Bridge (DAB) converter, with particular emphasis on reliable operation under open-circuit switch fault conditions. The research was motivated by the increasing demand for resilient power electronic converters in applications such as electric vehicle charging, battery energy storage systems, and renewable energy integration, where uninterrupted bidirectional power flow is critical.

A current-controlled switching strategy was first developed and implemented to ensure stable and efficient bidirectional power transfer between two battery systems. Unlike conventional phase-shift modulation, the adopted current-based control approach provided improved regulation of power flow and enhanced stability under dynamic operating conditions. Simulation results confirmed that the proposed control strategy successfully maintained bidirectional operation during both charging and discharging modes, with high efficiency across a wide range of output power levels.

To address converter reliability, this work focused on open-circuit switch faults, which are among the most common and challenging fault types in high-frequency power converters. An intelligent fault detection and diagnosis mechanism was developed by integrating wavelet-based feature extraction with an Artificial Neural Network (ANN) classifier. Wavelet decomposition was employed to extract time–frequency features from inductor current signals, allowing transient fault characteristics to be captured effectively. These features were then used to train the ANN to accurately distinguish between normal operation and individual switch fault conditions.

The ANN demonstrated fast convergence during training and achieved high classification accuracy during validation and testing, confirming its strong generalization capability. Simulation results showed that open-circuit faults at switches T1, T2, T5, and T6 were consistently detected within approximately 0.21–0.23 seconds. Following fault identification, the proposed passive fault-tolerant control (PFTC) strategy based on redundancy was activated, enabling the converter to recover stable operation within approximately 0.28–0.29 seconds. Post-fault current waveforms

returned to within acceptable tolerance bands with minimal oscillation, indicating effective fault mitigation and system robustness.

A detailed fault analysis was further supported by current flow diagrams, which illustrated how the conduction paths were altered under each fault condition. These diagrams provided clear physical insight into the observed current waveform behaviour and confirmed that the recovery process was directly linked to the activation of healthy and redundant switching paths. The combined use of waveform analysis and current flow interpretation strengthened the validity of the proposed fault-tolerant approach.

In addition, a comparative performance evaluation was conducted using Multiple Linear Regression (MLR), Support Vector Regression (SVR), and ANN models. The ANN consistently outperformed the other models in terms of Mean Squared Error (MSE), Root Mean Squared Error (RMSE), and Mean Absolute Percentage Error (MAPE), demonstrating its superior capability in modelling nonlinear fault characteristics inherent in DAB converters.

Overall, the results confirm that the proposed AI-enhanced fault-tolerant DAB converter successfully achieves fast fault detection, accurate fault classification, and reliable recovery without interrupting bidirectional power flow. By combining wavelet-based signal processing, ANN-based diagnosis, and redundancy-based passive fault tolerance, this research contributes a practical and robust solution for improving the reliability of modern power electronic systems systems.

5.2 Future Work

Although the proposed framework has demonstrated strong performance through comprehensive simulation studies, several directions for future research can be identified. First, experimental hardware implementation is recommended to validate the proposed fault detection and fault-tolerant control strategy under real-world operating conditions, including switching noise, sensor inaccuracies, and component non-idealities. Hardware-in-the-loop (HIL) testing could serve as an intermediate step before full experimental deployment.

Second, the current study focuses exclusively on single open-circuit switch faults. Future work may extend the fault diagnosis framework to include short-circuit faults, sensor failures, incipient faults, and multiple simultaneous fault scenarios. This

would further enhance the applicability of the proposed approach in complex and safety-critical systems.

Third, while a conventional ANN was employed in this research, advanced deep learning architectures such as convolutional neural networks (CNNs) or recurrent neural networks (RNNs) could be explored to improve fault classification accuracy under more complex operating conditions. Adaptive or online learning techniques may also be investigated to enable real-time model updating and improved long-term performance.

Finally, future studies may examine the integration of the proposed fault-tolerant strategy into larger energy systems, such as multi-converter DC microgrids or vehicle-to-grid (V2G) platforms, to evaluate scalability and system-level impacts. These extensions would further support the development of intelligent, resilient, and sustainable power electronic infrastructures use.

REFERENCES

[1] Y. Guan, Y. Xie, Y. Wang, Y. Liang, and X. Wang, "An Active Damping Strategy for Input Impedance of Bidirectional Dual Active Bridge DC-DC Converter: Modeling, Shaping, Design, and Experiment," *IEEE Trans. Ind. Electron.*, vol. 68, no. 2, 2021, doi: 10.1109/TIE.2020.2969126.

[2] H. Wen, J. Li, H. Shi, Y. Hu, and Y. Yang, "Fault Diagnosis and Tolerant Control of Dual-Active-Bridge Converter with Triple-Phase Shift Control for Bidirectional EV Charging Systems," *IEEE Trans. Transport. Electron.*, vol. 7, no. 1, 2021, doi: 10.1109/TTE.2020.3045673.

[3] M. Berger, I. Kocar, H. Fortin-Blanchette, and C. Lavertu, "Open-Phase Fault-Tolerant Operation of the Three-Phase Dual Active Bridge Converter," *IEEE Trans Power Electron*, vol. 35, no. 4, 2020, doi: 10.1109/TPEL.2019.2933487.

[4] A. Chambayil and S. Chattopadhyay, "A Dual Active Bridge Converter with Multiphase Boost Interfaces for Single-Stage Bidirectional DC-AC Conversion," *IEEE Trans Ind Appl*, vol. 57, no. 3, 2021, doi: 10.1109/TIA.2021.3058202.

[5] H. Zhang, Z. Liu, Y. Song, P. Han, and J. Liu, "A Current-Stress-Optimized Design Method for Dual Active Bridge Converters with Improved ZVS Capability under Wide Output Voltage Conditions," *IEEE Trans. Ind. Electron.*, vol. 71, no. 6, 2024, doi: 10.1109/TIE.2023.3292861.

[6] Y. Harrye, A. Abdalla, and H. A. Mahasneh, "The Generalization of Bidirectional Dual Active Bridge DC/DC Converter Modulation Schemes: State-of-the-Art Analysis under Triple Phase Shift Control," *Energies (Basel)*, vol. 16, no. 22, 2023, doi: 10.3390/en16227577.

[7] F. Rajabi, K. El Mokhtari, and J. J. McArthur, "MACHINE LEARNING-BASED FAULT DETECTION AND PRELIMINARY DIAGNOSIS FOR TERMINAL AIR-HANDLING UNITS," in *Proceedings of the European Conference on Computing in Construction*, 2023. doi: 10.35490/EC3.2023.213.

[8] T. Bakir, B. Boussaid, P. F. Odgaard, M. N. Abdelkrim, and C. Aubrun, "Artificial neural network based on wavelet transform and feature extraction for a wind turbine diagnosis system," in *2016 14th International Conference on Control, Automation, Robotics and Vision, ICARCV 2016*, 2016. doi: 10.1109/ICARCV.2016.7838818.

[9] S. N. Rekha, P. A. Jeyanthy, and D. Devaraj, "Wavelet transform based open

circuit fault diagnosis in the converter used in wind energy systems," in *Proceedings of the 2017 IEEE International Conference on Intelligent Techniques in Control, Optimization and Signal Processing, INCOS 2017*, 2017. doi: 10.1109/ITCOSP.2017.8303152.

[10] Q. Zhang *et al.*, "Improved assessment sensitivity of time-varying cavitation events based on wavelet analysis," *Ultrasonics*, vol. 138, 2024, doi: 10.1016/j.ultras.2023.107227.

[11] M. S. Priyadarshini, M. Bajaj, L. Prokop, and M. Berhanu, "Perception of power quality disturbances using Fourier, Short-Time Fourier, continuous and discrete wavelet transforms," *Sci Rep*, vol. 14, no. 1, 2024, doi: 10.1038/s41598-024-53792-9.

[12] W. Y. Yerima, O. M. Ikechukwu, K. N. Dang, and A. Ben Abdallah, "Fault-Tolerant Spiking Neural Network Mapping Algorithm and Architecture to 3D-NoC-Based Neuromorphic Systems," *IEEE Access*, vol. 11, 2023, doi: 10.1109/ACCESS.2023.3278802.

[13] Z. Shen, X. Zhao, C. Zhang, L. Zhang, and X. Liu, "Adaptive fault-tolerant method based on long-short term memory neural network," *Xi Tong Gong Cheng Yu Dian Zi Ji Shu/Systems Engineering and Electronics*, vol. 45, no. 3, 2023, doi: 10.12305/j.issn.1001-506X.2023.03.25.

[14] M. I. Rahman, K. H. Ahmed, and D. Jovcic, "Analysis of DC Fault for Dual-Active Bridge DC/DC Converter Including Prototype Verification," *IEEE J Emerg Sel Top Power Electron*, vol. 7, no. 2, 2019, doi: 10.1109/JESTPE.2018.2856759.

[15] C. Song, Y. Yang, A. Sangwongwanich, and F. Blaabjerg, "Open-Circuit Fault Analysis and Fault-Tolerant Control for 2/3-Level DAB Converters," in *Proceedings of the Energy Conversion Congress and Exposition - Asia, ECCE Asia 2021*, 2021. doi: 10.1109/ECCE-Asia49820.2021.9479285.

[16] Z. Li, C. Li, S. Li, and X. Cao, "A Fault-Tolerant Method for Motion Planning of Industrial Redundant Manipulator," *IEEE Trans Industr Inform*, vol. 16, no. 12, 2020, doi: 10.1109/TII.2019.2957186.

[17] L. Caseiro and A. Mendes, "Fault analysis and non-redundant fault tolerance in 3-level double conversion ups systems using finite-control-set model predictive control," *Energies (Basel)*, vol. 14, no. 8, 2021, doi: 10.3390/en14082210.

[18] M. Umair, N. M. Hidayat, A. Sukri Ahmad, N. H. Nik Ali, M. I. M. Mawardi,

and E. Abdullah, "A renewable approach to electric vehicle charging through solar energy storage," *PLoS One*, vol. 19, no. 2 February, 2024, doi: 10.1371/journal.pone.0297376.

[19] P. Shi, X. Wang, X. Meng, M. He, Y. Mao, and Z. Wang, "Adaptive Fault-Tolerant Control for Open-Circuit Faults in Dual Three-Phase PMSM Drives," *IEEE Trans Power Electron*, vol. 38, no. 3, 2023, doi: 10.1109/TPEL.2022.3223411.

[20] E. Garcia-Rodriguez, E. Reyes-Archundia, J. A. Gutierrez-Gnecchi, A. Mendez-Patino, M. V. Chavez-Baez, and J. C. Olivares-Rojas, "Detection of Power Quality Disturbances in Real Time Based on FPGA," in *Proceedings of the 25th Autumn Meeting on Power, Electronics and Computing, ROPEC 2023*, 2023. doi: 10.1109/ROPEC58757.2023.10409364.

[21] C. Zhang, Y. Zhu, C. Yu, J. Bao, Q. Wang, and G. Buja, "Power Quality Disturbance Identification Algorithm Based on Empirical Wavelet Transform and Time-Domain Kurtosis Feature Analysis," in *IEEE International Symposium on Industrial Electronics*, 2023. doi: 10.1109/ISIE51358.2023.10227977.

[22] Chinedu Alex Ezeigweneme, Chinedu Nnamdi Nwasike, Adedayo Adefemi, Abimbola Oluwatoyin Adegbite, and Joachim Osheyor Gidiagba, "SMART GRIDS IN INDUSTRIAL PARADIGMS: A REVIEW OF PROGRESS, BENEFITS, AND MAINTENANCE IMPLICATIONS: ANALYZING THE ROLE OF SMART GRIDS IN PREDICTIVE MAINTENANCE AND THE INTEGRATION OF RENEWABLE ENERGY SOURCES, ALONG WITH THEIR OVERALL IMPACT ON THE INDUSTRI," *Engineering Science & Technology Journal*, vol. 5, no. 1, 2024, doi: 10.51594/estj.v5i1.719.

[23] S. S. Khan, H. Wen, H. Shi, Y. Hu, L. Jiang, and G. Chen, "Multiple Open-Circuit Fault Detection and Isolation Using Universal Low-Cost Diagnosis Circuits for Reconfigurable Dual-Active-Bridge Converters," *IEEE Trans Power Electron*, vol. 38, no. 5, 2023, doi: 10.1109/TPEL.2023.3234592.

[24] A. F. Amiri, S. Kichou, H. Oudira, A. Chouder, and S. Silvestre, "Fault Detection and Diagnosis of a Photovoltaic System Based on Deep Learning Using the Combination of a Convolutional Neural Network (CNN) and Bidirectional Gated Recurrent Unit (Bi-GRU)," *Sustainability (Switzerland)*, vol. 16, no. 3, 2024, doi: 10.3390/su16031012.

[25] J. He, Y. Chen, J. Lin, J. Chen, L. Cheng, and Y. Wang, "Review of Modeling,

Modulation, and Control Strategies for the Dual-Active-Bridge DC/DC Converter," 2023. doi: 10.3390/en16186646.

[26] S. Shao *et al.*, "Modeling and Advanced Control of Dual-Active-Bridge DC-DC Converters: A Review," 2022. doi: 10.1109/TPEL.2021.3108157.

[27] A. F. Qusayer and S. M. S. Hussain, "Communication Assisted Protection Scheme Based on Artificial Neural Networks for Multi-Microgrid," *IEEE Access*, vol. 12, 2024, doi: 10.1109/ACCESS.2024.3352027.

[28] S. Rahimpour, O. Husev, D. Vinnikov, N. V. Kurdkandi, and H. Tarzamni, "Fault Management Techniques to Enhance the Reliability of Power Electronic Converters: An Overview," *IEEE Access*, vol. 11, 2023, doi: 10.1109/ACCESS.2023.3242918.

[29] C. Yu *et al.*, "High Efficiency Bidirectional Dual Active Bridge (DAB) Converter Adopting Boost-Up Function for Increasing Output Power," *IEEE Trans Power Electron*, vol. 37, no. 12, 2022, doi: 10.1109/TPEL.2022.3192048.

[30] Y. Zeng, Z. Zhao, J. Zheng, H. Li, S. Ji, and L. Yuan, "A Self-Restoring Fault-Tolerant Method for Controller Cooperation Simulation of Power Electronics Systems," *IEEE Trans. Ind. Electron.*, vol. 71, no. 1, 2024, doi: 10.1109/TIE.2023.3250742.

[31] H. A. Abd el-Ghany, M. I. Elmezain, E. M. Rashad, and E. S. Ahmed, "Discrete-wavelet-based scheme for protection coordination of hybrid AC/DC distribution networks," *Alexandria Engineering Journal*, vol. 90, 2024, doi: 10.1016/j.aej.2024.01.060.

[32] F. M. Shakiba, S. M. Azizi, M. Zhou, and A. Abusorrah, "Application of machine learning methods in fault detection and classification of power transmission lines: a survey," *Artif Intell Rev*, vol. 56, no. 7, 2023, doi: 10.1007/s10462-022-10296-0.

[33] I. Segovia Ramírez and F. P. García Márquez, "Machine Learning for Fault Detection and Diagnosis of Large Photovoltaic Plants Through Internet of Things Platform," *SN Comput Sci*, vol. 5, no. 1, 2024, doi: 10.1007/s42979-023-02348-1.

[34] Q. Yuan, Q. Tu, L. Yan, and K. Xia, "Fault diagnosis of H-bridge cascaded five-level inverter based on improved support vector machine with gray wolf algorithm," *Energy Reports*, vol. 9, 2023, doi: 10.1016/j.egyr.2023.03.017.

[35] F. L. N.A., "Wavelet analysis-based techniques for processing voice and video

signals in network communications," *International Journal of Computational Systems Engineering*, vol. 8, no. 3/4, 2024, doi: 10.1504/ijcsyse.2024.10059073.

[36] R. S. Jawad and H. Abid, "HVDC Fault Detection and Classification with Artificial Neural Network Based on ACO-DWT Method," *Energies (Basel)*, vol. 16, no. 3, 2023, doi: 10.3390/en16031064.

[37] S. Roy and S. Debnath, "A wavelet based PSD approach for fault detection and classification in grid connected inverter interfaced microgrid," *Measurement (Lond)*, vol. 226, 2024, doi: 10.1016/j.measurement.2023.114079.

[38] X. Li, X. Zhang, F. Lin, and F. Blaabjerg, "Artificial-Intelligence-Based Design for Circuit Parameters of Power Converters," *IEEE Trans. Ind. Electron.*, vol. 69, no. 11, 2022, doi: 10.1109/TIE.2021.3088377.

[39] X. Zhang, L. Xinze, M. Hao, H. Jingjing, and Z. Zheng, "The Proposed Artificial-Intelligence-Based Design (AI-D) for Circuit Parameters of Power Converters," in *Automated Design of Electrical Converters with Advanced AI Algorithms*, 2023. doi: 10.1007/978-981-99-0459-4_4.

[40] X. Zhang, W. Yang, L. Yan, M. Bin Kaleem, and W. Liu, "Adaptive internal short-circuit fault detection for lithium-ion batteries of electric vehicles," *J Energy Storage*, vol. 84, 2024, doi: 10.1016/j.est.2024.110874.

[41] Akanksha Sharma and Dr. Charu Saraf, "Comparing MLR and SVR in Evaluating the Impacts of Climate Change on Sugarcane Production in Saharanpur District," *International Research Journal on Advanced Engineering and Management (IRJAEM)*, vol. 3, no. 01, 2025, doi: 10.47392/irjaem.2025.0008.

[42] B. Bezyan and R. Zmeureanu, "Detection and Diagnosis of Dependent Faults That Trigger False Symptoms of Heating and Mechanical Ventilation Systems Using Combined Machine Learning and Rule-Based Techniques," *Energies (Basel)*, vol. 15, no. 5, 2022, doi: 10.3390/en15051691.

[43] A. Kothakota *et al.*, "Modeling and optimization of process parameters for nutritional enhancement in enzymatic milled rice by multiple linear regression (MLR) and artificial neural network (ANN)," *Foods*, vol. 10, no. 12, 2021, doi: 10.3390/foods10122975.

[44] J. Meerasri and R. Sothornvit, "Artificial neural networks (ANNs) and multiple linear regression (MLR) for prediction of moisture content for coated pineapple cubes," *Case Studies in Thermal Engineering*, vol. 33, 2022, doi:

10.1016/j.csite.2022.101942.

[45] D. L. de Souza, M. H. Granzotto, G. M. de Almeida, and L. C. Oliveira-Lopes, "Fault Detection and Diagnosis Using Support Vector Machines - A SVC and SVR Comparison," *Journal of Safety Engineering*, vol. 3, no. 1, 2014, doi: 10.5923/j.safety.20140301.03.

[46] S. Karimian, S. Falahat, Z. E. Bakhsh, M. J. G. Rad, and A. Barkhordari, "A comparative study on predicting the characteristics of plasma activated water: artificial neural network (ANN) & support vector regression (SVR)," *Journal of Theoretical and Applied Physics*, vol. 18, no. 4, 2024, doi: 10.57647/j.jtap.2024.1804.48.

[47] Z. Chen, P. Wang, B. Li, E. Zhao, Z. Hao, and D. Jia, "Artificial Neural Networks-Based Fault Diagnosis Model for Distribution Network," *Distributed Generation and Alternative Energy Journal*, vol. 38, no. 5, 2023, doi: 10.13052/dgaej2156-3306.38513.

[48] E. Egrioglu and E. Bas, "A new deep neural network for forecasting: Deep dendritic artificial neural network," *Artif Intell Rev*, vol. 57, no. 7, 2024, doi: 10.1007/s10462-024-10790-7.

[49] B. Li, C. Delpha, D. Diallo, and A. Migan-Dubois, "Application of Artificial Neural Networks to photovoltaic fault detection and diagnosis: A review," 2021. doi: 10.1016/j.rser.2020.110512.

[50] C. F. Rodríguez-Hernández, M. Musso, E. Kyndt, and E. Cascallar, "Artificial neural networks in academic performance prediction: Systematic implementation and predictor evaluation," *Computers and Education: Artificial Intelligence*, vol. 2, 2021, doi: 10.1016/j.caeai.2021.100018.

[51] A. Chouhan, P. Gangsar, R. Porwal, and C. K. Mechefske, "Artificial neural network–based fault diagnosis for induction motors under similar, interpolated and extrapolated operating conditions," 2021. doi: 10.1177/09574565211030709.

[52] Z. Yuan, G. Xiong, and X. Fu, "Artificial Neural Network for Fault Diagnosis of Solar Photovoltaic Systems: A Survey," 2022. doi: 10.3390/en15228693.

[53] G. Rayjade, A. Bhagure, P. B. Kushare, R. Bhandare, V. Matsagar, and A. Chaudhari, "Performance evaluation of machine learning algorithms and impact of activation functions in artificial neural network classifier for bearing fault diagnosis," *JVC/Journal of Vibration and Control*, vol. 31, no. 9–10, 2025, doi:

10.1177/10775463241235778.

[54] Q. Sun, X. Yu, H. Li, F. Peng, and G. Sun, "Fault detection for power electronic converters based on continuous wavelet transform and convolution neural network," *Journal of Intelligent and Fuzzy Systems*, vol. 42, no. 4, 2022, doi: 10.3233/JIFS-211632.

[55] S. S. Ghosh *et al.*, "Wavelet-based rapid identification of IGBT switch breakdown in voltage source converter," *Microelectronics Reliability*, vol. 152, 2024, doi: 10.1016/j.microrel.2023.115283.

[56] T. Kamiya, Y. Nakamura, H. Cho, Y. Ishida, and H. Shiraishi, "Partial Discharge Detection Method for High Voltage Converter System Using Wavelet Transform and Convolutional Neural Network," in *2022 9th International Conference on Condition Monitoring and Diagnosis, CMD 2022*, 2022. doi: 10.23919/CMD54214.2022.9991715.

[57] L. S. Azuara Grande, R. Granizo, and S. Arnaltes, "Wavelet Analysis to Detect Ground Faults in Electrical Power Systems with Full Penetration of Converter Interface Generation," *Electronics (Switzerland)*, vol. 12, no. 5, 2023, doi: 10.3390/electronics12051085.

[58] K. S. A. El-Naeem, M. A. Nayel, M. Abdelrahem, and I. Alkabbany, "Detecting Open-Circuit Faults in Power Electronic Converters Using Continuous Wavelet Transform and Convolutional Neural Networks for Simultaneous Charging Systems," *Arab J Sci Eng*, 2025, doi: 10.1007/s13369-025-10780-z.

[59] J. S. Farkhani, Ö. Çelik, K. Ma, C. L. Bak, and Z. Chen, "Fault Detection, Classification, and Location Based on Empirical Wavelet Transform-Teager Energy Operator and ANN for Hybrid Transmission Lines in VSC-HVDC Systems," *Journal of Modern Power Systems and Clean Energy*, vol. 13, no. 3, 2025, doi: 10.35833/MPCE.2023.000925.

[60] D. Wang *et al.*, "Model Predictive Control Using Artificial Neural Network for Power Converters," *IEEE Trans. Ind. Electron.*, vol. 69, no. 4, 2022, doi: 10.1109/TIE.2021.3076721.

[61] A. A. Ibrahim, A. Zilio, T. Younis, D. Biadene, T. Caldognetto, and P. Mattavelli, "Optimal Modulation of Triple Active Bridge Converters by an Artificial-Neural- Network Approach," *IEEE Trans. Ind. Electron.*, vol. 71, no. 3, 2024, doi: 10.1109/TIE.2023.3270529.

[62] J. Gurram, N. S. Babu, and G. N. Srinivas, "Artificial neural network based DC-

DC converter for grid connected transformerless PV system," *International Journal of Power Electronics and Drive Systems*, vol. 13, no. 2, 2022, doi: 10.11591/ijpeds.v13.i2.pp1246-1254.

[63] D. Guiza, D. Ounnas, S. Youcef, and A. Bouden, "PID based on a single artificial neural network algorithm for DC-DC boost converter," *Indonesian Journal of Electrical Engineering and Computer Science*, vol. 31, no. 1, 2023, doi: 10.11591/ijeecs.v31.i1.pp160-169.

[64] M. S. Mahdavi, M. S. Karimzadeh, T. Rahimi, and G. B. Gharehpetian, "A Fault-Tolerant Bidirectional Converter for Battery Energy Storage Systems in DC Microgrids," *Electronics (Switzerland)*, vol. 12, no. 3, 2023, doi: 10.3390/electronics12030679.

[65] A. K. Rana and A. V. Ravi Teja, "A Fault-Tolerant Power Converter with Multi-Switch Fault Diagnosis and Repair Capability for 4-Phase 8/6 SRM Drives," *IEEE IEEE Trans. Transport. Electron.*, vol. 8, no. 3, 2022, doi: 10.1109/TTE.2022.3161090.

[66] M. M. Masoom, M. Kumar, and N. Kumar, "Design and Characterization of Solar PV Fed Fault Tolerant Multiport Converter With Reduced Current Ripple," *IEEE Trans Ind Appl*, vol. 61, no. 4, 2025, doi: 10.1109/TIA.2025.3544565.

[67] J. C. Núñez, A. Martínez, J. Pastor-Rodríguez, O. Sandoval, R. Posada, and M. Adam, "Current status of control strategies in energy recovery systems in electric vehicles," *Dyna (Spain)*, vol. 97, no. 1, 2022, doi: 10.6036/10134.

[68] N. Wang, X. Pan, and S. F. Su, "Finite-time fault-tolerant trajectory tracking control of an autonomous surface vehicle," *J Franklin Inst*, vol. 357, no. 16, 2020, doi: 10.1016/j.jfranklin.2019.05.016.

[69] J.-C. Núñez, A. Martínez, J. Pastor-Rodríguez, O. Sandoval, R. Posada, and M. Adam, "Current status of control strategies in energy recovery systems in electric vehicles; [Estado actual de estrategias de control en sistemas de recuperación de energía en vehículos eléctricos]," *Dyna (Spain)*, vol. 97, no. 1, 2022.

[70] Y. Yao, W. Huang, R. Li, M. Yu, J. Liu, and J. Wu, "Active Fault-Tolerant Control for Three-Level T-Type Converter With Unbalanced Neutral-Point Voltage Modulation," *IEEE Trans Power Electron*, vol. 40, no. 10, 2025, doi: 10.1109/TPEL.2025.3576810.

[71] A. R. Lopez, J. Y. Rumbo-Morales, G. Ortiz-Torres, J. E. Valdez-Resendiz, G. Vazquez, and J. C. Rosas-Caro, "Fault-Tolerant Control Implemented for

Sustainable Active and Reactive Regulation of a Wind Energy Generation System," *Sustainability (Switzerland)*, vol. 16, no. 24, 2024, doi: 10.3390/su162410875.

[72] D. Du and Z. Li, "Research on weakly conservative passive fault-tolerant control method considering the fault distribution," *Engineering Science and Technology, an International Journal*, vol. 61, 2025, doi: 10.1016/j.jestch.2025.101948.

[73] A. Zaidi, M. Chrigui, and N. Zanzouri, "Cascade sliding mode control implementation in photovoltaic power supply for camping-car applications," *Journal of Energy Systems*, vol. 7, no. 2, 2023, doi: 10.30521/jes.1205696.

[74] F. Ahmad, M. Adnan, A. A. Amin, and M. G. Khan, "A comprehensive review of fault diagnosis and fault-tolerant control techniques for modular multi-level converters," 2022. doi: 10.1177/00368504221118965.

[75] A. Aslam and M. Raza, "Design and Implementation of Active Control Method for Minimizing Circulating Current in MMC-VSC System," *IEEE Access*, vol. 13, 2025, doi: 10.1109/ACCESS.2025.3588713.

[76] F. Rojas, C. Jerez, C. M. Hackl, O. Kalmbach, J. Pereda, and J. Lillo, "Faults in Modular Multilevel Cascade Converters - Part II: Fault Tolerance, Fault Detection and Diagnosis, and System Reconfiguration," *IEEE Open Journal of the Industrial Electronics Society*, vol. 3, 2022, doi: 10.1109/OJIES.2022.3213508.

[77] L. Huang, W. Zhao, J. Ji, T. Tao, Y. Du, and Q. Zhang, "Enhanced Fault Tolerance of Dual Three-Phase Permanent Magnet Motor with Three-Redundancy Control," *IEEE Transactions on Energy Conversion*, vol. 38, no. 3, 2023, doi: 10.1109/TEC.2023.3267786.

[78] W. A. Salem, O. Mohamady, M. Draz, and G. El-bayoumi, "Promoting the Maneuverability and Fault-Tolerant Control Capabilities of Dual-System/Hybrid VTOL UAVs," *Arab J Sci Eng*, vol. 49, no. 5, 2024, doi: 10.1007/s13369-023-08255-0.

[79] J. Harikumaran, G. Buticchi, M. Galea, and P. Wheeler, "Open Phase Fault Tolerant Control of Multi Three Phase Machines," *IEEE Open Journal of Power Electronics*, vol. 2, 2021, doi: 10.1109/OJPEL.2021.3115404.

[80] H. S. Johar, A. Bhattacharyya, and S. S. Rao, "Fault-Tolerant Brushless DC Motor Drive for Aerospace Applications," *Def Sci J*, vol. 73, no. 6, 2023, doi: 10.14429/DSJ.73.18898.

[81] S. S. Khairullah, F. N. Qassabbashi, and J. A. Kareem, "Design and analysis of fault-tolerant sequential logic circuits for safety-critical applications," *Bulletin of Electrical Engineering and Informatics*, vol. 13, no. 1, 2024, doi: 10.11591/eei.v13i1.5713.

[82] F. Zhang, Z. Zhang, Z. Zhang, T. Wang, J. Han, and Y. Amirat, "A Fault-Tolerant Control Method Based on Reconfiguration SPWM Signal for Cascaded Multilevel IGBT-Based Propulsion in Electric Ships," *J Mar Sci Eng*, vol. 12, no. 3, 2024, doi: 10.3390/jmse12030500.

[83] S. M. Banteywalu, G. Bekele, B. Khan, V. De Smedt, and P. Leroux, "A high-reliability redundancy scheme for design of radiation-tolerant half-duty limited dc-dc converters," *Electronics (Switzerland)*, vol. 10, no. 10, 2021, doi: 10.3390/electronics10101146.

[84] J. Wu, H. Wang, M. Ma, Q. Chen, and J. Liang, "Mode analysis and fault-tolerant method of open-circuit fault for a three-level dual active bridge DC-DC converter," *Microelectronics Reliability*, vol. 150, 2023, doi: 10.1016/j.microrel.2023.115100.

[85] F. Ahmad, M. Ahmad, F. Hayat, S. ud Din, M. Adnan, and A. A. Amin, "Modified triple modular redundancy based fault-tolerant three-phase matrix converter design with AI driven diagnostic capabilities," *Results in Engineering*, vol. 25, 2025, doi: 10.1016/j.rineng.2025.104454.

[86] Y. Xu, Z. Zhao, and S. Yin, "Performance Optimization and Fault-Tolerance of Highly Dynamic Systems Via Q-Learning With an Incrementally Attached Controller Gain System," *IEEE Trans Neural Netw Learn Syst*, vol. 34, no. 11, 2023, doi: 10.1109/TNNLS.2022.3155876.

[87] M. Bindi *et al.*, "Comparison Between PI and Neural Network Controller for Dual Active Bridge Converter," in *2021 IEEE 15th International Conference on Compatibility, Power Electronics and Power Engineering, CPE-POWERENG 2021*, 2021. doi: 10.1109/CPE-POWERENG50821.2021.9501168.

[88] M. Madhiarasan and M. Louzazni, "Analysis of Artificial Neural Network: Architecture, Types, and Forecasting Applications," *Journal of Electrical and Computer Engineering*, vol. 2022, 2022, doi: 10.1155/2022/5416722.

[89] V. K. Awaar, P. Jugge, S. T. Kalyani, and M. Eskandari, "Dynamic Voltage Restorer–A Custom Power Device for Power Quality Improvement in Electrical Distribution Systems," 2023. doi: 10.1007/978-981-19-7956-9_4.

[90] T. T. Le, M. K. Nguyen, T. D. Duong, C. Wang, and S. Choi, "Open-Circuit Fault-Tolerant Control for a Three-Phase Current-Fed Dual Active Bridge DC-DC Converter," *IEEE Transactions on Industrial Electronics*, vol. 70, no. 2, 2023, doi: 10.1109/TIE.2022.3156036.

[91] P. Wang, D. Guo, J. Hu, W. Wang, and D. Xu, "Natural Power Factor Correction and Soft Switching Design for a Single-Stage Bidirectional Dual Active Bridge AC-DC Converter," *IEEE Trans Power Electron*, vol. 39, no. 5, 2024, doi: 10.1109/TPEL.2024.3364391.

APPENDICES

APPENDIX 1

Research Activities

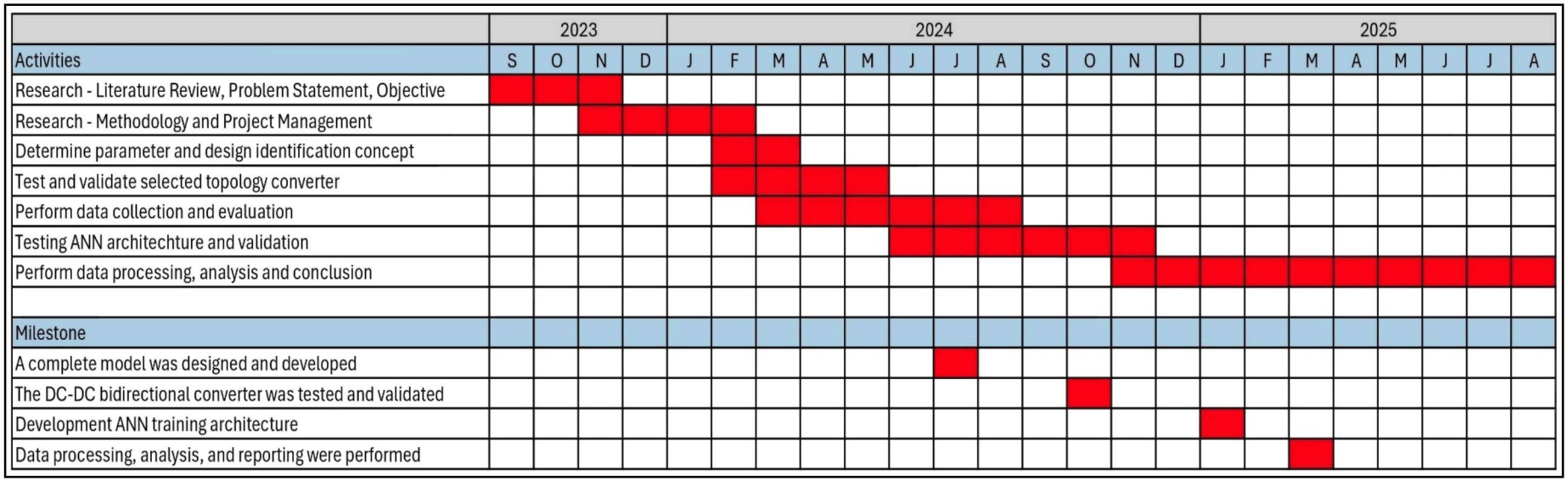

APPENDIX 2

DAB Simulation Circuit

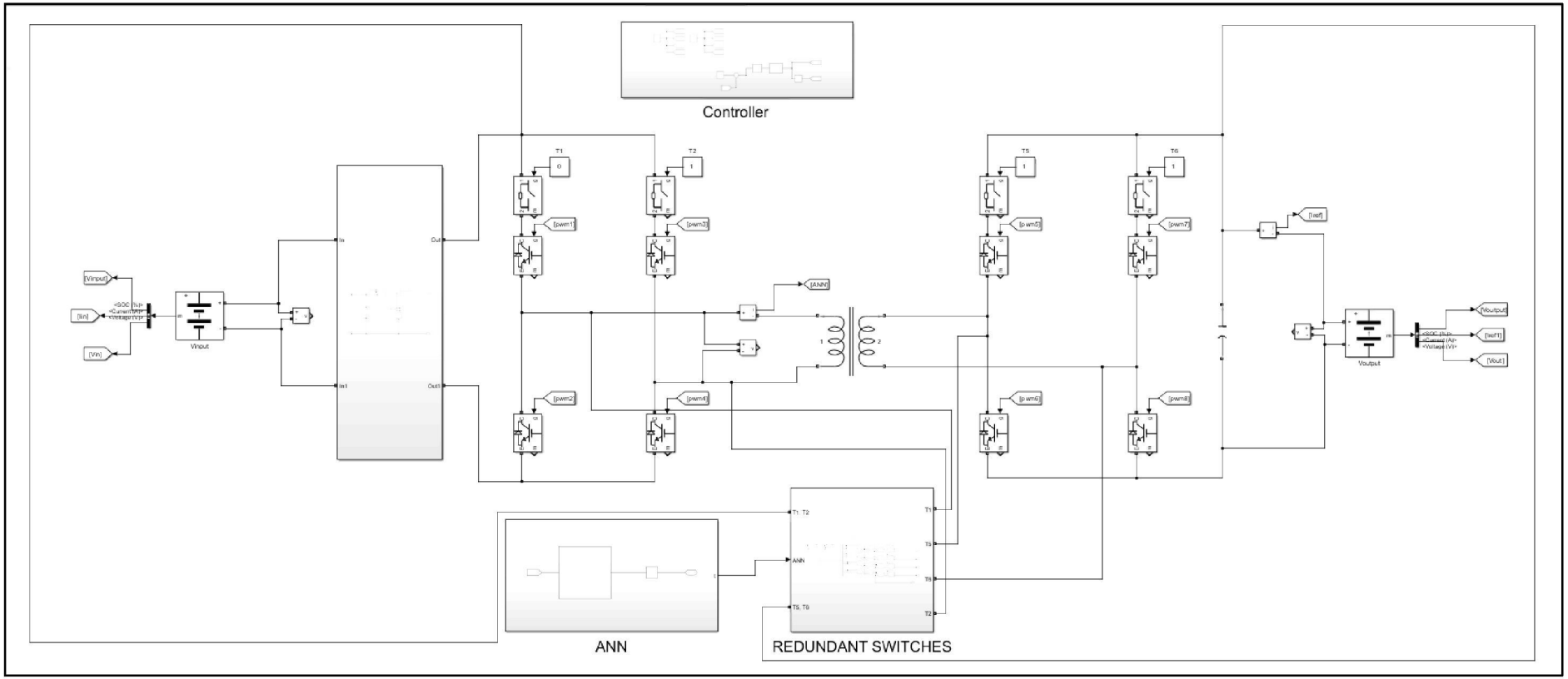

AUTHOR'S PROFILE

Mohamad Syazwan Bin Mohamed obtained his Bachelor of Electrical Engineering (Power System) from Universiti Teknologi MARA (UiTM), Malaysia, in 2023. He is currently pursuing a Master's degree at the School of Engineering, College of Engineering, Universiti Teknologi MARA (UiTM), Shah Alam, Malaysia, and serves as a Research Assistant for Petronas Research Sdn. Bhd., which has been funding the project from 2022 to 2024. He is also a Graduate Member of the Board of Engineers Malaysia (BEM). His research interests include power electronic converters, electric vehicles, energy storage systems, and solar energy.

LIST OF PUBLICATIONS

1. Published

M. Syazwan, N. M. Hidayat, K. Naidu, M. Umair, M. A. N. Zelan and N. H. Nik Ali, "Redundancy-Based Fault-Tolerant Control for Dual Active Bridge Converters," 2024 IEEE 22nd Student Conference on Research and Development (SCOReD), Selangor, Malaysia, 2024, pp. 645-651, doi: 10.1109/SCOReD64708.2024.10872649

2. Under Review

M. Syazwan, N. M. Hidayat, K. Naidu, M. Umair, and N. H. Nik Ali, "Adaptive Fault-Tolerant Control Strategy in Dual Active Bridge Converter," (Under review)